

Novel solid base catalysts for Michael additions

Synthesis, Characterization and Application

DISSERTATION

zur Erlangung des akademischen Grades

doctor rerum naturalium

(Dr. rer. nat.)

im Fach Chemie

eingereicht an der

Mathematisch-Naturwissenschaftlichen Fakultät I

Humboldt-Universität zu Berlin

von

M.Sc. (Chemistry) Zhijian Li

geboren am 27.04.1977 in Fujian, P.R. China

Präsident der Humboldt-Universität zu Berlin

Prof. Dr. Jürgen Mlynek

Dekan der Mathematisch-Naturwissenschaftlichen Fakultät I

Prof. Thomas Buckhout, PhD

Gutachter:

1. Prof. Dr. Erhard Kemnitz

2. Prof. Dr. Heiner Lieske

Tag der mündlichen Prüfung: 18.08.2005

Abstract

In contrast to solid acid catalysts, much fewer efforts have been made to study solid base catalysts. In this thesis, preparation, characterization and application of oxides and modified oxide as solid base catalysts were studied. The catalysts include MgO prepared by different methods, potassium-modified ZrO₂, calcined Mg-Al hydrotalcites, and a novel catalyst system Mg(O,F), which was prepared by sol-gel method for the first time. The catalysts were studied by N₂ adsorption/desorption measurement, XRD, FTIR, XPS, TG-DTA-DTG and NMR. Acid-base properties of the catalysts were investigated by TPD, FTIR spectroscopy and microcalorimetry to correlate with the catalytic behavior. Calcined Mg-Al hydrotalcite and Mg(O,F) are found to be highly active and selective catalysts for liquid-phase Michael additions of CH-acid compounds with methyl vinyl ketone.

Keywords:

Solid base catalyst, Michael addition, acid-base properties, heterogeneous catalysis, MgO, ZrO₂, hydrotalcite, Mg(O,F), sol-gel

Abstrakt

Im Gegensatz zu „festen Säuren“ sind „feste Basen“ wesentlich seltener Untersuchungsgegenstand in ihrer Anwendung als Katalysatoren in der heterogenen Katalyse.

In der vorliegenden Promotionsarbeit wurden entgegen diesem Trend die Herstellung, Charakterisierung und Anwendung basischer Oxide sowie modifizierter Oxide in ihrer Eignung als feste Basen in der Katalyse untersucht. Zu diesen Katalysatoren gehören MgO, hergestellt nach unterschiedlichen Methoden, Kalium modifiziertes ZrO₂, calcinierte Mg-Al Hydrotalcite und ein neuartiges Katalysatorsystem auf der Basis von Mg(O,F)-Kompositionen, die zum ersten Mal nach einem Sol-Gel-Fluorierungsverfahren hergestellt wurden.

Die Katalysatoren wurden mittels N₂ Adsorptions/Desorptionsuntersuchungen (BET), XRD, FTIR, XPS, TG-DTA-DTG und MAS NMR untersucht. Die Säure-Basen-Eigenschaften der Katalysatoren wurden durch TPD, FTIR Spektroskopie und Mikrokalorimetrie charakterisiert und mit den katalytischen Eigenschaften korreliert. Calcinierte Mg-Al Hydrotalcite und Mg(O,F) waren in diesem Zusammenhang am stärksten aktiv und auch selektiv wie für die Flüssigphasenreaktion der Michael-Addition von CH aciden Verbindungen mit Methylvinylketon gezeigt wurde.

Stichworte:

„Feste Basen“-Katalysator, Michael-Addition, Säure-Basen-Eigenschaften, heterogene Katalyse, MgO, ZrO₂, Hydrotalcite, Mg(O,F), Sol-Gel -Fluorierung

Table of Contents

Acknowledgements	III
List of Abbreviations, Acronyms and Symbols	IV
Chapter 1 Introduction	1
1.1 General introduction – from catalyst to solid base catalyst	2
1.2 Types of solid base catalysts	5
1.3 Application of solid base catalysts in liquid-phase reactions	15
1.4 Main reactions investigated in this thesis: Michael additions	23
1.5 Scope and outline of this thesis	24
Chapter 2 Experimental section	26
2.1 Chemicals	27
2.2 Catalyst preparation	28
2.3 Characterization	28
2.4 Reaction	31
Chapter 3 MgO as solid base catalysts in Michael addition	33
3.1 Introduction	34
3.2 Preparation and characterization of MgO prepared by different methods	35
3.3 Catalytic behavior of MgO catalysts	38
3.4 Conclusions	40
Chapter 4 Characterization and catalytic behavior of potassium-modified ZrO₂ base catalysts	42
4.1 Introduction	43
4.2 Preparation and characterization of potassium-modified ZrO ₂	43
4.3 Catalytic behavior of potassium-modified ZrO ₂	49
4.4 Conclusions	51
Chapter 5 Application of calcined Mg-Al hydrotalcites for Michael additions...	53
5.1 Introduction	54
5.2 Preparation and characterization of calcined Mg-Al hydrotalcites	56
5.3 Catalytic behavior of calcined Mg-Al hydrotalcites	63
5.4 Acid-base properties of calcined Mg-Al hydrotalcites	68
5.5 Correlation of catalytic behavior and the acid-base properties	81

5.6 Conclusions	85
Chapter 6 Sol-gel preparation, characterization and catalytic behavior of Mg(O,F).....	86
6.1 Introduction	87
6.2 Sol-gel preparation	88
6.3 Characterization of Mg(O,F)	90
6.4 Catalytic behavior of Mg(O,F)	105
6.5 Conclusions	109
Chapter 7 Summary and conclusions	110
Zusammenfassung	114
References	117
Lebenslauf	126
Selbständigkeitserklärung	127

Acknowledgements

First and foremost, I would like to thank my advisor Prof. Dr. Erhard Kemnitz, for offering me the opportunity to study in his group. I would like to express my deepest gratitude and appreciation for his inspiring discussions, valuable suggestions and encouragement throughout my study. I learn a lot and am very grateful.

I would deeply like to thank Dr. Hillary A. Prescott for her patient help, support and encouragement throughout the duration of this thesis.

I am very grateful to the cooperation with the group of Prof. Dr. Heiner Lieske from Institut für Angewandte Chemie Berlin-Adlershof (ACA). I would like to thank Dr. Annette Trunschke for teaching me FTIR, Dr. Jens Deutsch for his help in the reactions. The discussions with them and the suggestions from them are very helpful.

I am very grateful to Dr. Michael Feist for thermal analysis; Prof. Aline Auroux for microcalorimetric measurement; Sigrid Bäßler for TPD measurement and fluoride analysis; Elfriede Lieske for gas-phase reaction test; Thoralf Krahle for solving the XRD problems; Dr. D. Heidemann for solid state NMR measurement; Dr. J. Radnik and Dr. Ercan Ünveren for XPS measurement; Dr. Irmela Hähnert for TEM measurement.

I would also like to thank Dr. Krishna Murthy Janmanchi, Dr. Udo Groß, Dr. Candra Shekar, Dr. Sergey I. Troyanov and Dr. Stephan Rüdiger for many helpful discussions, advices and help.

I would like to thank all the members and visiting scholars in Prof. Kemnitz's group I ever met, Dr. Irmina Kris Murwani, Kerstin Scheurell, Mike Ahrens, Pratap Patil, Gehen Eltanany, Sushil K. Maurya, Dr. Yuexiang Zhu, Dr. Martin Wloka, Sakthivel Ramasamy, for their support and help in various ways.

Most of all, I would like to thank my wife and my family for encouraging me to face the difficulty and continually supporting.

At last, I would like to thank all my friends in Berlin, who have contributed to making my years of stay in Berlin not only educational, but also enjoyable.

Thank you!

Zhijian Li

July 2005

List of Abbreviations, Acronyms and Symbols

Å	angstrom
Ar	Argon
a.u.	arbitrary units
BE	binding energy
BET	Brunauer-Emmett-Teller and their adsorption model
BJH	Barret-Joyner-Halenda and their adsorption model
°C	degree Celsius
CHT	calcined hydrotalcite
CDCl ₃	chloroform-d
DMSO- <i>d</i> ₆	dimethyl- <i>d</i> ₆ sulphoxide
DTA	differential thermal analysis
DTG	differential thermogravimetry
EDX	energy-dispersive X-ray emission spectroscopy
Et	ethyl
Et ₂ O	ether
ESR	electron spin resonance
FTIR	fourier transformation infrared spectroscopy
GC	gas chromatography
HT	hydrotalcite
IC	ionic current
ICP-OES	inductively coupled plasma-optical emission spectroscopy
K	kelvin
MAS NMR	magic angle spinning nuclear magnetic resonance
Me	methyl
MS	mass spectrometry
NMR	nuclear magnetic resonance
PAS	photoacoustic spectroscopy
PDF No.	powder diffraction file number

pK_a	negative log of ionization constant
PTFE	p oly t etra f luoroethylene
Py	p yr i dine
RT	room t emperature
S_{BET}	specific surface area calculated by BET method
STP	standard t emperature and p ressure
TEM	t ransmission e lectron m icroscopy
THF	t etra h ydro f uran
TG	t hermo g ravimetric analysis
TPD	temperature- p rogrammed d esorption
XRD	X -ray d iffraction
XPS	X -ray p hotoelectron s pectroscopy

“Chemistry without catalysis would be like a sword without a handle, a light without brilliance, a bell without sound.....”

--- Alwin Mittasch

Chapter 1

Introduction

1.1 General introduction – from catalyst to solid base catalyst

Catalysis and Catalyst

Catalysis, from the Greek *kata* (*cata*), meaning down, and *lyein* (*lysis*) meaning to loosen, to free [1], may come from the “philosopher’s stone” or “quinta essential” of the medieval alchemists.

The chemical concept of catalysis was first developed by the great Swedish chemist Berzelius (1779–1848) in 1835 to correlate observations made by other chemists in Europe [2,3], such as the enhanced conversion of starch to sugar by acids; the hastening of gas combustion by platinum; the stability of hydrogen peroxide in acid solution but its decomposition in the presence of alkali and transition metals, such as manganese, silver, platinum, and gold; and the observation that the oxidation of alcohol to acetic acid was accomplished in the presence of finely divided platinum [4]. According to the definition of catalysis introduced by Berzelius and scientifically defined firstly by the German chemist Ostwald (1853–1932) in 1894, **catalyst** is a substance which alters the rate of approaching of chemical equilibrium without itself being changed or substantially consumed in the process [5]. In a catalyzed reaction the catalyst generally enters into chemical combination with the reactants but is ultimately regenerated so that the amount of catalyst remains unchanged. All the remarkable phenomenon involved catalyst can be called catalysis.

Catalysts may achieve astonishing activities. Very small quantities of catalyst can catalyze the reactions containing thousands or even millions of times their own weight of chemicals. Equally astonishing is just how selective they can be. A catalyst may increase the rate of only one reaction out of many competing reactions [6,7]. This just is the significant phenomenon of catalysis. Whereas normally in nature the law is valid: the cause is equal to the effect, catalytic phenomena are of an entirely different nature. The conceptual importance of catalysis is based on its surprising nature [8]. It is also interesting to note that over 80% of industrial processes involve catalysts and the number is rising; more than half of the elements in the periodic table are involved in catalytic systems.

Heterogeneous (Solid) catalysts

Catalysts are classified roughly according to their phase behavior into homogeneous and heterogeneous catalysts. For heterogeneous catalysis, catalyst and reactants are in different phases. The reactants may be either gases or liquids (or solutions) and usually the catalyst is a solid. Therefore, heterogeneous catalysts are also called as solid catalysts.

Catalysis takes place always and everywhere. Catalysis by solid materials has been observed quantitatively at temperatures as low as 78 K and as high as 1500 K; at pressures between 10^{-9} and 10^3 bar; with reactants in the gas phase or in liquid phase; with or without assistance of photons, radiation, or electron transfer at electrodes; with pure metals as unreactive as gold and as reactive as sodium; with multi-component and multi-phase inorganic compounds and acidic organic polymers; and at site time yields as low as 10^{-5}s^{-1} (one turnover per day) and as high as 10^9s^{-1} (gas kinetic collision rate at 10 bar) [9].

Nowadays the increasing social and environmental pressure on industry to substitute traditional homogeneous-catalyzed reactions by environmentally friendly technologies represents the most important driving force for the development of heterogeneous catalysis. Indeed, the solid catalysts have many advantages over liquid catalysts. They are non-corrosive and environmentally benign, presenting fewer disposal problems. Their reuse is possible and their separation from liquid products is much easier. Furthermore, they can be designed to give higher activity, selectivity and longer catalyst life.....

Today, heterogeneous catalytic processes may be divided into two large groups: *redox* reactions and *acid-base* reactions. The first group includes all those reactions in which the catalyst affects the homolytic bond rupture in the reactant molecules with the appearance of unpaired electrons, and formation of homolytic bonds with the catalyst with the participation of catalyst electrons. The second group includes reactions in which the reactants form heterolytic bonds with the catalyst by using the free electron pair of the catalyst or reactants, or the free electron pair formed in the course of reaction by heterolytic rupture of bonds in the reactant molecules [10]. Therefore, heterogeneous catalysts can be divided into redox catalysts and acid-base catalysts.

Solid acid-base catalysts

In general terms, a solid acid catalyst may be understood as a solid on which the color of a basic indicator changes, or as a solid on which a base is chemically adsorbed. On the contrary, a solid base catalyst may be understood as a solid on which the color of an acidic indicator changes, or as a solid on which an acid is chemically adsorbed. More strictly, following both Brønsted (-Lowry) and Lewis definitions [11]: a Brønsted acid is a *proton donor* and Brønsted base is a *proton acceptor*; a Lewis acid is an *electron-pair acceptor* and Lewis base is an *electron-pair donor*. A solid acid shows a tendency to donate a proton or to accept an electron pair, whereas a solid base tends to accept a proton or to donate an electron pair. These definitions are adequate for an understanding of the acid-

base phenomena shown by various solids, and are convenient for a clear description of solid acid and base catalysis. However, it should be noted that the same site could serve as a Brønsted base as well as a Lewis base, depending on the nature of the adsorbate in the reaction [11].

Solid base catalysts

So far, solid acid catalysts have been extensively studied and applied in numerous reactions due to the demand in the great progress of petroleum and petrochemical industry in the past 40 years. However, in contrast to solid acid catalysts, much fewer efforts have been made to study solid base catalysts. From a statistical survey made by Tanabe and Hölderich [12], in industrial processes until 1999, the classification of the types of catalysts into solid acid, solid base, and solid acid-base bifunctional catalysts gives the numbers as 103, 10 and 14, respectively. Obviously, the total number of solid base-related catalysts including solid base and acid-base bifunctional catalysts is much less than that of solid acid catalysts.

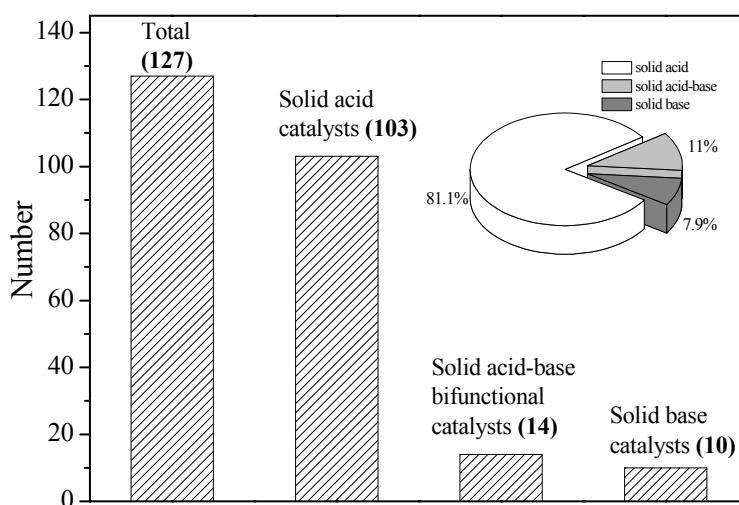


Fig.1.1 Number of the solid catalysts in the industrial processes [12]

Actually, numerous reactions such as isomerizations, alkylations, condensations, additions, and cyclizations are carried out industrially by using liquid bases catalysts. The replacement of liquid bases by cleaner catalytic alternatives is quite necessary in the view of environmentally benign. Solid base catalysts are non-stoichiometric, non-corrosive and reusable, which can be a good alternative.

1.2 Types of solid base catalysts

Table 1.1

Types of solid base catalysts

Type	Typical catalyst	Details of the catalyst
Single metal oxide	Alkaline earth oxide	MgO, CaO, SrO, BaO
	Rare earth oxide	La ₂ O ₃ , YbO ₂
	Transition metal oxide	ZrO ₂
Mixed oxide	Mg-Al mixed oxide	MgO-Al ₂ O ₃
	Mg-Ti mixed oxide	MgO-TiO ₂
Zeolite	Alkali ion-exchanged zeolite	Cs-exchanged zeolite X, Y
	Alkali metal or metal oxide occluded zeolite	Cs-occluded zeolite X, Y
Mesoporous material	Modified mesoporous material	MgO/SBA-15
	Functionalized mesoporous	MCM-41 functionalized with amino groups
	Mesoporous silicon oxynitride	-
Supported catalyst	compound: Na, K, KF, KNO ₃ , K ₂ O	KF/Al ₂ O ₃ , Na/NaOH/Al ₂ O ₃ ,
	Support: C, Al ₂ O ₃ , SiO ₂ , ZrO ₂ , MgO	Na/MgO
Clay and modified clay	Hydrotalcite, calcined and rehydrated hydrotalcite	Mg-Al hydrotalcites
	Chrysotile	-
	Sepiolite	Magnesium silicate
Oxynitride	Silicon oxynitride	SiON
	Aluminophosphate oxynitride	AlPON
	Zirconophosphate oxynitride	ZrPON
Other	Modified natural phosphate (NP)	Calcined NaNO ₃ /NP

The first study of heterogeneous basic catalysts, which was pointed out by Hattori [13], was that Pines et al. [14] studied sodium metal dispersed on alumina acted as an effective catalyst for double bond migration of alkenes in the 1950s. In the following 50 years, until now, the studies of solid base catalysts have been continuous and progressed steadily. From a single metal oxide, such as MgO, to functionalized mesoporous materials, a variety of solid base catalysts have been developed and studied. Here, the solid base catalysts are

divided into the types displayed in Table 1.1. Although some excellent reviews [13,15,16,17,18,19] are available about the solid base catalysts, some selected types of solid base catalysts, such as basic zeolites, functionalized mesoporous basic materials, oxynitrides, $\text{KF/Al}_2\text{O}_3$ and solid superbase catalysts will be briefly discussed in the following. Some other kinds of catalysts will also be further introduced later in the following chapters.

Basic zeolites

Generally, zeolites are aluminosilicates that are constructed from TO_4 tetrahedra (T = tetrahedral atom, e.g., Si, Al) with each apical oxygen atom shared with an adjacent tetrahedron. It is well known that zeolites are usually used as solid acid catalysts [20]. At the beginning of the 1990s, zeolites were used as base catalysts in their ion-exchanged and impregnated forms [19].

There are two main kinds of basic zeolites: alkali ion-exchanged zeolites and metal oxide or metal occluded zeolites. The latter can also be called as modified zeolites, supported zeolites, loaded zeolites or added zeolites. In general, the basic sites in alkali ion-exchanged zeolites are regarded as the framework oxygens and therefore related to the negative charge density on the oxygen atoms, which depend on the zeolite structure and chemical composition. The basic strength and the density of basic sites in alkali ion-exchanged zeolites decrease with an increase in framework Si/Al ratio, while basic strength increases with an increase in electropositivity of the countercation in zeolites [15,17]. Thus, the relatively high aluminum content of zeolite X (Si/Al = 1–1.5) results in a substantial framework negative charge, which makes zeolite X one of the most basic zeolites when in the alkali-exchanged form. Normally, the basic strength of alkali ion-exchanged zeolites decreases in the following order: $\text{Cs}^+ > \text{Rb}^+ > \text{K}^+ > \text{Na}^+ > \text{Li}^+$ [15,17,21]. This kind of basic zeolites is regarded as weak bases. Therefore, they can be handled in ambient atmosphere, since adsorption of carbon dioxide or water is not too strong, and they can be removed by high-temperature treatment.

Occlusion of alkali metal oxide clusters in zeolite cages via decomposition of impregnated alkali salts results in a further increase in the basicity of basic zeolites. Preparation of fine particles of alkali oxides inside the cavities of zeolites was developed by Hathaway and Davis [22,23,24]. They impregnated CsNaX and CsNaY zeolite with cesium acetate aqueous solution and calcined at 723 K to decompose cesium acetate into cesium oxide occluded in the cavities. Very active basic sites are formed by this method. In

the decomposition reaction of isopropanol to produce acetone, the activity of the impregnated CsNaY zeolite was an order of magnitude greater than that found for the impregnated CsNaX zeolite with the identical loadings of cesium acetate. The impregnated CsNaY zeolite was also found to show an order of magnitude greater acetone activity than the parent CsNaY zeolite [22]. The work of Hathaway and Davis was extended by Tsuji et al. [25,26], and they found that potassium and rubidium oxide could be formed in addition to cesium oxide. The resulting zeolite possesses basic sites stronger than those of simple ion-exchanged zeolite and is able to isomerize 1-butene at 273 K with high *cis/trans* 2-butene ratios. Recently, alkali earth oxides, such as MgO and BaO were also introduced into zeolites to produce strong basic sites [27,28].

Other basic zeolites containing alkali metals in cages have been studied as strong solid base catalysts. Impregnation of zeolite with NaN₃ or CsN₃ followed by controlled thermal decomposition of the alkali azide can form either ionic or neutral metal clusters [29,30,31,32]. Martens and co-workers [29,30] first prepared occluded metallic sodium zeolites, by the thermal decomposition of sodium azide adsorbed on the zeolite. These catalysts were active in the isomerization of *cis*-2-butene and the hydrogenation of acetylene, benzene and *cis*-2-butene.

Meanwhile, loading of low-valent Yb or Eu species on Y-zeolites by impregnation from Yb or Eu metal dissolved in liquid ammonia also resulted in strong basic catalysts [33,34]. Again, the loaded zeolites had a high catalytic activity for the isomerization of 1-butene at 273 K, when they were heated under vacuum at about 470 K.

It is also worth to mention that the microporous titanasilicate ETS-10 is found to be more basic than alkali ion-exchanged faujasite [35,36]. In the isopropanol conversion, Cs-exchanged X-type zeolite gave a 49.4% selectivity for acetone, while Cs-exchanged ETS-10 gave a 85.8% selectivity at 623 K.

The basicity (amount and strength) of basic zeolites have been extensively studied by theoretical approaches and experimental characterizations [15], including infrared (IR) spectroscopy of adsorbed probe molecules such as carbon dioxide [26,37], pyrrole [21,38], and chloroform [39], TPD [26,40], XPS [41,42,43], UV-Vis spectroscopy [44,45], microcalorimetry [46,47] and NMR [48,49,50]. Meanwhile, to investigate the active species, ¹³³Cs MAS NMR, ESR and Raman spectroscopy were also used.

By generating framework and/or extra-framework basic sites mentioned above, it is possible to prepare basic zeolites with a very large spectrum of basicities. Then, depending on the reaction to be catalyzed, it should be possible to select the most suitable basic

zeolite from the very mild alkaline-exchanged zeolites up to very strong alkali- or alkaline-oxide-cluster containing zeolites. Therefore, until now, basic zeolites have been used as catalysts in a number of base-catalyzed reactions, such as toluene alkylations with methanol [51,52] or ethylene [46], dehydrogenation of alcohols [22], double bond isomerizations [26,40], Knoevenagel condensations [53,54,55], aldol condensations [56,57] and cycloaddition of CO₂ to epoxides [58]. However, an industrial process utilizing a basic zeolite has not been commercialized [17].

For an excellent discussion of basic zeolites, a comprehensive review by Barthomeuf [15] is available.

Mesoporous basic materials

Although basic zeolites have been used in a broad spectrum of reactions, in some cases they are limited in the application of the synthesis of fine chemicals because their small pore openings prevent bulky molecules from reaching the active sites in zeolite cages. New families of mesoporous silicas, such as MCM-41 [59] and SBA-15 [60], open the new opportunities for supports due to tuneable larger pore sizes.

Basic mesoporous materials may be prepared by following routes: a) cation exchange with alkali (e.g. Na⁺, K⁺, Cs⁺) metal ions; b) impregnation with alkali salts solution and calcination; c) functionalization with organic groups. The preparations of the former two kinds of mesoporous materials are similar to those of basic zeolites.

The use of mesoporous materials MCM-41 as carriers for basic guest species was proposed by Kloetstra and Bekkum [61,62]. They found sodium and cesium cation-exchanged MCM-41s were mild, selective, water-stable and recyclable catalysts for base-catalyzed Knoevenagel condensation [61]. Meanwhile, they obtained finely dispersed cesium oxide clusters in the pores of MCM-41 by impregnation of MCM-41 with cesium acetate in aqueous or methanolic solution and calcination, when the cesium content was not higher than 10 wt%. The CsO_y/MCM-41 catalyst had strong base activity in Michael addition [61]. However, the catalyst did not show a good thermal and chemical stability. After repeated calcinations or after use, aggregation of the cesium oxide particles and a significant reduction of the specific surface area were observed [63]. Kloetstra and Bekkum further improved the thermal stability substantially and lowered the catalyst moisture sensitivity by addition of equimolar amounts of lanthanum, which gave the MCM-41 supported binary cesium-lanthanum oxide. The resulting catalyst was applied in Michael addition [62] and novel isomerization of ω-phenylalkanals to phenyl alkyl ketones

[64]. Recently, basic mesoporous material was also prepared by *in-situ* coating of SBA-15 with basic MgO in one-step procedure by adding acetate salt into the initial mixture of raw materials for synthesis [65].

Functionalized mesoporous basic material can also be prepared by the immobilization of an organic base, such as amino groups, cinchonine, β -aminoalcohols or quaternary organic ammonium hydroxides, on the surface of a carrier material. There have been various attempts to fix functional groups on the surface of mesoporous silica. Macquarrie first reported the one-pot synthesis of surface-modified mono-disperse MCM-type silica [66], and further found MCM-type silicas having aminopropyl groups were effective base catalysts for the Knoevenagel reactions [67]. The amino groups can also be introduced by post-synthesis using the reactivity of the OH groups [68,69]. Triazabicyclo[4,4,0]dec-5-ene (TBD) is an extremely strong organic base and particularly active both in the free form and immobilized on an organic resin. Subba Rao et al. [70] prepared a catalyst based on TBD immobilized on MCM-41. They reported high activity for base-catalyzed reactions such as Michael addition and Knoevenagel condensation. Rodriguez et al. [71] prepared strong and stable Brønsted base catalysts by anchoring quaternary organic tetraalkylammonium hydroxide on MCM-41. Corma and co-workers [72] grafted a proton sponge, 1,8-bis(dimethylaminonaphthalene) (DMAN), onto amorphous and pure-silica MCM-41. The results showed that DMAN supported MCM-41 was an excellent base catalyst for the Knoevenagel condensation between benzaldehyde and different active methylene compounds as well as for the Claisen-Schmidt condensation of benzaldehyde and 2'-hydroxyacetophenone to chalcones and flavanones.

The organic-inorganic hybrid materials are less strongly basic than the corresponding free organic molecules and possess a wide distribution of base sites with different strengths, which has been explained by an H-bonding interaction of the amine function with residual silanol groups. At the same time, these organic-inorganic hybrid materials maintain the advantages of the inorganic support, notably a high surface area and structural stability at elevated temperature and pressure. Thus, mesoporous silicas with a variety of organic bases have been tested for a variety of reactions, including the syntheses of monoglycerides from fatty acids and glycidol [68, 73], Knoevenagel condensations [70,71,74,75], aldol condensations [71,74], and Michael additions [70,71]. Moreover, it is worth noting that the immobilization of a chiral amine on MCM-41 can give a heterogeneous catalyst for enantioselective reactions [76].

Oxynitrides

Lednor and Rulter first prepared silicon oxynitride, $\text{Si}_2\text{N}_2\text{O}$, by a gas-solid reaction of amorphous silica with ammonia at 1373 K [77] and further found that the material had a solid base character in the Knoevenagel condensations [78, 79]. After that, aluminophosphate oxynitrides (ALPON), synthesized by nitridation under NH_3 of high-surface-area amorphous aluminophosphate precursors at around 1073 K (the temperature and time of nitridation could be changed to modify the nitrogen content in the final solid), [80,81,82,83,84] were described as a new family of solid basic catalysts, showing very promising behavior to the synthesis of methyl isobutyl ketone [80] and in Knoevenagel condensations [81,84]. The incorporation of nitrogen in the aluminophosphate anionic framework seems to be an effective way to modify the surface acid-base properties of the precursors and particularly to decrease the number of acid sites and to increase the number of basic sites. Zirconophosphate oxynitride (ZrPON) [85,86,87], galloaluminophosphate oxynitride (AlGaPON) [88,89] and aluminovanadate oxynitride (VAION) [90,91], which were prepared in a similar method, have also been reported as solid base catalysts. Recently, Xia and Mokaya [92] extended the preparation method and successfully prepared highly ordered mesoporous silicon oxynitride materials as solid base catalysts.

For oxynitrides, the identification of the basic sites is more difficult than that on oxide basic catalysts because several species present at the surface can act as basic sites. Among them the nitride nitrogen (N^{3-}), the $-(\text{NH})-$, and the $-\text{NH}_2$ group could be candidates, but the oxygen and the hydroxyl whose charge would be modified by the vicinity of the less electronegative framework nitrogen cannot be neglected [90]. Nevertheless, it seems that the acid-base properties of oxynitrides may be tuned by adjusting the O/N ratio.

In most cases, these oxynitrides are known to catalyze Knoevenagel condensations. However, application of this kind of catalysts to other types of reactions is highly desirable.

KF/ Al_2O_3

Most of heterogeneous basic catalysts are in the form of oxides and the basic sites are O^{2-} ions with different environments depending on their types. If the basic sites are constituted by elements other than O^{2-} , the catalysts are expected to show different catalytic properties [13]. Among the catalysts of the non-oxide type, potassium fluoride supported on alumina ($\text{KF}/\text{Al}_2\text{O}_3$) is most widely studied. $\text{KF}/\text{Al}_2\text{O}_3$ was introduced by Clark [93] as an effective solid catalyst to promote base-catalyzed organic reactions. The reactions using $\text{KF}/\text{Al}_2\text{O}_3$ as catalyst include Michael additions, Knoevenagel

condensations, aldol condensations and so on. Though $\text{KF}/\text{Al}_2\text{O}_3$ has wide application in organic chemistry because of its easy workup after reactions, the idea of its catalytically active species is still controversial and the mechanisms of the appearance of the basicity of $\text{KF}/\text{Al}_2\text{O}_3$ are not clarified. Moreover, conflicting conclusions have been reported on its base strength: most authors consider it to be weak or moderate base, but some note high or even super base.

Hattori and co-workers [94] reported that treating $\text{KF}/\text{Al}_2\text{O}_3$ at high temperature 573–673 K under high vacuum is essential for obtaining the high catalytic activity for double-bond isomerization of 1-pentene; the activity showed a sharp maximum at 623 K. The dependence of the catalytic activity on evacuation temperature was also found for the Tishchenko reaction of benzaldehyde [95] and the disproportionation of trimethylsilylacetylene [96]. Hattori and co-workers also found that the main containing F species on $\text{KF}/\text{Al}_2\text{O}_3$ was K_3AlF_6 , which was formed by the reaction of KF with alumina; however, it was not related to the formation of active sites, which gave a peak at -150 ppm in ^{19}F MAS NMR [97]. Insufficient coordination of KF only with surface OH^- groups may result in the formation of the so-called ‘half-naked’ and thus active F^- ions [98], which was supported by ^{19}F MAS NMR. Ando et al. concluded that there could be three basic species of KF/alumina [99,100]: (a) the presence of active fluoride, (b) the presence of $[\text{Al}-\text{O}^-]$ ion which generates OH^- when water is added, and (c) the cooperation of F^- and $[\text{Al}-\text{OH}]$.

Recently, the effect of the support on the properties of $\text{KF}/\text{Al}_2\text{O}_3$ was investigated. The basicity of supported KF can be significantly increased by a proper choice of support. The higher basicity is probably due to the dispersion of KF in small crystals [101]. More recently, CsF supported on α -alumina was also found to be an efficient basic catalyst [102].

Solid superbases

To activate a reactant under mild conditions, a catalyst with very strong basic sites may be needed. Moreover, in the possible commercial industry chemical processes, effective application of superbase catalyst to side chain alkylation for alkyl-aromatics, and high selectivity for double-bond-isomerization of olefinic compounds without causing tar-formation as well as in place of solid acid catalysts having problem of deactivation are highly desirable [103]. Normally, catalysts which possess base sites stronger than $H_- = 26$ are called superbases [5,11]. There have been some attempts to prepare those superbase catalysts (see Table 1.2).

Table 1.2

Types of solid superbase catalysts [104]

Catalyst	Starting material (preparation method)	Pretreatment Temperature (K)	Strength (H_-)
CaO	CaCO ₃	1173	26.5
SrO	Sr(OH) ₂	1123	26.5
NaOH/MgO	(NaOH impregnated)	823	26.5
KNO ₃ / Al ₂ O ₃ , KNO ₃ / ZrO ₂	(dry ground)	873	26.5
Na/MgO	(Na vaporized)	923	35
Na/Al ₂ O ₃	(Na vaporized)	823	35
Na/NaOH/Al ₂ O ₃	(NaOH, Na impregnated)	773	37
KNH ₂ /Al ₂ O ₃	(KNH ₂ impregnated)	573	>37
K(NH ₃)/Al ₂ O ₃	(ammoniacal K impregnated)	523–573	>37

Pines and co-workers [14,105,106] loaded alkali metals on supports by deposition of the metal vapor and used them as highly active catalysts for the isomerization of alkenes and the related compounds. The catalysts were regarded as superbase. Kijenski and Malinowski [107,108] also reported that sodium metal deposited on MgO (Na/MgO) showed a high catalytic activity for the isomerization of alkenes at 293 K and the base sites were stronger than $H_- = 35$. Ushikubo et al. [109] also prepared a superbase catalyst by addition of metallic sodium to MgO by decomposing NaN₃ to evolve metallic sodium vapor. The resulting catalyst acted as an efficient catalyst for decomposition of methyl formate to CO and methanol. Sun and Klabunde [110] found nanocrystalline MgO doped with potassium metal were capable of alkene isomerization and alkene alkylation, including the conversion of propylene–ethylene mixtures to pentene and heptene.

Suzukamo et al. [111,112] prepared a superbase catalyst by addition of alkali hydroxides to alumina followed by further addition of alkali metals. The resulting catalyst, Na/NaOH/Al₂O₃, a pale blue solid, possessed basic sites stronger than $H_- = 37$ and catalyzed various base-catalyzed reactions, such as double bond migrations of 5-vinylbicyclo[2.2.1]hept-2-ene to 5-ethylidenebicyclo[2.2.1]hept-2-ene at the reaction temperature 243–373 K, 2,3-dimethylbut-1-ene to 2,3-dimethylbut-2-ene at 293 K, and saffrole to isosaffrole at 293 K and side chain alkylations of alkylbenzenes at the reaction temperature 293–433 K.

Baba et al. [113,114] obtained a superbase K(NH₃)/Al₂O₃ by loading potassium onto alumina in liquid ammonia and heating the resulting material under vacuum at 523–573 K. The resulting catalyst showed extremely high catalytic activity for the isomerization of

alkene and had much higher activity than that of Al_2O_3 loaded with alkali metals by vapor deposition. The active species are not metallic, but probably amide- or imide-like species. However, Al_2O_3 loaded with KNH_2 was found to be more active than $\text{K}(\text{NH}_3)/\text{Al}_2\text{O}_3$ for the isomerization of 2,3-dimethylbut-1-ene. Using $\text{KNH}_2/\text{Al}_2\text{O}_3$, even toluene can be activated to react with silanes at 329 K [115]. Moreover, the NH_2 groups in $\text{KNH}_2/\text{Al}_2\text{O}_3$ even react with methane ($\text{p}K_a = 50$) [116]. The basic strength of both catalysts was estimated to be at least $H_- = 37$.

Yamaguchi [117] and Wang et al. prepared superbases by dispersing potassium salts such as KNO_3 , K_2CO_3 , KHCO_3 on alumina [118] or zirconia [119] followed by thermal treatments. The dispersed compounds are decomposed partly during the thermal treatment, but the origin of the basic sites is not clear yet. The catalysts possessed a base strength of at least $H_- = 26.5$ and have the advantage of easy preparation.

Acid-base bifunctional catalysts

Acidity and basicity are a pair of concepts and any kind of solid base (or solid acid) possesses more or less acid sites (or base sites), even for the catalysts which are simply regarded to be base (or acid) catalysts. The catalysts having suitable acid-base pair sites sometimes show pronounced activity, even if the acid-base strength of a bifunctional catalyst is much weaker than the acid or base strength of acid or base. ZrO_2 was found to be a very important acid-base bifunctional catalyst and has been used in industrial applications [120]. The possible solid acid-base bifunctional catalysts are given in Table 1.3.

Table 1.3

Possible solid acid-base bifunctional catalysts

Type	Details of the catalyst	Typical catalyst
Single metal oxide	Rare earth oxide	La_2O_3
	Transition metal oxide	ZrO_2
Mixed oxide	Mg-Al mixed oxide	$\text{MgO-Al}_2\text{O}_3$
Oxynitride	Aluminophosphate oxynitride	AlPON

Future prospects and problem to be solved

The role of basic active sites and their correlate with the catalytic behavior

Until now, the nature of the basic sites on some solid base catalysts, for example $\text{KF}/\text{Al}_2\text{O}_3$ and $\text{KNH}_2/\text{Al}_2\text{O}_3$, are not very clear. Moreover, the role of alumina as a support for

some catalyst systems is also not clear. It is quite necessary to explore new or proper characterization method to confirm the nature of the active sites. Meanwhile, there are a number of examples of heterogeneous base-catalyzed reactions which cannot be understood only in terms of number and strength of the basic sites, since the catalytic behavior of solid base catalysts are not simple copies of those of homogeneous basic catalysts. In situ spectroscopic techniques (IR, NMR) may be efficient methods to carry out the study. These techniques will furnish new and detailed information on the adsorbates on the working catalysts, thus helping to elucidate reaction mechanisms and find out the active sites. As catalysts, it is also important to define the reaction environment around the active sites to enhance the rate and selectivity of base-catalyzed reactions. On the other hand, theoretical calculations of the surface sites and the reaction mechanisms are quite helpful for exploration of solid base catalysis. So far the results of the quantum chemical calculations which have been done explain well the experimental results, and give us valuable information about the solid base catalysis. Unfortunately, the theoretical calculations have been done only for limited cases. An attempt to calculate for many cases is highly desirable. Keen insight into the surface reaction mechanisms and functions required for the reactions together with the accumulation of the data will enable to design the solid base catalysts active for desired reactions.

The roles of acid-base cooperative effects

In a lot of base-catalyzed reactions, acid sites on the surface of the catalysts were found to have cooperative effect to enhance the activity. However, the cooperative effect has not been well investigated. It is necessary to find an efficient way to further prove the mechanism of the cooperative effect.

Leaching problem for some kinds of catalysts in liquid-phase reactions

Some kinds of solid catalysts, such as Na/NaOH/Al₂O₃, metal or metal oxide occluded zeolites, show good activity in gas-phase reactions. However, when these catalysts were used in liquid-phase reactions, the problem of leaching of the active sites should be considered and studied.

Application of solid base catalysts

Novel reactions should be studied not only from the known homogeneous base-catalyzed reactions, but also from a wider range of reactions which might proceed through “anionic or anion-like” intermediates. Finally, solid bases should be utilized in industrial processes.

1.3 Application of solid base catalysts in liquid-phase reactions

Traditionally, heterogeneous catalysis has been associated with the production of petrochemicals and bulk chemicals for a long time, whereas fine and speciality chemicals are produced predominantly with non-catalytic organic synthesis or via homogeneous catalysis. Recently, heterogeneous catalysis is beginning to be used in the fine-chemicals industry because of the need for more environmentally friendly production technology. This tendency is assisted by the availability of novel catalytic materials and modern techniques of creating and investigating specific active sites on catalyst surfaces [121,122].

In the field of fine chemical production, important steps in the synthesis of relatively large and complex molecules include carbon-carbon bond forming reactions such as Knoevenagel condensations or Michael additions. Bases are usually used in organic reactions to deprotonate and form carbanion intermediates, which are important intermediates in many organic reactions for fine-chemical synthesis. This is why base-catalyzed reactions usually find more applications in intermediates and fine chemical synthesis. Replacing the conventional homogeneous base catalysts, mostly solutions of alkali metal hydroxides and alkoxides, by solids can be desirable for various reasons, e.g., to suppress undesired side reactions (polymerization, self-condensation) or avoid salt formation due to the necessary neutralization of the soluble bases. The amount of by-products (largely inorganic salts) per kilogram of product is generally much larger in fine chemicals and pharmaceuticals than bulk chemicals (see Table 1.4). The use of heterogeneous base catalysts has reached great development in different areas of organic synthesis due to their environmental compatibility combined with the good yield and selectivity that can be achieved.

Table 1.4

The E factor (kg by-product/kg product) [121]

Industry segment	Product tonnage	Kg by-product/kg product
Bulk chemicals	$10^4 - 10^6$	< 1 – 5
Fine chemicals	$10^2 - 10^4$	5 – 50
Pharmaceuticals	$10 - 10^3$	25 – > 100

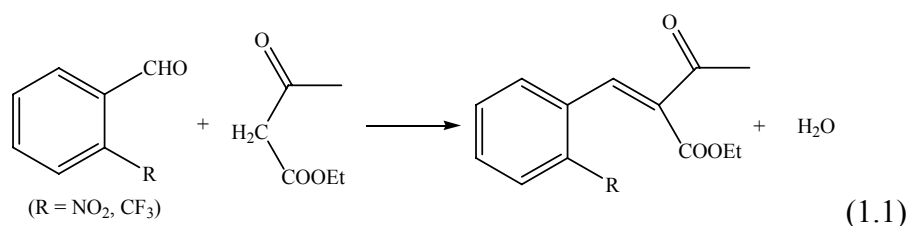
Therefore, in the following section, application of solid catalysts in liquid-phase reactions, especially in C–C bond formation reactions for fine chemicals will be discussed.

Some typical reactions, such as Knoevenagel condensation and aldol condensation, will be detailed below.

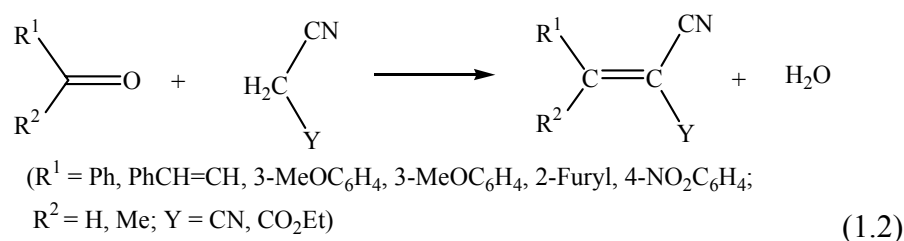
Knoevenagel condensation

Knoevenagel condensations are the reactions between a ketone and active methylene compounds and proceed over a variety of basic solid catalysts, including alkali-ion-exchanged zeolites, alkali-ion-exchanged sepiolite, oxynitrides, and hydrotalcite-related catalysts and so forth.

The Knoevenagel condensations of benzaldehyde and substituted benzaldehydes with ethylcyanoacetate, ethylmalonate, and ethylacetoacetate [Eq.(1.1)] were catalyzed by basic faujasite zeolites [53,54] to obtain intermediates for the production of dihydropyridine derivatives. The catalytic activity increased with the basicity of the zeolite.

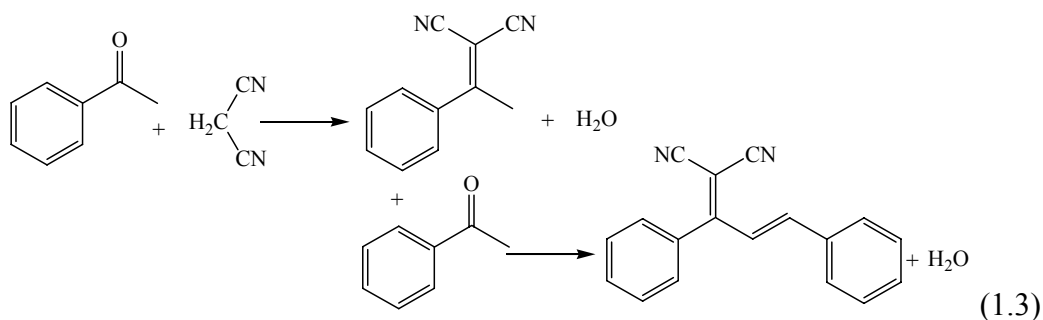


Rehydrated hydrotalcite was reported by Kantam et al. to give quantitative yields for a variety of Knoevenagel condensations [Eq.(1.2)] at room temperature using toluene or DMF as solvent in liquid phase [123]. Mesoporous silicas modified with amino groups [74] and mesoporous silicon oxynitride [92] were also effective in similar reactions.

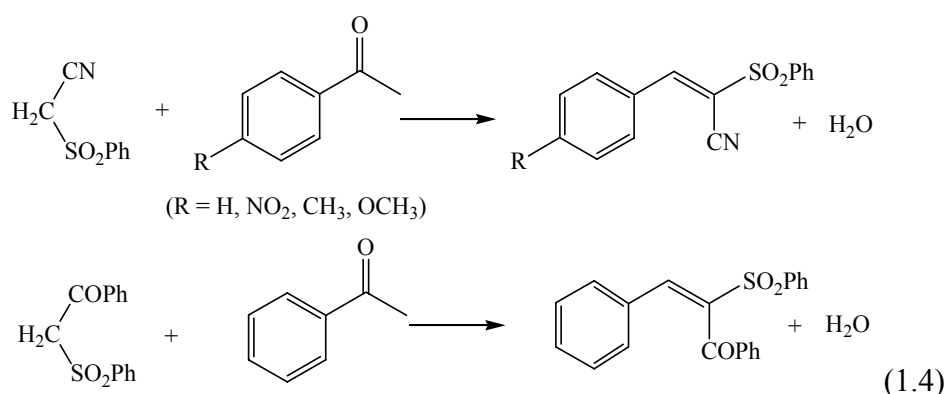


Knoevenagel condensations of malononitrile with cyclohexanone, benzophenone and *p*-amino acetophenone yield alkenes containing electron withdrawing nitrile groups, which facilitate additions to the double band. These alkenes are useful in anionic polymerization reactions leading to plastics, synthetic fibers or the production of liquid crystals. They can be synthesized using ion-exchanged zeolite X, sepiolite and hydrotalcite as catalysts [124].

Dicyanomethylene derivative dyes could be prepared by two-step synthesis using different solid bases via Knoevenagel condensations [Eq.(1.3)]. The first step is the condensation of acetophenone and malononitrile to give the corresponding α -methylbenzylidene-malononitrile, which was catalyzed by a variety of solid bases such as MgO, calcined hydrotalcites, and ALPONS. Subsequent condensation with benzaldehyde gives the 1,1-dicyano-1,3-butadiene dye, which was catalyzed efficiently by ALPON. Interestingly, the reaction can also be performed in a one-pot system using an optimized ALPON as catalyst [125].



Knoevenagel condensation is also chosen for the synthesis of unsaturated arylsulfones. For instance, phenylsulfonylacetonitrile and phenylsulfonylacetophenone reacted with benzaldehyde and 4-substituted benzaldehydes using high-surface-area MgO, calcined Mg-Al hydrotalcites or ALPON type materials leading to α -phenylsulfonyl-cinnammonitrile and derivatives as well as α -phenylsulfonylchalcone [Eq.(1.4)] [126].



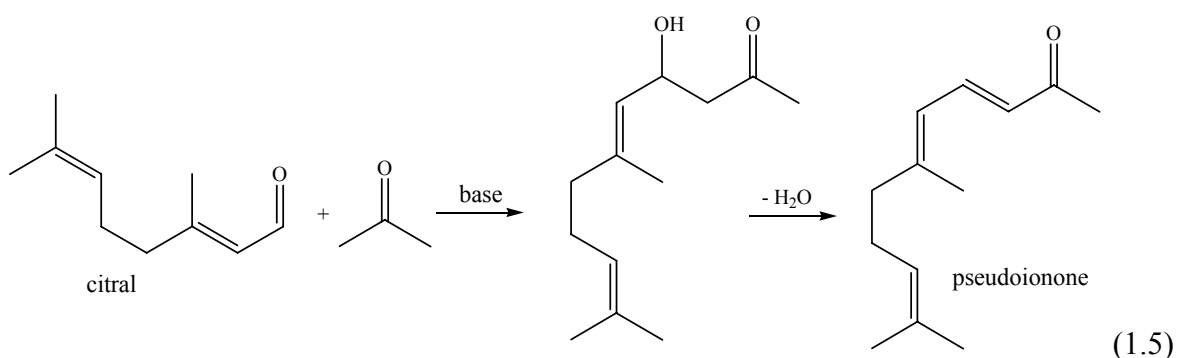
Aldol condensation

The aldol condensation is an important reaction for carbonyl compound (aldehyde or ketone) coupling via C–C bond formation. Aldol self-condensation of acetone to diacetone alcohol is catalyzed by a variety of solid bases, such as alkaline earth oxides, La₂O₃ and

ZrO₂, and Ba(OH)₂ [13]. Alkaline earth oxides are active for the reaction in the following order: BaO > SrO > CaO > MgO [127] and the active sites are suggested to be surface OH groups. This reaction can also be catalyzed by meixnerite-like hydrotalcite-based catalysts with high selectivity towards the desired product [128].

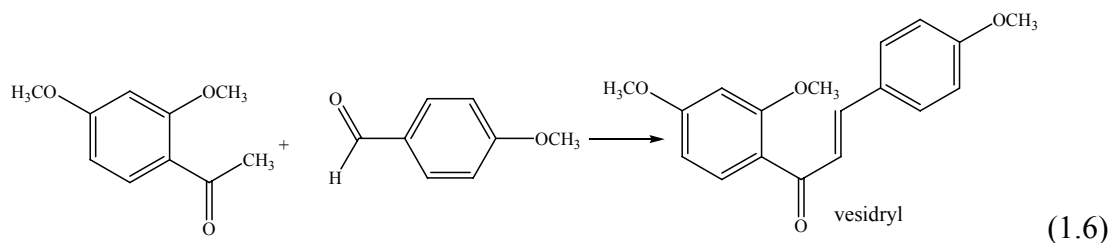
For aldol condensations, generally, product aldols will undergo dehydration in presence of acid sites besides basic sites. For example, when Choudary et al. used diamino-functionalized mesoporous silica as a catalyst, the reaction products were a mixture of the aldols and their dehydration products [74].

Properly activated hydrotalcite was used in condensation of citral (a mixture of geranial and neral with a proportion of 25 and 75 wt%, respectively) and acetone into pseudoionone [Eq.(1.5)], which is an intermediate in the commercial production of vitamin A [129]. The results showed that even at 273 K this reaction was catalyzed by modified hydrotalcites with a conversion of 65% and a selectivity of 90%, when the citral concentration is not too high (~1 wt%).

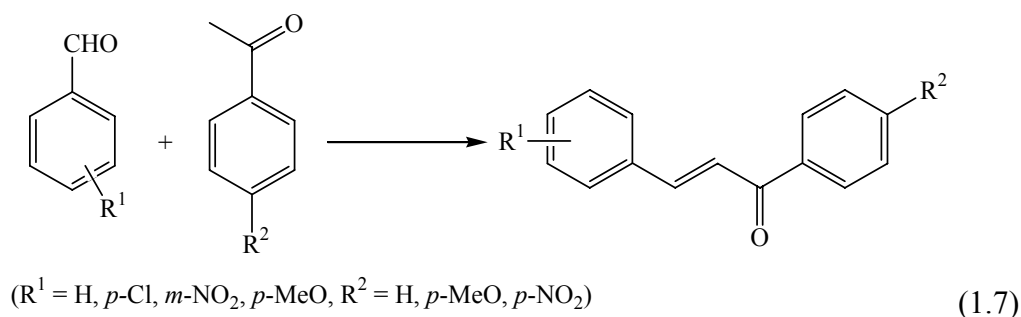


However, Climent et al. found both calcined hydrotalcites and rehydrated hydrotalcites could perform the same reaction at 333 K with excellent conversions and selectivities with relatively low acetone to citral ratios. It was worth noting that rehydrated hydrotalcites showed an improved reaction rate [130]. Moreover, under the reaction conditions, it was possible to avoid the inhibiting effect of citral found at 273 K [129]. Using rehydrated hydrotalcites, attractive results have also been reported in the condensation between aromatic aldehydes like benzaldehyde or substituted benzaldehydes and acetone [123].

In an aldol condensation between a ketone and an aldehyde (Claisen-Schmidt condensation), vesidryl, which is of pharmacological interest owing to its diuretic and choleric properties, was produced from substituted acetophenone and substituted benzaldehyde [Eq.(1.6)]. By use of calcined hydrotalcite as a catalyst (5 wt%), 85% yield of vesidryl was obtained at 170 °C after 20 h [131].



A strongly basic catalyst, which was obtained by impregnation of natural phosphate with a solution of sodium nitrate, followed by calcination at 900 °C, could also catalyze the Claisen-Schmidt condensations [Eq.(1.7)] to produce chalcones with high yields [132]. The catalyst could be easily recovered and efficiently reused.



Among aldol condensations, nitroaldol condensation (Henry reaction) is the reaction of a nitro compound with a carbonyl compound to form a nitroalcohol under basic conditions. The products, nitroalcohols, can be converted by hydrogenation to β -aminoalcohols, which are then converted to pharmacologically important chemicals; or proceed further to afford nitroalkene. Again, a classical nitroaldol reaction is also routinely performed by use of homogeneous basic catalysts such as alkali metal hydroxides, alkoxides, amines, and ammonium acetate.

The nitroaldol condensation of propionaldehyde and nitromethane gave the product, 1-nitro-2-hydroxybutane, in the presence of different solid bases at 313 K [133]. Among the solid bases studied, MgO was the most active. The activity was not so strongly dependent on the pretreatment temperature and was scarcely retarded by exposure to air. The condensation of aromatic aldehydes with nitroalkanes over alkaline ion-exchanged zeolites affords nitroalkenes directly. Thus, in the reaction of benzaldehyde and chlorobenzene with nitromethane, CsNaX gave the corresponding nitroalkenes in 68% and 80% yields, respectively, at 413 K [134].

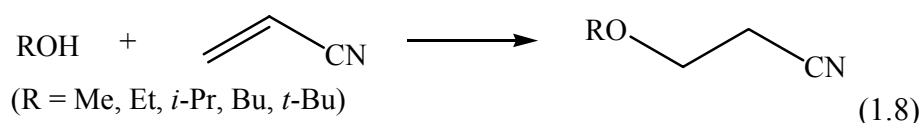
Mg–Al mixed oxides prepared by calcination of hydrotalcite catalyzed the nitroaldol condensation to nitroalcohols with diastereoselective. For example, when 3-nitrobenzaldehyde and nitroethane was refluxed in THF, 1-(3-nitrophenyl)-2-nitropropan-1-ol was obtained in a 95% yield with a threo/erythro ratio of 12.5 [135].

Conjugate addition of alcohols

Conjugate addition of alcohols to α,β -unsaturated carbonyl compound forms a new carbon–oxygen bond to yield valuable ethers. The reactions are catalyzed by homogeneous base catalysts such as alkali hydroxides and alkoxides. Conjugate addition of methanol to 3-buten-2-one proceeds to form 4-methoxybutan-2-one over the solid bases such as alkaline earth oxides, strontium hydroxide, barium hydroxide, and $\text{KF}/\text{Al}_2\text{O}_3$, $\text{KOH}/\text{Al}_2\text{O}_3$ at a reaction temperature of 273 K [136]. MgO treated at 673 K gave the highest activity. The catalytic activities of MgO , CaO , and $\text{KF}/\text{Al}_2\text{O}_3$ were not affected by exposure of the catalysts to carbon dioxide or air.

Among conjugate additions, cyanoethylation of alcohols is a widely used reaction for the synthesis of drug intermediates and organic compounds of industrial interest. Again, high activities for this reaction were reported for high temperature activated MgO catalyst (1073 K in vacuum) [137].

Cyanoethylation of alcohols such as methanol, ethanol, and 2-propanol with acrylonitrile [Eq.(1.8)] proceeds at 273 K over alkaline earth oxides and hydroxides, $\text{KF}/\text{Al}_2\text{O}_3$ and $\text{KOH}/\text{Al}_2\text{O}_3$. The reaction was not poisoned by adsorption of carbon dioxide at room temperature [138].



Hydrotalcite by rehydration after calcination was found to be also a highly active catalyst for cyanoethylation of alcohols, such as methanol, ethanol, and 2-propanol, with acrylonitrile at 50 °C. The catalyst was reusable without appreciable loss in activity and was air stable [139].

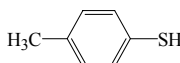
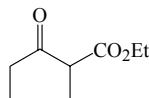
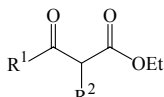
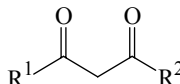
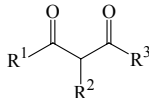
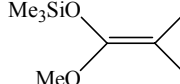
Michael addition

Michael addition is widely used as C–C bond coupling reaction in the production of pharmaceuticals and fine chemicals. The reaction is also conventionally catalyzed with

soluble bases, such as KOH or amines. Normally, it involves nucleophilic addition of a carbanion, formed by abstraction of a proton from a C–H bond of the organic donor molecule by a base, to α,β -unsaturated carbonyl compounds. Environmental and economical concerns are driving forces in the replacement of soluble bases by suitable solid catalysts. The latter are easy to separate, recover, and thus, reuse. So far, several solid base catalyst systems, such as $\text{Ba}(\text{OH})_2$, MgO , $\text{KF}/\text{Al}_2\text{O}_3$, $\text{Na}/\text{NaOH}/\text{Al}_2\text{O}_3$, and modified Mg-Al hydrotalcite have been used in Michael additions. The efficient catalyst varies with the type of the reactants. Moreover, some transition metal complexes as heterogeneous Lewis acid catalysts instead of conventional strong bases, like montmorillonite-enwrapped scandium, nickel (II) and cobalt (II) complexes were also applied in Michael additions. Some Michael additions of different donors to methyl vinyl ketone (MVK) catalyzed by solid catalysts in liquid phases are listed in Table 1.5.

Table 1.5

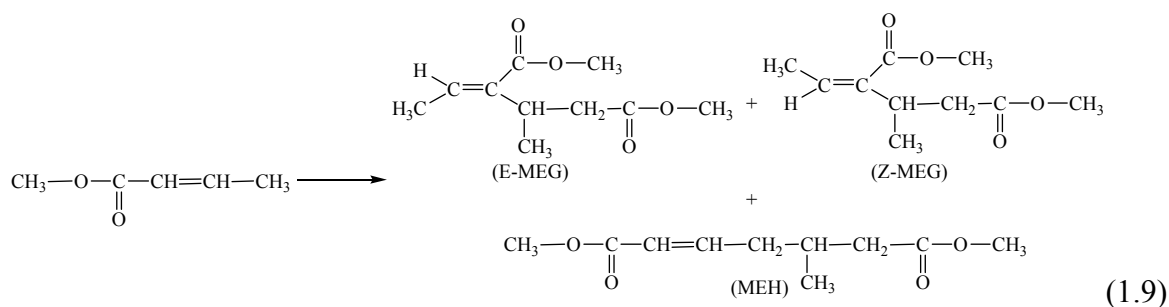
Michael additions of different donors to methyl vinyl ketone (MVK) catalyzed by solid catalysts in liquid phase.

Michael donor	Catalyst	Main supposed active sites	Reference
CH_3NO_2	KF/alumina, KOH/alumina, MgO	Lewis base or Brønsted base	[97,140]
	Modified Mg-Al hydrotalcite	Brønsted base	[141]
	Tetraalkylammonium hydroxide and chiral amines on MCM-41	Brønsted base	[142,143]
	Organosilicon compounds	Lewis acid and Brønsted base	[144]
	Nickel (II) and cobalt (II) complexes	Lewis acid	[145]
	Montmorillonite-enwrapped scandium	Lewis acid	[146]
	TS-1, Ti- β molecular sieve	Lewis acid	[147]

From Table 1.5, interestingly, not only solid base catalysts but also solid acid catalysts can catalyze the Michael additions of different donors to methyl vinyl ketone (MVK) catalyzed in liquid phase.

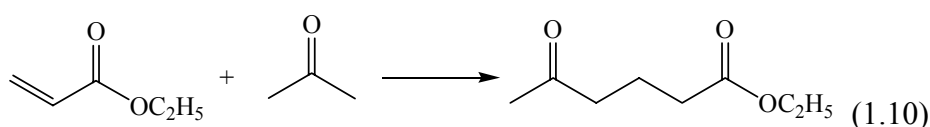
Partially dehydrogenated Ba(OH)₂ catalyzes Michael additions of chalcones with active methylene compounds such as ethyl malonate, ethyl acetoacetate, acetylacetone, nitromethane, and acetophenone [148].

Potassium fluoride supported on alumina (KF/Al₂O₃) is active for the following Michael additions at room temperature: nitromethane [149], nitroethane, 1,3-diphenyl-2-propen-1-one [150], and dimenone with 3-buten-2-one (methyl vinyl ketone) [151].



For a self-Michael addition of methyl crotonate [Eq.(1.9)], MgO exhibits a higher activity than the other basic catalysts such as CaO, SrO, BaO, KF/alumina, KX zeolite [152]. For Michael addition of nitromethane to α,β -unsaturated carbonyl compounds, KF/alumina and KOH/alumina exhibit high activities, while MgO and CaO exhibit low activities [140]. The factors to be considered for an efficient catalyst are basic strength of the site, acidity of reactant, and charge on the carbon atom at β -position to carbonyl group.

Mesoporous silica having *N,N*-dimethyl-3-aminopropyl groups prepared by a templated sol-gel method are shown to be a good catalyst for Michael addition reactions of nitroalkanes to 3-buten-2-one and 2-cyclohexen-1-one. No leaching of the catalytic component was observed [153].



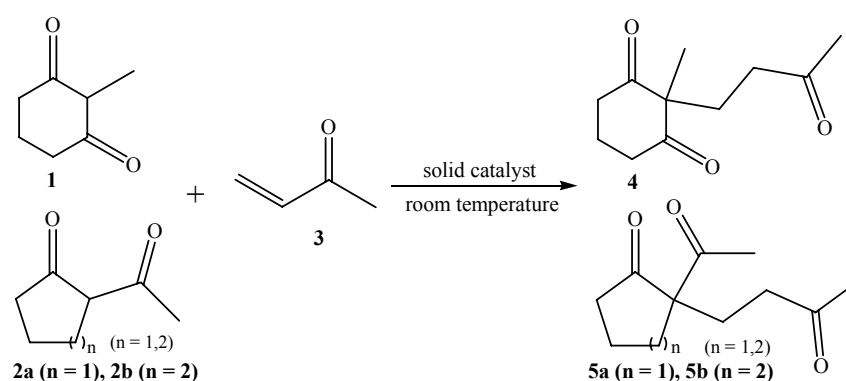
Na/NaOH/Al₂O₃ and Zeolite X containing metallic sodium clusters or cesium oxide were applied in Michael addition of ethyl acrylate and acetone forming 5-oxohexanoic acid ethyl ester [Eq.(1.10)]. After 24 h at 90 °C, about 50–80% conversions with 60–70% selectivities were achieved and the catalysts were reusable [154].

Recently, Choudary et al. found that a rehydrated Mg-Al hydrotalcite with an expected Mg/Al ratio of 2.5, which was obtained by calcination hydrotalcite at 450 °C and then

rehydrating at room temperature under a flow of dry nitrogen gas saturated with water vapor, was an efficient and very selective catalyst for Michael additions. For most of the reactions they investigated, more than 88% yield of 1,4-addition products were produced in 2 hours. Moreover, the authors observed that the as synthesized or just calcined hydrotalcite showed no activity for the reactions and ascribed the excellent catalytic behavior of the rehydrated hydrotalcite to Brønsted base sites [141].

1.4 Main reactions investigated in this thesis: Michael additions

The main Michael addition reactions investigated in this thesis are shown in Scheme 1.1. Table 1.6 summarizes the results of the Michael additions using a variety of catalysts in the literature for these reactions.



Scheme 1.1 Michael additions of 2-methylcyclohexane-1,3-dione (**1**), 2-acetylcyclopentanone (**2a**), and 2-acetylcyclohexanone (**2b**) to methyl vinyl ketone (**3**) to obtain Michael adducts: 2-methyl-2-(3-oxo-butyl)-cyclohexane-1,3-dione (**4**), 2-acetyl-2-(3-oxo-butyl)-cyclopentanone (**5a**), and 2-acetyl-2-(3-oxo-butyl)-cyclohexanone (**5b**).

As shown in Table 1.6, in most cases, homogeneous catalysts such as KOH and amines or metal complexes were used in these reactions. In the Michael additions of 2-methylcyclohexane-1,3-dione to methyl vinyl ketone, at room temperature, using triethylamine as catalyst and methanol as solvent, only 42% yield of product was obtained. However, increasing the reaction temperature and using hydroquinone as catalyst, about 100% yield of product was obtained. It is worth noting using acetic acid could also perform the reaction.

Table 1.6

Catalysts in the literatures used for the Michael additions

Catalyst	Solvent	Reaction conditions	Yield	Ref.
Reaction 1: Michael addition of 2-methylcyclohexane-1,3-dione to methyl vinyl ketone				
Triethylamine	Methanol	RT	42%	[155]
Et ₃ N	Acetonitrile	20 °C, 24 h, 750.06 Torr	67%	[156]
KOH	Methanol	Heating, 4 h	-	[157]
Hydroquinone	H ₂ O	70–80 °C, 4 h	~100%	[158]
Acetic acid	H ₂ O	75 °C, 1 h	-	[159]
Reaction 2: Michael addition of 2-acetylcyclopentanone to methyl vinyl ketone				
Montmorillonite-enwrapped scandium	H ₂ O	50 °C, 1 h	97%	[146]
	-	50 °C, 1 h	99%	[146]
Ni(OAc) ₂ ·4H ₂ O with ligand	CHCl ₃	23 °C, 16 h	41% ^a	[160]
Reaction 3: Michael addition of 2-acetylcyclohexanone to methyl vinyl ketone				
FeCl ₃	CH ₂ Cl ₂	25 °C, 18 h	79% ^a	[160]
Ni(OAc) ₂ ·4H ₂ O with ligand	CHCl ₃	23 °C, 16 h	57% ^a	[160]
P-BEMP ^b	THF	RT, 23 h	98%	[161]

a: with stereoselective

b: *N*-phenyl-tris(dimethylamino)iminophosphorane immobilized on polystyrene resin

Although some catalysts including normal liquid base and metal complexes have been used in these Michael additions, few solid base catalysts have been involved in the reactions investigated in this thesis. Solid base catalysts are non-stoichiometric, non-corrosive, reusable and environmentally benign. Therefore, solid base catalysts are good alternative for Michael additions.

1.5 Scope and outline of this thesis

The aim of this thesis is to study preparation, characterization and application of oxides and modified oxide as solid base catalysts and find efficient catalysts for the liquid-phase Michael additions, meanwhile, to understand how catalytic performances are influenced by acid-base properties of the catalysts. The catalysts include MgO, potassium-modified ZrO₂, calcined Mg-Al hydrotalcites, and a novel catalyst system Mg(O,F), which was prepared by sol-gel method for the first time.

In **Chapter 2**, general experiment and characterization methods are described. In **Chapter 3**, MgO catalysts – a common solid base, prepared by different ways are first involved in the Michael addition. In **Chapter 4**, potassium-modified ZrO_2 are studied in both gas phase and liquid phase reactions. The leaching test of potassium-modified ZrO_2 in the liquid phase reaction has also been performed. **Chapter 5** concentrates on the calcined Mg-Al hydrotalcites. The Michael additions of 1,3-diones with different $\text{p}K_{\text{a}}$ values to methyl vinyl ketone are examined on calcined commercial Mg-Al hydrotalcites including an Al-rich ($\text{Mg}/\text{Al} = 0.6$) sample. Acid-base properties of the catalysts are investigated by FTIR spectroscopy and microcalorimetry. In **Chapter 6**, based on the results of former chapters, a novel catalyst system oxide/hydroxidefluoride $\text{Mg}(\text{O},\text{F})$ is prepared by sol-gel method for the first time and used in the Michael addition. In the final chapter, **Chapter 7**, results from the previous chapters are briefly summarized.

Chapter 2

Experimental Section

2.1 Chemicals

Inorganic chemicals

AlO(OH) (Pural SB)	SASOL Germany GmbH
Magnesium (Mg)	Aldrich, small turnings, 99.98%
Magnesium carbonate (MgCO_3)	Fluka, 99%
Magnesium hydroxide [Mg(OH)_2]	Fluka, 99%
Magnesium fluoride (MgF_2)	Aldrich, 98%
Magnesium nitrate hexahydrate [$\text{Mg(NO}_3)_2 \cdot 6\text{H}_2\text{O}$]	Fluka, 99%
Potassium acetate ($\text{KC}_2\text{H}_3\text{O}_2$)	Merck, 99%
Potassium bromide (KBr)	Fluka, 99%
Potassium carbonate (K_2CO_3)	Fluka, 99%
Potassium hydrocarbonate (KHCO_3)	Merck, 99%
Potassium hydroxide (KOH, pellets)	Merck, 85%
Potassium nitrate (KNO_3)	Fluka, 99%
Carbon dioxide (CO_2)	Messer Griesheim, 99.995 vol.-%
Hydrofluoric acid (HF)	Merck, 40%
Hydrofluoric acid (HF, gas)	Solvay Fluor, Germany
Hydrotalcite (Pural MG30, 50, 61, 70)	SASOL Germany GmbH
Zirconyl chloride octahydrate ($\text{ZrOCl}_2 \cdot 8\text{H}_2\text{O}$)	Fluka, 99%

Organic chemicals

1-Butene	Aldrich, 99%
Methyl vinyl ketone	Aldrich, 99%
2-Methylcyclohexane-1,3-dione	Acros, 98%
2-Acetylcyclopentanone	Aldrich, 98%
2-Acetylcyclohexanone	Acros, 99%
Dimethyl phthalate	Acros, 99%
Methanol	Aldrich, 99%
2-methoxycarbonylcyclopentanone	Acros, 99%
Pyridine	Merck, 99%
DMSO- d_6	Chemotrade, 99.5%
CDCl_3	Chemotrade, 99.5%

2.2 Catalyst preparation

Wet impregnation, thermal decomposition and sol-gel methods are used in the preparation of the catalysts. The details are shown in the following chapters.

2.3 Characterization

Element analysis

C, N, H contents were determined by elemental analysis (Leco CHNS-932 element analyzer). K, Zr, Mg, Al contents were determined by ICP-OES (UNICAM 701). F contents were determined according to Seel by the method described in [162]. 10–20 mg of sample was dissolved by melting in a mixture of $\text{K}_2\text{CO}_3/\text{Na}_2\text{CO}_3$ in a platinum crucible. The mixture was cooled down to room temperature and dissolved in distilled water. About 1 g of silica and 20 mL of 98% H_2SO_4 were slowly added to the solution. This solution was then distilled under a water vapor flow in order to support the formation of H_2SiF_6 and its evaporation. After the condensation of H_2SiF_6 , the fluoride content in the aqueous solution was determined with an F^- sensitive electrode.

X-ray diffraction (XRD)

X-ray powder diffraction (XRD) analysis was performed with Cu $\text{K}\alpha$ radiation ($\lambda = 1.5418 \text{ \AA}$, 40 kV, and 35 mA) using RD 7 (Rich. Seifert GmbH & Co. KG, Freiberg, Germany) over the 2θ range from 5 to 65° or 90° .

N_2 adsorption/desorption experiments

Nitrogen adsorption/desorption experiments were carried out at 77 K using a Micromeritics ASAP 2010 system; samples were degassed at 200°C (or 100°C) overnight. The specific surface area was calculated using the BET method. Pore volumes and pore distributions were calculated using the BJH method.

CO_2 -TPD

CO_2 -TPD was used to measure the strength of basic sites. The pelleted sample (approximately 300 mg, 0.3–0.5 mm diameter fraction) was pretreated in a nickel reactor under Ar (70 mL/min) at 600°C for 1 h. The sample was then cooled to 50°C and exposed to a stream of Ar and CO_2 . The sample was flushed for over 1 h at 50°C to remove

physisorbed CO₂, after which, the TPD program (10 °C/min, up to 600 °C, held for 30 min) was started. The desorption of gas phase CO₂ was detected by monitoring the band at 2349 cm⁻¹ with FTIR spectroscopy (FTIR system 2000, Perkin-Elmer).

¹H NMR

¹H NMR experiments were performed on a Bruker AVANCE 400 spectrometer.

²⁷Al MAS NMR

²⁷Al MAS NMR experiments were performed by accumulating 64 spectra on a Bruker AVANCE 400 spectrometer at a resonance frequency of 104.3 MHz with excitation of $\pi/6$ pulses and a repetition time of 5 s. A commercial Bruker 4-mm probe was used to perform the MAS experiments with a spinning rate of 10 kHz. An aqueous 1 M solution of aluminum chloride was used as reference for the chemical shifts.

¹⁹F MAS NMR

Solid state NMR experiments were done on a Bruker AVANCE 400 spectrometer using a 2.5 mm double-bearing magic angle spinning (MAS) probe with a decoupling channel optimized for ¹⁹F observation. The samples were characterized at room temperature by measurements of ¹⁹F ($I = 1/2$, 282.4 MHz) nucleus at an ultrafast spinning speed of 30 kHz to reduce most of the ¹⁹F dipolar interactions and obtain high-resolution spectra. A recycle delay of 10 s and 64 scans were used. ¹⁹F chemical shifts were referenced to CFCl₃ at 0 ppm and accurate to ± 1 ppm.

Thermal analysis

Thermogravimetry (TG) and differential thermal analysis measurements (DTA) were performed using a NETZSCH STA409C system equipped with a skimmer-coupled mass spectrometer in air with a heating rate of 10 °C/min from room temperature up to 700 °C (reference: Al₂O₃).

FTIR measurements

FTIR spectra of KBr pellets were recorded on a Perkin-Elmer 2000 spectrometer in transmission mode. About 500 mg of KBr were pressed with 1.5–2.0 mg of the sample, and then the samples were measured in the regions 400–4000 cm⁻¹.

FTIR studies were also carried out on self-supporting wafers (10–40 mg) in a transmission IR quartz cell with CaF₂ window. Pyridine (Merck, 99%) was freshly distilled and stored over zeolite A. The samples were pretreated in flowing synthetic air for 1 h and evacuated for 30 min both at 550 °C. The adsorption of pyridine was then performed at 40 °C with 0–15 mbar pyridine with subsequent evacuation for 10 min to remove physisorbed pyridine. The IR spectra were measured every 50 °C during temperature programmed desorption (TPD) from 100 to 300 °C (heating rate of 10 °C/min) after evacuation for 10 min at each temperature. In the case of CO₂ adsorption (Messer Griesheim, 99.995 vol.-%), the samples were pretreated under vacuum at 400 °C for 1 h. The measurement conditions were identical to those used after pyridine adsorption except for the evacuation time during TPD of 10 min, which was lengthened to 30 min. IR spectra (64 accumulations, resolution of 2 cm⁻¹) were recorded on a Digilab FTS-60A spectrometer. The spectra were normalized with the wafer weight; the spectrum measured prior to adsorption was used as the background spectrum.

Microcalorimetric measurements

Microcalorimetric measurements were carried out in Prof. Auroux's group (Institut de Recherches sur la Catalyse, France).

Gas-phase CO₂ adsorption

Microcalorimetric data were collected using a heat flow Tian-Calvet-type calorimeter (C 80, Setaram) connected to a volumetric line with an online injection system for pulsing reactive gases. CO₂ (> 99.9%) was pulsed from a storage vessel. After each pulse, the equilibrium pressure was measured with a differential pressure gauge (Barocel, Datametries). The calorimetric and volumetric data (pressure, adsorbed volume, heats of adsorption, differential and integral enthalpies) were stored and analyzed by a microcomputer. The sample (70–100 mg) was pretreated under vacuum overnight at 400 °C. The first adsorption cycle was complete after a final equilibrium pressure of 0.6 Torr was reached at 40 °C; the system was then evacuated to remove the physisorbed CO₂, and a second adsorption cycle was performed. For all the samples measured here, the level of irreversible adsorption was almost constant above 0.2 Torr. Thus, the amounts of totally adsorbed (chemisorbed and physisorbed) and irreversibly (chemisorbed) CO₂ were determined from the difference between the isotherms of the first and second cycle of adsorption, respectively.

Liquid-phase adsorption: benzoic acid in toluene

Liquid-phase experiments were performed on a Titrys calorimeter (Setaram) with a stirring system. The samples (about 200 mg) were pretreated under vacuum overnight at 400 °C and then transferred to the calorimetric cell, which contained toluene (1.5 mL). The reference cell contained the same amount of toluene before injection. At 70 °C, the solution of benzoic acid in toluene (0.0307 mol/L) was injected stepwise (0.2 mL, injection rate: 0.05 mL/min) every 2 h. The amount of unreacted benzoic acid was measured by UV spectrofluorimetry.

X-ray photoelectron spectroscopy (XPS)

In chapter 5, X-ray photoelectron spectroscopy (XPS) was performed on VG ESCALAB 220 iXL spectrometer with a Mg $K\alpha$ source and a monochromated Al $K\alpha$ source, respectively [measurements were carried out in Institut für Angewandte Chemie Berlin-Adlershof e.V. (ACA)]. In chapter 6, Narrow scan X-ray photoelectron spectra (XPS) were acquired using Kratos Axisultra electron spectrometer with monochromatised Al $K\alpha$ excitation ($h\nu = 1486.6$ eV) operated at 75 W and in CAE 20mode [measurements were carried out in Bundesanstalt fuer Materialforschung und -prüfung (BAM), Berlin]. Before recording the spectra the samples were stored overnight in the Extended PrepLock chamber in a vacuum better than 10^{-6} mbar in order to degas. The vacuum in the spectrometer was better than 10^{-8} mbar. Binding energy data were referenced to the aliphatic C 1s peak at 284.8 eV. Charge neutralization system was used. The spectrometer energy scale was calibrated following ISO 15427.

Transmission electron microscopy (TEM)

Transmission electron microscopy (TEM) was performed on Hitachi H-8110 (200 kV, LaB6 gun) with energy dispersive X-ray detector.

2.4 Reaction**Gas-phase reaction: Double-bond isomerization of 1-butene**

The isomerization of 1-butene was performed in a down-flow, fixed-bed glass reactor. Equal volumes of the pelleted, calcined catalyst (about 300–450 mg, 0.3–0.5 mm diameter fraction) were exposed to the feed stream mixture of nitrogen (10 mL/min) and 1-butene (0.6 mL/min) at 150 °C. Prior to the reaction, the catalyst was pretreated in N₂ at 600 °C

for 2 h. On-line gas chromatography (Shimadzu GC-17A, FID, quartz capillary: PONA (methylsiloxane), 50 m, 0.2 mm \times 0.5 μ m) was used to determine the composition of the reaction mixture of 1-butene and *cis/trans*-2-butene after a time-on-stream (TOS) of 10, 30, 60 and 90 min. Due to 100% product selectivity, the reaction conversion is given by the yield of 2-butene product. Product yields were normalized by the mass of the catalyst used at 30 min in order to compare the catalysts' results with each other.

Liquid-phase Michael additions

Generally, the reaction was carried out in a 50-mL round-bottom flask at room temperature. Methyl vinyl ketone (22.5 mmol, Aldrich, 99%), a CH-acid compound (15.0 mmol) [2-methylcyclohexane-1,3-dione (Acros, 98%, slightly soluble in methanol), 2-acetylcyclopentanone (Aldrich, 98%) or 2-acetylcyclohexanone (Aldrich, 97%)], dimethyl phthalate (3.75 mmol, Acros, 99%, internal NMR standard), and the solvent, methanol (10 mL, Aldrich, 99%), were stirred together for 30 min to saturate the mixture before the powdered catalyst was added. In general, a catalyst weight of 0.225 g was used. The reaction mixture (0.1 to 0.3 mL) was sampled at certain times and centrifuged. The separated solution was then concentrated on a rotary evaporator to remove solvent and unreacted methyl vinyl ketone. The yield of the target product was analyzed by ^1H NMR spectroscopy (solvent: DMSO- d_6 or CDCl_3) using the integrals of the CH_3 signals of the Michael adducts: 2-methyl-2-(3-oxo-butyl)-cyclohexane-1,3-dione (1.11 and 2.04 ppm, DMSO- d_6), 2-acetyl-2-(3-oxo-butyl)-cyclopentanone (2.14 and 2.09 ppm, CDCl_3), 2-acetyl-2-(3-oxo-butyl)-cyclohexanone (2.08 ppm, CDCl_3 , only one CH_3 -signal used because the other overlapped with that of 1,3-dione reagent), 2-oxo-1-(3-oxo-butyl)-cyclopentanecarboxylic acid methyl ester (2.11 and 3.68 ppm) and dimethyl phthalate (3.83 ppm in DMSO- d_6 and 3.88 ppm in CDCl_3).

Chapter 3

MgO as solid base catalysts in Michael addition

3.1 Introduction

Alkaline earth oxides are generally used as solid base catalysts. Among them, MgO is the most widely used. MgO has been extensively studied as a promising catalyst [13,163,164,165], modifier or promoter [166,167,168] and catalyst support [169,170,171] in heterogeneous catalysis. MgO exhibits high activities in numerous base-catalyzed organic reactions, such as self-Michael addition to form methyl diesters [163], the Tishchenko reactions [164], the Meerwein-Ponndorf-Verley reactions [165], dimerisation of ethanol to butanol [172], and self-condensation of propanol [173].

The basicity of MgO has been studied by FTIR, CO₂-TPD. Normally, MgO acts as strong base catalyst. Coluccia and Tench [174] proposed a surface model for MgO (Fig. 3.1). There are several types of Mg–O ion pairs with different coordination numbers. Ion pairs of low coordination numbers exist at corners, edges, or high Miller index surfaces of the (100) plane [175]. Different basic sites generated by increasing the pre-treatment temperature appear to correspond to the ion pairs of different coordination numbers. However, the correspondence between the catalytically active sites for different reaction types and the coordination number of the ion pairs is not definite yet [13].

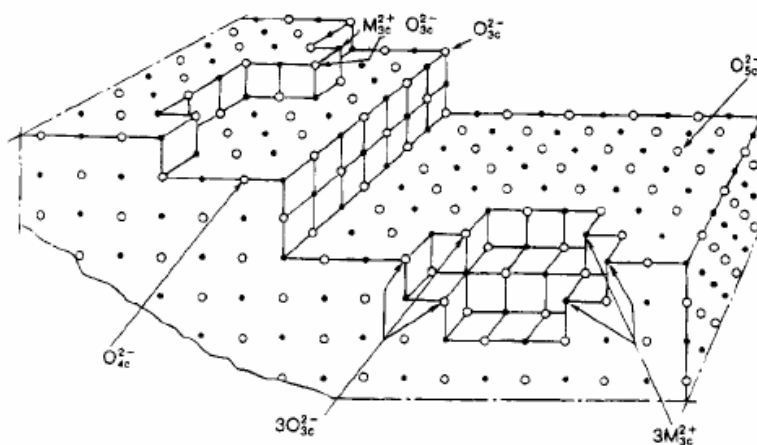


Fig. 3.1 Ions in low coordination on the surface of MgO [174]

MgO can be prepared by simple thermal decomposition of magnesium compounds such as Mg(OH)₂, MgCO₃, Mg(NO₃)₂ under controlled conditions. However, the pretreatment time, calcination temperature, gas environment can influence the properties of the resulting MgO catalysts, and therefore decide the catalytic behaviour. Choudhary et al. studied the influence of precursors used in preparation of MgO and its surface properties and catalytic

activity in oxidative coupling of methane and found MgO obtained from magnesium carbonate and magnesium acetate were comparable and were much better than MgO obtained from the other precursors [176]. However, Aramendia et al. found in Meerwein-Ponndorf-Verley reaction of cyclohexanone with isopropyl alcohol, the most active catalyst was the solid prepared by rehydration and subsequent calcination of a magnesium oxide that was previously obtained from commercially available magnesium hydroxide [165]. Nanoscale and high surface area MgO can also be prepared from $\text{Mg}(\text{OCH}_3)_2$ by use of autoclave hypercritical drying (aerogel) procedure [177]. Meanwhile, aerogel prepared MgO showed higher reactivity than commercial and conventionally prepared MgO in Wadsworth–Emmons reactions [178]. However, the same MgO was poorer catalyst in toluene benzylation by benzyl chloride [179]. Therefore, for different reactions, various MgO catalysts may have quite different catalytic behaviors.

MgO has been proved as a good catalyst in a self-Michael addition of methyl crotonate [152], but not in the Michael additions of nitromethane to α,β -unsaturated carbonyl compounds [140]. The factors to be considered MgO as an efficient catalyst for Michael addition depend on the strength of the basic sites, the acidity of reactant, and the charge on the carbon atom at β -position to carbonyl group. Because of the importance of MgO as a solid base catalyst, in this chapter, various MgO prepared from different precursors were first tested in the liquid-phase Michael addition of 2-methylcyclohexane-1,3-dione to methyl vinyl ketone to get the preliminary result.

3.2 Preparation and characterization of MgO prepared by different methods

Table 3.1 shows the preparation and characteristics of the MgO catalysts prepared from different precursors. In most cases, simple thermal decomposition of various precursors at different temperatures was used to prepare MgO. All the calcination time is 4 h. As shown in Table 3.1, MgO-1 was prepared by calcination of $\text{Mg}(\text{NO}_3)_2 \cdot 6\text{H}_2\text{O}$ at 600 °C in air, and very low surface area, 1.8 m^2/g , was obtained. MgO-2 and MgO-3 were obtained by thermal decomposition of MgCO_3 at 600 and 500 °C in air, respectively. MgO-3 had a higher surface area (106.6 m^2/g) than MgO-2 (76.6 m^2/g) because a lower calcination temperature was used. MgO-4 was obtained by calcination at 600 °C of dried $\text{Mg}(\text{OH})_2$, which was prepared by precipitation of MgCl_2 using KOH and dried at 110 °C. MgO-4 had a surface area of 76.7 m^2/g . MgO-5 to MgO-7 were prepared by calcination of dried

$\text{Mg}(\text{OH})_2$ (the hydroxide was precipitated from $\text{Mg}(\text{NO}_3)_2$ solution with KOH and dried at 110 °C) at 600, 500, 400 °C, respectively. The surface area of these three MgO increased with decreasing calcination temperature. This is due to an increase in the crystal size caused by sintering of MgO at the higher temperatures.

Table 3.1

Preparation and characteristics of MgO catalysts

Sample	Precursor	Preparation	S_{BET} (m^2/g)	V_p^a (cm^3/g)	d_p^b (Å)
MgO-1	$\text{Mg}(\text{NO}_3)_2$	calcination at 600 °C in air	1.8	0.017	381
MgO-2	MgCO_3	calcination at 600 °C in air	76.6	0.337	175
MgO-3	MgCO_3	calcination at 500 °C in air	106.4	0.321	120
MgO-4	MgCl_2	precipitation ^c and calcination at 600 °C in air	76.7	0.971	508
MgO-5	$\text{Mg}(\text{NO}_3)_2$	precipitation ^c and calcination at 600 °C in air	75.0	0.960	258
MgO-6	$\text{Mg}(\text{NO}_3)_2$	precipitation ^c and calcination at 500 °C in air	116.5	1.095	375
MgO-7	$\text{Mg}(\text{NO}_3)_2$	precipitation ^c and calcination at 400 °C in air	170.2	1.074	252
$\text{Mg}(\text{OH})_2$	$\text{Mg}(\text{NO}_3)_2$	precipitation and dried at 110 °C in air	-	-	-

a: BJH desorption cumulative pore volume of pores between 17.0 and 3000.0 Å diameter

b: Average pore diameter by BET

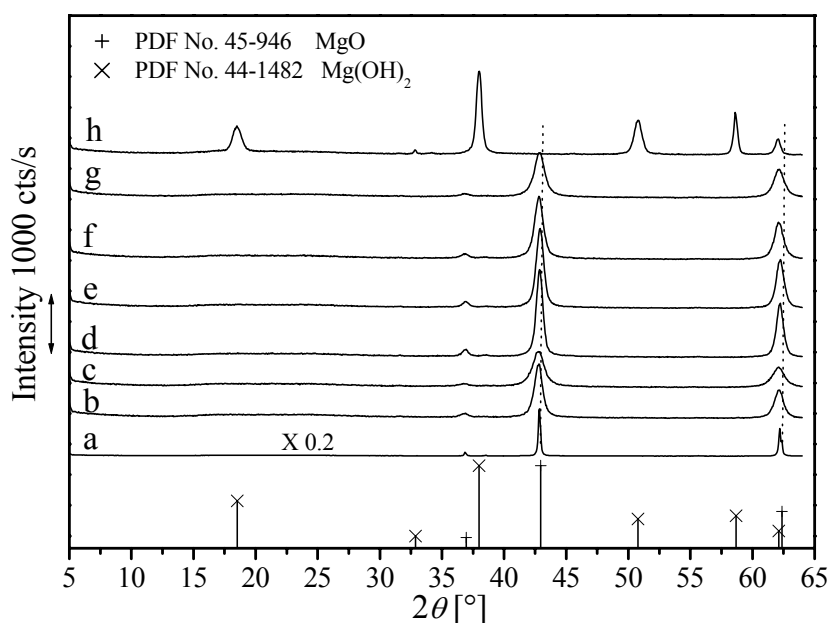
c: $\text{Mg}(\text{OH})_2$ was dried at 110 °C in air before calcination

Fig. 3.2 XRD patterns of MgO. MgO-1 (a), MgO-2 (b), MgO-3 (c), MgO-4 (d), MgO-5 (e), MgO-6 (f), MgO-7 (g), $\text{Mg}(\text{OH})_2$ (h)

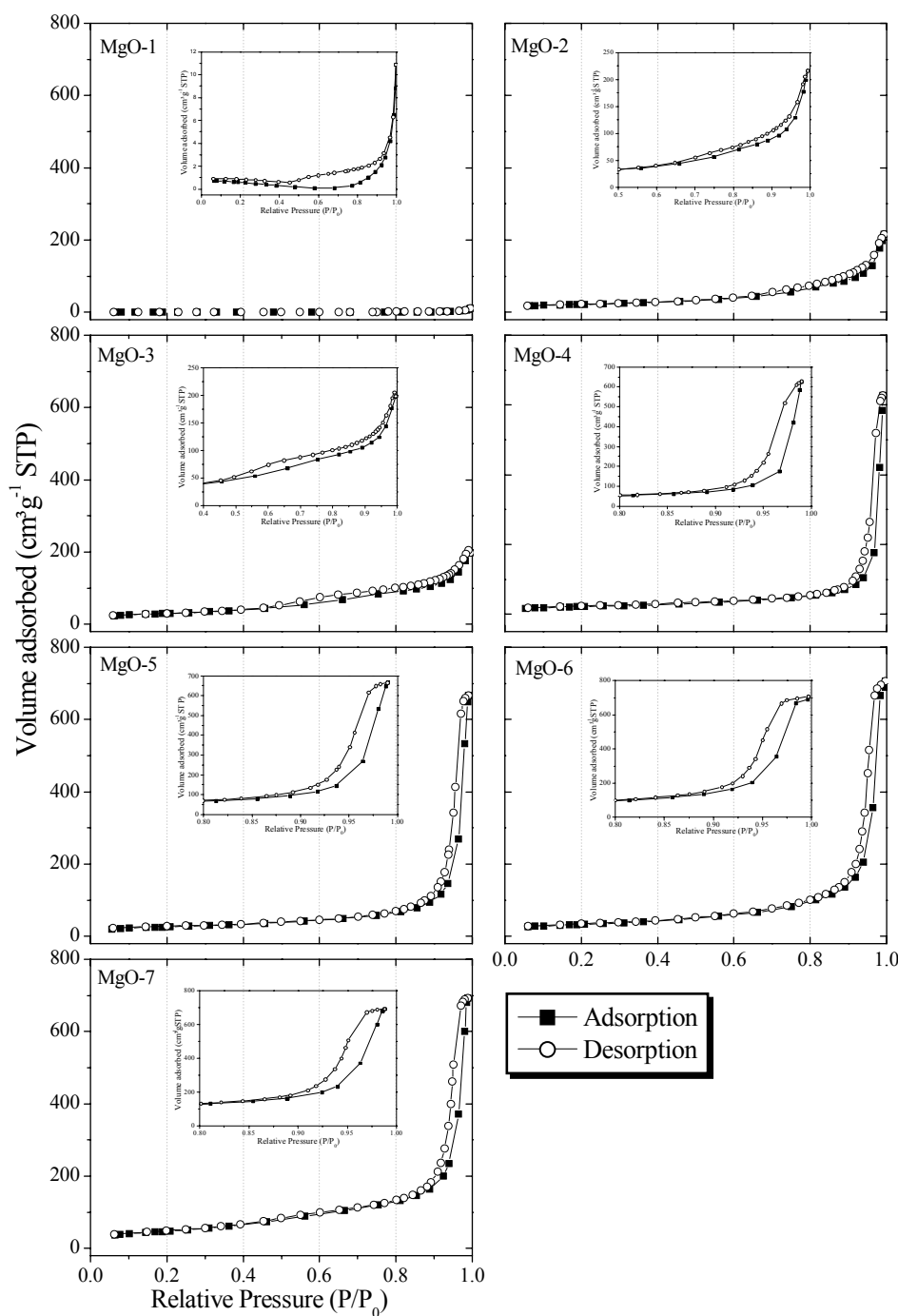


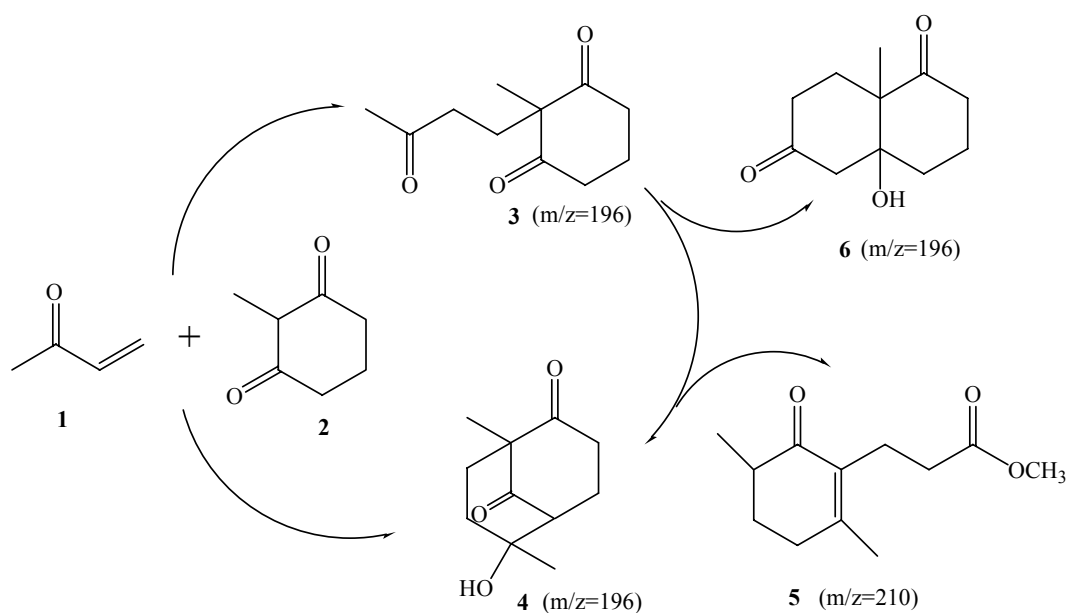
Fig. 3.3 N₂ adsorption/desorption isotherms of MgO catalysts

XRD patterns of MgO catalysts are shown in Fig. 3.2. All the MgO catalysts are pure phases of periclase MgO (PDF No.45-946) that exhibits the three characteristic peaks at 2θ values of 37.0 (1 1 1), 43.0 (2 0 0) and 62.4 (2 2 0) degrees. The hydroxide (Fig. 3.1h) precipitated from $\text{Mg}(\text{NO}_3)_2$ exhibited a brucite-like $\text{Mg}(\text{OH})_2$ structure (PDF No.44-1482). If the strongest peak at around 43.0 degree for periclase is used as a reference for crystallinity, then MgO-1 with the smallest surface area is the most crystalline sample.

MgO-3 is the least crystalline. From MgO-5 to MgO-7, with the decrease of the calcination temperature, the crystallinity decreases.

The N₂ adsorption/desorption isotherms of MgO catalysts are shown in Fig. 3.3. Except of the MgO calcined from the precursor of Mg(NO₃)₂·6H₂O, all other MgO exhibited similar isotherms (type IV). According to IUPAC classification, they are typical of mesoporous materials [180]. The shape of isotherms and the hysteresis loop can give the information about the pore structure. The desorption isotherms of MgO-2 and MgO-3 followed different paths than the adsorption isotherm down to a P/P_0 value of 0.5 and 0.4, respectively. The hysteresis loop of MgO-3–MgO-7 closed at P/P_0 values of ca.0.8. These results indicated that MgO-2 and MgO-3 had smaller mesoporous than MgO-3–MgO-7. Based on the shape of hysteresis loops, all MgO have ‘ink-bottle’ pores, spheroidal cavities or voids between close-packed spherical-like particles.

3.3 Catalytic behavior of MgO catalysts



Scheme 3.1 Possible reaction procedure in the reaction of 2-methylcyclohexane-1,3-dione (1) with methyl vinyl ketone (2) using MgO as catalyst

When MgO was used as catalyst in Michael addition of 2-methylcyclohexane-1,3-dione to methyl vinyl ketone, in the ¹H NMR spectra of the reaction products, besides the signals of expected Michael adduct 2-(3-oxobutyl)-2-methylcyclohexane-1,3-dione (single peaks at 1.11 and 2.04 ppm, DMSO-*d*₆), additional main CH₃ signals at 0.97 and 1.23 ppm, were

found. Based on the results of NMR and GC-MS, another main product 6-hydroxy-1,6-dimethyl-2,9-dioxobicyclo[3.3.1]nonane was confirmed, which was formed by the aldol cyclization of Michael adduct 2-methyl-2-(3-oxo-butyl)-cyclohexane-1,3-dione. In case of MgO as catalyst, the possible reaction procedure is shown in Scheme 3.1. Besides the expected Michael addition, a consecutive aldol cyclization took place to give a bridged ketol (product 4, in Scheme 3.1). Negligible amount of product 5 and 6 were also detected by GC-MS.

Table 3.2

The results of the Michael addition using different MgO as catalysts

Catalyst	Yield of Michael adduct and (bridged ketol) %						
	0.5 h	1 h	2 h	4 h	6 h	8 h	24 h
MgO-1	-	-	6 (0)	21 (0)	43 (4)	67 (9)	57 (32)
MgO-2	-	61 (30)	56 (32)	48 (39)	26 (55)	21 (56)	18 (51)
MgO-3	65 (14)	64 (28)	55 (33)	30 (53)	24 (59)	18 (55)	13 (45)
MgO-4	51 (18)	59 (31)	52 (34)	34 (47)	14 (62)	14 (60)	4 (43)
MgO-5	43 (28)	65 (26)	59 (28)	42 (40)	17 (60)	15 (54)	6 (47)
MgO-6	70 (22)	66 (26)	59 (30)	39 (47)	27 (54)	19 (57)	10 (42)
MgO-7	68 (17)	65 (24)	58 (30)	43 (30)	30 (49)	21 (54)	13 (42)
Mg(OH) ₂	-	23 (0)	51 (0)	75 (18)	60 (32)	52 (38)	42 (43)

Table 3.2 shows the reaction results of the different MgO catalysts. For the catalyst MgO-1, prepared by the decomposition of $\text{Mg}(\text{NO}_3)_2$, at the beginning of the reaction (before the reaction time 4 h), no bridged ketol was formed, only 21% yield of Michael adduct was obtained in 4 h. At 8 h, the yield of bridged ketol was 9% and the yield of Michael adduct arrived maximum 67%. Compared with the other MgO catalysts, MgO-1 showed quite different behavior probably due to its unusual low surface area. For other MgO catalysts (MgO-2 to MgO-7), both Michael adduct and bridged ketol appeared at the beginning of the reaction (in 0.5–1 h). Within the reaction time of 8 h, with the decrease of the yields of Michael adduct from the maxima of about 60–70% (after 0.5 h for MgO-3, MgO-6 and MgO-7; 1 h for MgO-4 and MgO-5) to 15–21% (8 h), the yields of bridged ketol increased from 25–30% (1 h) to 55–65% (8 h). However, in the literature, 60% isolated yield of bridged ketol was obtained after 38 h at 20 °C under high pressure using the same reactants and the homogeneous catalyst Et_3N [181]. For all cases, at 24 h, low yields of some possible known compounds (product 5 and 6 in Scheme 3.1) were obtained,

which could be the reason for the decrease of both Michael adduct and bridged ketol. In case of $\text{Mg}(\text{OH})_2$ as catalyst, within the reaction time of 2 h, 51% yield of Michael adduct with 100% selectivity was obtained. The Michael adduct yield went through a maximum of over 75% yield after 4 h but did not decrease as drastically as in the case of MgO (final yield : 42%, not less than 20%). The different behavior of $\text{Mg}(\text{OH})_2$ and MgO may ascribed to the different type of base sites on the surface. For the different MgO catalysts, the catalytic performances have slight difference. Many parameters, like the nature of the base sites on the MgO surface, the surface area of MgO, the crystallite size of MgO, can affect the reaction results. Since MgO did not catalyze the Michael addition selectively, the discussion here will not go further to point out what is the exact reason for the different catalytic behavior from one MgO catalyst to another. However, the behavior of MgO will be compared and discussed with other catalysts systems in the following chapter based on the characterization of its basic properties.

Here, the Michael adduct is an important precursor of Wieland-Miescher keton [182], which is particularly useful for the synthesis of biologically active compounds [183,184]. However, although bridged ketols are not normally the desired product of the reaction, they are proven to be versatile synthetic intermediates since they can be readily dehydrated to the bicyclic enones or converted to the fused Robinson products under mild acid conditions. Moreover, the bridgehead or angular carbomethoxy of the bicyclic or fused-ring compound, respectively, expands the possibilities for further synthetic transformations at this position [181]. In our case, by careful selection of the reaction time and catalyst, the reaction can, to an extent, be controlled to give high yields of the Michael adduct 2-(γ -oxobutyl)-2-methyl-cyclohexan-1,3-dione or the bridged ketol 6-hydroxy-1,6-dimethyl-2,9-dioxobicyclo [3.3.1]nonane, respectively.

In summary, MgO can not catalyze the Michael addition of 2-methylcyclohexane-1,3-dione to methyl vinyl ketone selectively. However, either Michael adduct or bicyclic ketol can be selected to be the dominant product by choosing the MgO catalyst and reaction time. Moreover, two-step reaction can be performed in one-pot system.

3.4 Conclusions

MgO prepared by different methods or conditions have various textural properties. MgO with surface area from 1.8 to 170.2 m^2/g and pore volume from 0.01 to 1.0 cm^3/g can be prepared. MgO-1 prepared by calcination of $\text{Mg}(\text{NO}_3)_2 \cdot 6\text{H}_2\text{O}$ at 600 °C in air has very

low surface area of 1.8 m²/g; however, MgO-7 prepared by calcination of dried Mg(OH)₂ at 400 °C has a high surface area of 170.2 m²/g.

All the MgO catalysts can not catalyze the Michael addition of 2-methylcyclohexane-1,3-dione to methyl vinyl ketone selectively because a consecutive aldol cyclitization occurred. Michael adduct or bicyclic ketol can be selected to be the dominant product by choosing the MgO catalyst and the reaction time. The catalytic behavior of MgO in Michael addition is ascribed to its strong basicity.

Chapter 4

*Characterization and catalytic behavior of
potassium-modified ZrO₂ base catalysts*

4.1 Introduction

ZrO₂ has attracted more and more attention as a promising catalyst and catalyst support because of its high thermal stability, amphoteric nature, and redox properties [185]. Until now, ZrO₂ has been transformed into strong, solid acid catalysts by modification with sulfate [186,187,188,189], WO₃ [190], MoO₃ [191], or B₂O₃ [192,193]. These ZrO₂-based solid acid catalysts show high activity and selectivity in many reactions. However, few efforts have been made to turn ZrO₂ into a base catalyst by taking advantage of its natural basicity, although several studies have been done on a highly effective alkali-modified ZrO₂ catalyst for the oxidative coupling of methane [194,195]. In general, it is common to prepare base catalysts by modifying or supporting alkali metal oxides on various supports [13]. Various alkali metal oxides have been loaded on different supports, such as magnesium oxide [196], zeolites [22,25,40], alumina [117,118,197], silica [198], by the decomposition of alkali compounds. These catalysts have proved to be excellent solid base catalysts for numerous vapor-phase probe reactions, such as isopropanol dehydrogenation [22,197,198], the isomerization of 1-butene [26, 199] and *cis*-but-2-ene [119], the methylation of phenol [198], toluene [200], and catechol [201] with methanol. However, alkali metal oxides supported catalysts used in liquid phase base-catalyzed reactions have been investigated less. It is not clear whether this kind of catalyst is a real heterogeneous catalyst in liquid phase reactions. Recently, Wang et al. [119] used a dry impregnation process to prepare KNO₃/ZrO₂ superbases, which possessed a base strength of H_a = 27.0 and were very active for *cis*-but-2-ene isomerization under mild conditions. In this chapter, potassium-modified ZrO₂ were prepared by the calcination of hydrous zirconia and anhydrous zirconia after impregnation with potassium compounds. The catalytic activity of this system was studied in the vapor-phase isomerization of 1-butene and in the liquid-phase Michael addition of 2-methylcyclohexane-1,3-dione to methyl vinyl ketone [202].

4.2 Preparation and characterization of potassium-modified ZrO₂

Catalyst preparation

Hydrous zirconia, ZrO(OH)₂·aq, was prepared from ZrOCl₂·8H₂O (Fluka, 99%). Pure anhydrous ZrO₂ was obtained by calcination of hydrous zirconia at 600 °C in air for 4h. The supported catalysts were prepared by wet impregnation of ZrO(OH)₂ (ZRH samples)

Table 4.1

Characteristics of different potassium-modified zirconia catalysts (I)

Sample	Precursor	Modifying agent	XRD		S_{BET} (m ² /g)	V_{P}^{a} (cm ³ /g)	d_{p}^{b} (Å)
			bc	ac			
ZR	ZrO(OH) ₂	-	A	M	26.0	0.08	127
KC-ZRH	ZrO(OH) ₂	K ₂ CO ₃	A	T+M	7.4	0.04	212
KHC-ZRH	ZrO(OH) ₂	KHCO ₃	A	T+M	6.3	0.03	281
KAC-ZRH	ZrO(OH) ₂	KOAc	A	T+M	9.5	0.04	185
KN-ZRH	ZrO(OH) ₂	KNO ₃	A	M+T	4.8	0.04	322
KC-ZRO	ZrO ₂	K ₂ CO ₃	M	M	10.0	0.06	219
KHC-ZRO	ZrO ₂	KHCO ₃	M	M	11.7	0.07	236
KAC-ZRO	ZrO ₂	KOAc	M	M	11.1	0.06	220
KN-ZRO	ZrO ₂	KNO ₃	M	M	3.0	0.02	266

Characteristics of different potassium-modified zirconia catalysts (II)

Sample	X-content (wt%) ^c		K/Zr (mol) ^d
	bc	ac	
ZR	C:0.23, H:1.19	C:0.04, H:0.08	-
KC-ZRH	C:1.23, H:1.28	C:0.45, H:0.13	0.18
KHC-ZRH	C:1.19, H:1.33	C:0.46, H:0.14	0.19
KAC-ZRH	C:3.45, H:1.33	C:0.51, H:0.10	0.17
KN-ZRH	C:0.37, H:1.14, N:2.21	C:0.26, H:0.06, N:1.00	0.18
KC-ZRO	C:1.01, H:0.12	C:0.80, H:0.12	0.15
KHC-ZRO	C:1.30, H:0.22	C:0.72, H:0.16	0.16
KAC-ZRO	C:3.00, H:0.52	C:0.87, H:0.11	0.14
KN-ZRO	C:0.14, H:0.10, N:2.57	C:0.13, H:0.09, N:1.61	0.17

bc– before calcination, ac– after calcination at 600 °C in air

A– amorphous zirconia

M– monoclinic zirconia (PDF No.78-47)

T– tetragonal zirconia (PDF No.80-784)

T+M– tetragonal zirconia was the main phase

M+T– coexistence of the tetragonal and monoclinic phases

a: BJH desorption cumulative pore volume of pores between 17.0 and 3000.0 Å diameter

b: Average pore diameter by BET

c: Element analysis

d: ICP-OES results of calcined samples

and ZrO₂ (ZRO samples) powders with aqueous solutions of KHCO₃, K₂CO₃, KOAc and KNO₃ (in most cases, about 1.0 mL solution for 1.0 g powder). The theoretical K/Zr ratios were 0.2. After impregnation, the excess solution was evaporated at room temperature. The

samples were then dried at 110 °C (for the samples modified with KHCO_3 , 80 °C was used instead), calcined at 600 °C in flowing air for 4h, and stored in closed containers until used.

Characterization of potassium-modified ZrO_2

Table 4.1 gives the notations and characteristics of the samples. Fig. 4.1 shows the XRD patterns of some catalysts after calcination. Amorphous, hydrous zirconia formed monoclinic ZrO_2 after calcination at 600 °C (Fig. 4.1: a). However, after the modification of hydrous zirconia using C-containing potassium compounds mentioned above and calcination, the main phase of KC-ZRH, KHC-ZRH and KAC-ZRH (Fig. 4.1: b) was metastable, tetragonal ZrO_2 . Both the tetragonal and monoclinic phases were found in KN-ZRH (Fig. 4.1: c). It has been postulated that the K^+ ions are incorporated in the vacant sites on the surface of hydrous zirconia and stabilize the tetragonal ZrO_2 phase [119,203]. All of the ZRH samples, except for KN-ZRH, also have sharper and more intense XRD peaks than those of the pure ZrO_2 and the ZRO samples; this indicates higher sample crystallinity of the ZRH samples. Almost no phase or intensity change was found in the XRD patterns of the impregnated, anhydrous ZrO_2 samples after modification with potassium compounds (Fig. 4.1: d, KAC-ZRO).

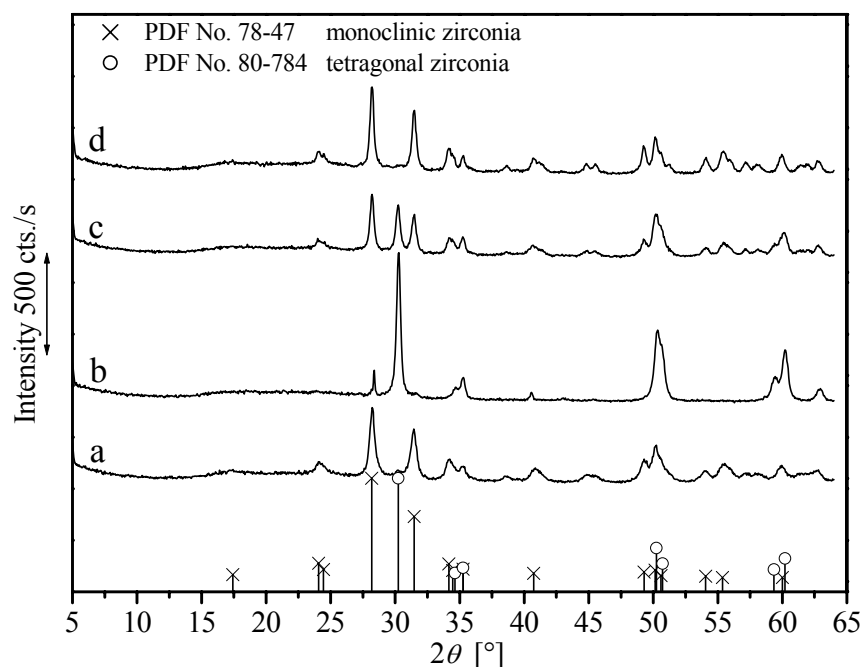


Fig. 4.1 XRD patterns of the catalysts after calcinations, a) ZR; b) KAC-ZRH; c) KN-ZRH; d) KAC-ZRO

The N₂ adsorption/desorption isotherms of all the samples (not shown) are of Type IV, according to IUPAC classification. The hysteresis loops, due to the capillary condensation associated with large mesopores, can be ascribed to the H2 Type [204]. There is not much difference between the adsorption/desorption isotherms of pure ZrO₂ and modified ZrO₂, but the specific surface areas of the modified samples are much lower than that of ZrO₂, whereas the pore volumes are only slightly smaller (Table 4.1). The decrease in surface area may be attributed to 1) rearrangements during the formation of the networks, 2) surface covering by potassium oxide produced at higher temperatures, or 3) the presence of bulk potassium compounds on the surface. On the other hand, the average pore diameters of the samples were somewhat larger (Table 4.1). The mesopore size distributions of some samples are shown in Fig. 4.3. The curves all show sharp maxima with narrow distributions. The pore diameters of pure anhydrous ZrO₂ and the modified samples were centered at about 70 and 100-180 Å, respectively (Fig. 4.2). Except for the KNO₃-modified samples with the lowest pore volume, the anhydrous ZrO₂ supported samples (KC-ZRO, KHC-ZRO, and KAC-ZRO) had pores with higher pore volumes than that of the hydrous ZrO₂ supported samples, KC-ZRH, KHC-ZRH, and KAC-ZRH. The carbon and nitrogen contents of the calcined samples indicate that the potassium compounds have not decomposed completely, which may be one reason for the decrease in surface area. The K/Zr mole ratios of calcined samples measured by ICP-OES were close to the nominal value of 0.2 (Table 4.1).

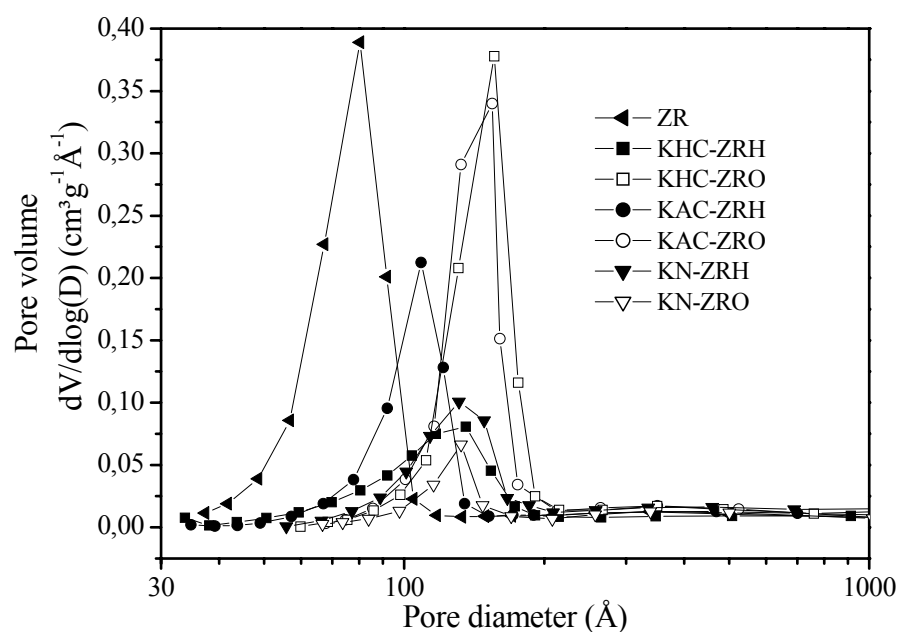


Fig. 4.2 Pore size distributions of the indicated catalysts

TG-DTG-DTA was used to investigate the decomposition of potassium compounds on ZrO_2 . The profiles of KHC-ZRH and KHC-ZRO are shown in Fig. 4.3. From the profiles of KHC-ZRH, a broad, endothermic effect, two DTG peaks, and 13% weight loss were observed from 100 to 400 °C, which can be ascribed to the evolution of water in hydrous zirconia and the decomposition of KHCO_3 . This was confirmed by an increase in the ionic currents of $m/z = 18$ (H_2O^+) and 44 (CO_2^+) with maxima at around 135 and 228 °C. A sharp exothermic effect at about 516 °C was observed without weight loss for the crystallization of amorphous ZrO_2 .

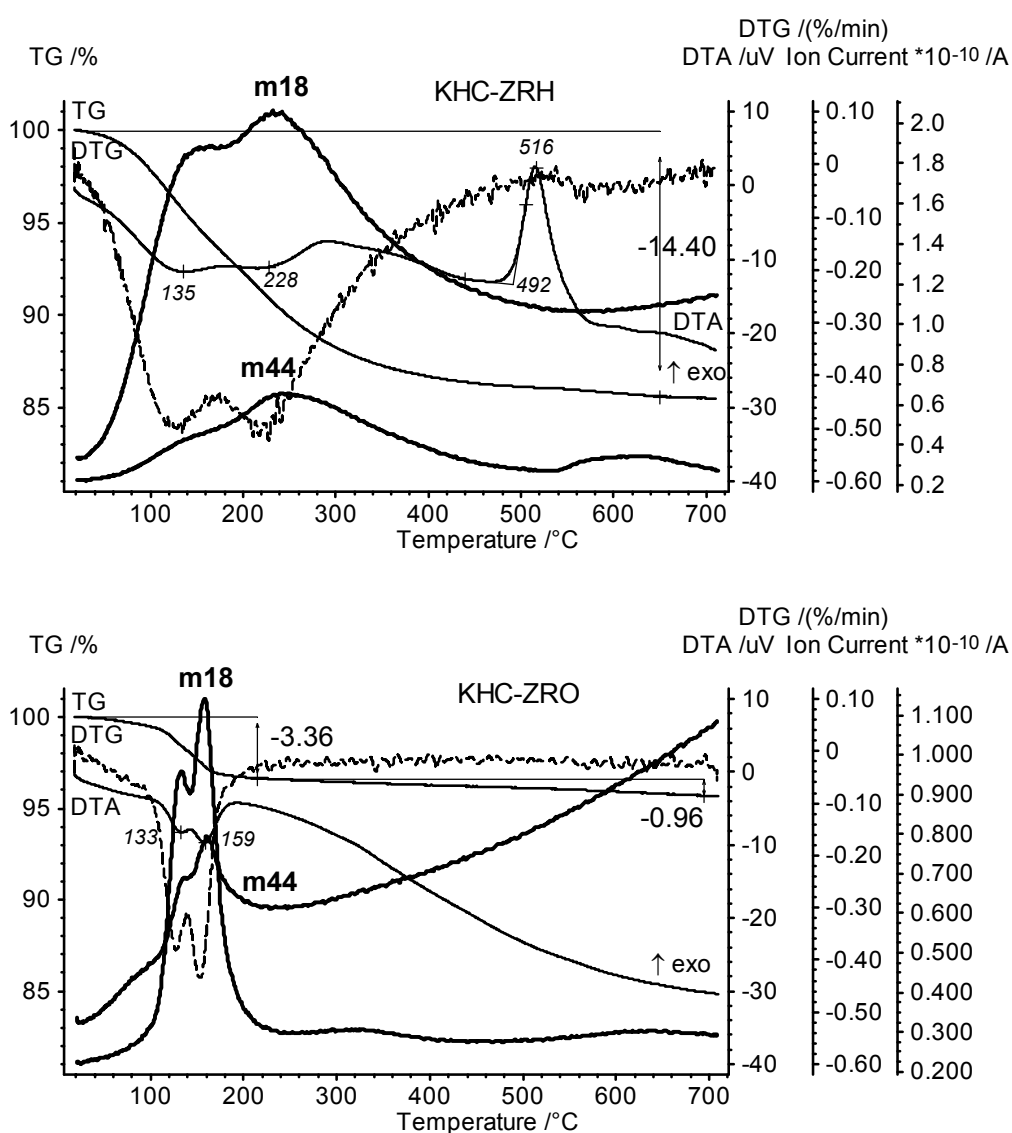


Fig. 4.3 TG-DTG-DTA profiles of KHC-ZRH (above) and KHC-ZRO (below) dried at 80 °C before calcination

The exothermic effect for the crystallization of pure ZrO_2 is at about 410°C in DTA curve [189]. Thus, the introduction of potassium ions in ZrO_2 shifts the crystallization temperature of ZrO_2 to higher temperatures. The sulfation of zirconia has the same effect [189]. In the measurement of KHC-ZRO, two endothermic effects and corresponding DTG peaks at around 133 and 159°C clearly indicate the decomposition of KHCO_3 on ZrO_2 with about 3% weight loss between 100 and 200°C , which is different from that of KHC-ZRH. The carbon contents of KHC-ZRH and KHC-ZRO after thermal analysis up to 700°C were 0.33% and 0.63%, respectively, which corresponds with the elemental analysis of these samples after calcination at 600°C (0.46 and 0.72%, respectively, in Table 4.1). These results indicate that the loaded potassium compounds do not completely decompose; this is also reported by Wang et al. for $\text{KNO}_3/\text{ZrO}_2$. For a sample with 20% KNO_3 on ZrO_2 , the percentage of decomposed KNO_3 was only 7.6% [119]. This and our results could be explained by the formation of layers of thermally stable potassium compounds on the zirconia surface.

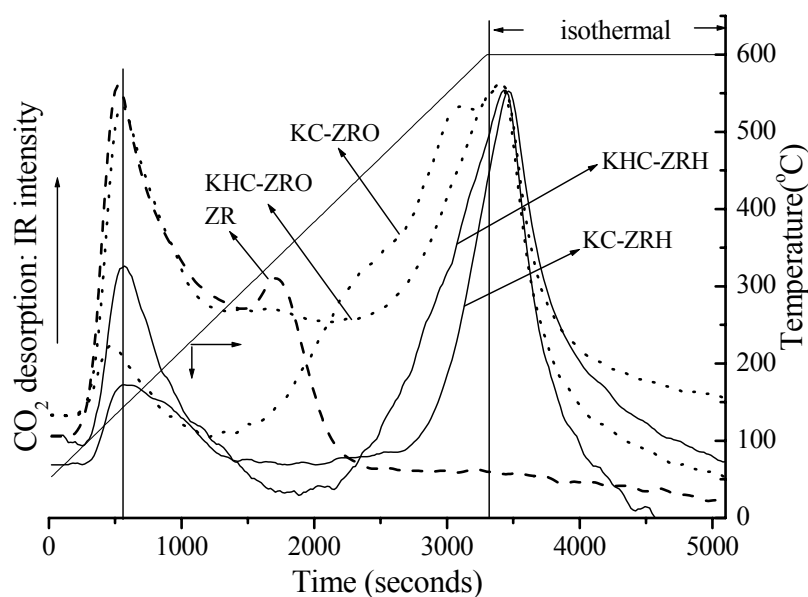


Fig. 4.4 Temperature-programmed desorption of CO_2

The CO_2 -TPD results (Fig. 4.4) show that pure ZrO_2 has basic sites indicated by two desorption maxima at about 135 and 335°C . The potassium-modified zirconia samples, like ZrO_2 , show an initial desorption maximum at around 140°C . A second step of CO_2 desorption at higher temperatures starts at around 400°C for KC-ZRH and KHC-ZRH, but at a lower temperature, 250 instead of 400°C , for the ZRO samples. This increase in the

CO₂ profile intensity continues up to 600 °C and lasts for 5–10 min under isothermal conditions. These results suggest that modified anhydrous zirconia (ZRO samples) has a wider distribution of basic sites than modified hydrous zirconia (ZRH samples). The second step of desorption of the modified samples indicates their stronger basic sites in comparison to those of ZrO₂.

CO₂ desorption at higher temperatures could be attributed to strong basic sites formed by K₂O extra-fine particles on the surfaces of ZrO₂ during decomposition. This has been reported by Zhu et al. [197]. He also excluded the possibility of some unusual oxides of potassium as the main basic sites on KNO₃/Al₂O₃. Hathaway et al. [22,23] and Kim et al. [40] also suggested in the case of Cs-modified zeolites that the decomposition product, cesium oxide, forms the active sites.

4.3 Catalytic behavior of potassium-modified ZrO₂

Table 4.2

The results of double-bond isomerization of 1-butene at 150 °C over calcined catalysts

Catalyst	Weight (mg)	Yield of 2-butene (%)				Yield/mass (%/mg) at 30 min	Average <i>cis/trans</i> ratios
		10 min	30 min	60 min	90 min		
ZR	330	24.1	21.7	19.1	16.7	0.066	4.0
KC-ZRH	395	69.7	54.2	42.4	35.2	0.137	5.3
KC-ZRH ^a	395	75.2	62.9	49.6	40.7	0.159	5.1
KHC-ZRH	361	62.7	44.3	30.2	22.8	0.123	5.3
KAC-ZRH	411	74.1	63.8	52.1	44.7	0.155	5.0
KAC-ZRH ^a	411	63.2	58.5	50.2	44.8	0.142	5.2
KN-ZRH	379	9.1	6.8	5.6	4.7	0.018	3.9
KC-ZRO	380	51.9	40.8	30.8	25.1	0.107	5.1
KHC-ZRO	350	53.1	36.8	25.9	21.0	0.105	5.3
KAC-ZRO	316	56.5	41.3	29.6	23.4	0.131	5.0
KN-ZRO	329	4.1	3.6	2.7	2.1	0.011	2.5

a: second run (the same reaction procedure was repeated again)

Both acid and base catalysts can catalyze the double-bond isomerization of 1-butene. Generally, the *cis/trans* ratio of 2-butene produced by isomerization of 1-butene is higher for base-catalyzed reactions [40,199]. The results of the double-bond isomerization of 1-butene are given in Table 4.2 with the normalized yields of 2-butene at 30 min for the catalysts. *Cis-* and *trans*-2-butene are the exclusive products found at 150 °C (100% product selectivity); skeletal isomerization or alkylation did not occur. Unmodified ZrO₂,

which was inactive at 60 °C in [205], had a low catalytic activity at 150 °C. About 21% yield of 2-butene with a *cis/trans* ratio of 3.9 was obtained after 30 min. The potassium modification of ZrO₂ resulted in an increase in the yield of 2-butene, i.e., from 21.7 up to (at the most) 63.8% after 30 min, except for the KNO₃-modified samples (Table 4.2). The improved activity is indicated by a) the yield/mass ratio at 30 min of 0.066 (pure zirconia) and 0.10–0.16 (potassium-modified ZrO₂) and b) the higher *cis/trans* ratios (more than 5.0). This can be explained by the stronger basic sites on catalysts produced by modification and confirmed with CO₂-TPD (Fig. 4.4). According to the literature [26,199], strong active basic sites are essential for the catalysis of 1-butene isomerization. Why the KNO₃-modified samples give yields of 2-butene lower than that of ZrO₂ and lower *cis/trans* ratios is not clear. The catalysts prepared from the modification of hydrous zirconia are slightly more active than the corresponding catalysts from anhydrous zirconia; this could be a result of the difference in the distribution of basic sites indicated by CO₂-TPD. At the same time, the locations of the basic sites on the surface of the different zirconia (tetragonal or monoclinic) may also affect the reaction. The catalysts, KC-ZRH and KAC-ZRH, were reused without much decrease in conversion after treatment at 600 °C (Table 4.2).

The liquid-phase Michael addition of 2-methylcyclohexane-1,3-dione to methyl vinyl ketone used for the catalytic experiments is an important reaction for the synthesis of steroid pharmaceutical products.

Table 4.3

The results of Michael addition and leaching tests at room temperature

Catalyst	Yield of 2-methyl-2-(3-oxo-butyl)-cyclohexane-1,3-dione (%) ^a					Leaching test		
	2h	4h	6h	8h	24h	After separation of the catalyst		
						Before separation		
KC-ZRH	17	24	-	48	99	73 (14h)	95 (12h)	95 (24h)
KHC-ZRH	18	32	-	56	98	82 (14h)	96 (12h)	96 (24h)
KAC-ZRH	16	30	41	52	96	-	-	-
KC-ZRO	39	63	82	93	89	66 (4h)	88 (16h)	85 (24h)
KHC-ZRO	59	79	90	86	86	75 (4h)	89 (16h)	89 (24h)
KAC-ZRO	36	62	81	92	96	-	-	-

a: related to 2-methylcyclohexane-1,3-dione

Pure ZrO₂ was catalytically inactive in this reaction, but the modification of ZrO₂ with potassium salts was successful in producing catalytic activity. Thus, the target product, 2-methyl-2-(3-oxo-butyl)-cyclohexane-1,3-dione, was formed selectively on the catalysts,

KC-ZRH, KHC-ZRH, and KAC-ZRH, within 24 h in yields of more than 95% (Table 4.3). In contrast, KN-ZRH and KN-ZRO gave yields of only 72 and 55%, respectively (not given in Table 4.3). The rate of product formation was highest on KC-ZRO, KHC-ZRO, and KAC-ZRO. Yields of about 80–90% were achieved within 6 h.

Leaching tests performed by filtration of the catalyst from the reaction mixture after 4 or 14 h show that the reaction continues after removal of the solid potassium-modified zirconia catalyst. The presence of potassium ions in solution was checked and confirmed by ICP-OES. It can be concluded that potassium compounds leach from the catalyst surface into the methanolic reaction mixture. This leaching and consequent homogeneous catalysis may be explained by the weak interaction of the potassium compounds with ZrO_2 and the solubility of potassium compounds in methanol. Consequently, exclusive heterogeneous catalysis can be ruled out for the liquid-phase reaction investigated on potassium-modified zirconia in methanol. However, the catalytic results differ from those obtained for the soluble base catalyst, KOH. When KOH is used, low product yield (40%) and a mixture of various products is found. This indicates that different K species are present in the methanol solution, and that the reaction may not be a straightforward example of homogeneous catalysis.

These results show that this catalyst system is less suitable for liquid-phase reactions, although the potassium-modified ZrO_2 samples do produce both higher selectivities and higher yields than KOH, and catalysts with potassium or alkali metal cations have been used successfully in vapor-phase reactions. The nature of the interaction between the support, ZrO_2 or Al_2O_3 , with potassium or other alkali metal cations is open to further discussion [18].

4.4 Conclusions

In summary, the properties and the activities of the catalysts can be influenced by a variety of parameters, such as the zirconia precursor and the potassium modifying agent. High product yields and selectivities were also obtained for the liquid-phase Michael addition of 2-methylcyclohexane-1,3-dione to methyl vinyl ketone in methanol, but leaching could not be prevented. The following can be concluded:

Modified hydrous zirconia forms the metastable, tetragonal ZrO_2 phase after calcination; the phase of modified anhydrous zirconia, on the other hand, is monoclinic. The specific surface areas of the modified samples are much lower than that of ZrO_2 . The potassium

compounds on hydrous zirconia decompose in a broader temperature range than those on anhydrous zirconia.

Stronger basic sites are produced after modification, and modified anhydrous zirconia has a wider distribution of basic site strengths than modified hydrous zirconia.

Potassium-modified zirconia, except for that modified with KNO_3 , give higher yields and *cis/trans* ratios of 2-butene in the double-bond isomerization of 1-butene and is reusable.

Potassium-modified zirconia is less suitable as a solid base catalyst for liquid phase reactions in methanol because of potassium leaching effects.

Chapter 5

Application of calcined Mg-Al hydrotalcites for Michael additions

5.1 Introduction

Hydrotalcite (HT)-like compounds, also known as layered double hydroxides (LDH) and anionic clays, are natural or synthetic crystalline materials consisting of positively charged two-dimensional sheets with water and exchangeable charge-compensating anions in the interlayer region. They may be represented by the general formula $[M^{2+}_{1-x}M^{3+}_x(OH)_2]^{x+}[A^{n-}_{x/n} \cdot mH_2O]^{x-}$. M^{2+} are divalent anions (*e.g.*, Mg^{2+} , Zn^{2+} , Mn^{2+} , Ni^{2+} , Co^{2+} , Fe^{2+}), M^{3+} are trivalent metal ions (*e.g.*, Al^{3+} , Cr^{3+} , Fe^{3+} , Co^{3+} , Ga^{3+}) and A^{n-} is the interlayer anion with charge n . The structure of hydrotalcite (HT) itself, $Mg_6Al_2(OH)_{16}CO_3 \cdot 4H_2O$, is similar to that of brucite, $Mg(OH)_2$, in which Mg^{2+} is octahedrally coordinated by hydroxyl groups. These octahedra share adjacent edges to form sheets or layers. In HT, part of the Mg^{2+} ions is replaced by Al^{3+} ions, resulting in positively charged layers. The space between the stacked brucite-like cation layers is filled with charge compensating anions (*e.g.*, CO_3^{2-} , Cl^- , NO_3^- , SO_4^{2-} , OH^- and many others) and water molecules. In naturally occurring HT, mostly carbonate is the interlayer anion. The synthesis, the textural and acid-base properties, and the catalytic application of hydrotalcites and hydrotalcite-related catalysts have been reviewed in [206,207,208,209]. Hydrotalcites and hydrotalcite-related materials are used in different forms as follows:

As-synthesized hydrotalcite

As-synthesized hydrotalcite is used as flame retardant, ion exchanger, adsorbent for waste water in industry. As-synthesized hydrotalcite can also be used as catalyst and showed a high catalytic activity for decomposition of 2-methyl-3-butyne-2-ol into acetone and acetylene [210]. Halide exchange reactions between alkyl chloride and bromide/iodide are catalyzed by the catalysts having Cl^- , Br^- , or I^- in the interlayers [211]. Moreover, after anion exchange with inorganic heteropolyacids, hydrotalcite may also exhibit acid properties, which mainly are associated with the anions in interlayers [206].

Calcined hydrotalcite

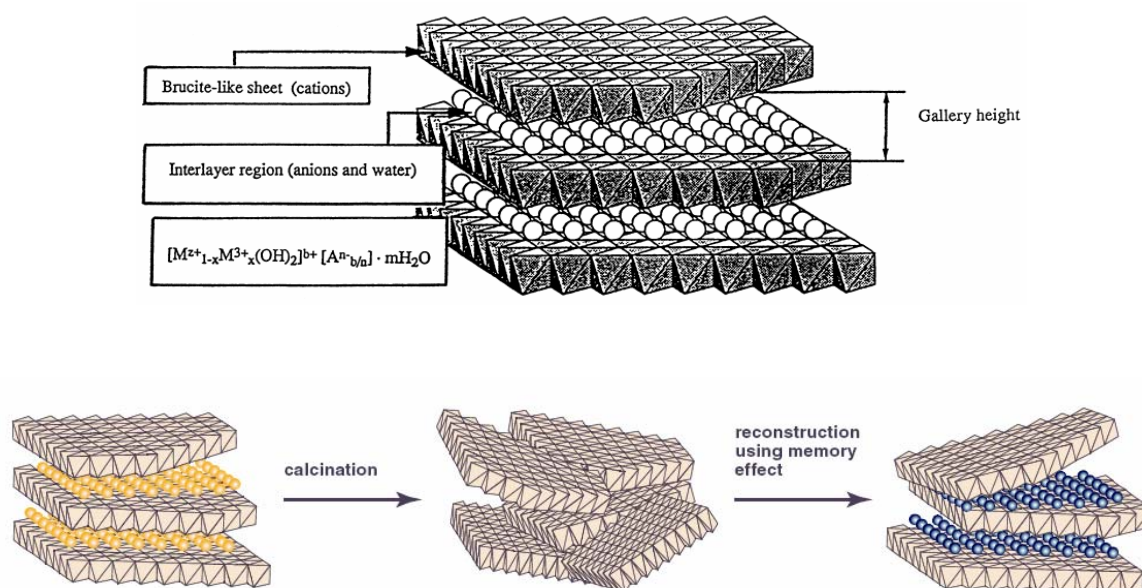
The calcined hydrotalcites are normally referred to as mixed oxides and most widely used as catalysts. The most interesting and important properties of the mixed oxides obtained by calcination are the following: a) high surface area; b) basic properties; c) homogeneous mixtures of oxides with very small crystal size; d) memory effect, which allows the reconstruction of the original hydrotalcite-related structure under mild conditions [206]. In the field of heterogeneous catalysis (hydrogenation, reforming, basic catalysis and catalyst support), properties a), b) and c) have found various applications [206,208]. Recently, in

base-catalyzed reactions, calcined hydrotalcites have attracted more attention. They are attractive alternatives to the use of dissolved alkali hydroxides or alkoxides.

Reconstructed hydrotalcite

When calcined hydrotalcites are rehydrated in water or in flowing nitrogen saturated with water, hydrotalcites structure are reconstructed. This is the “memory effect” of calcined hydrotalcites. The reconstructed material contains OH^- ions in the interlayers. It is also possible to introduce OH^- ions by direct ion exchange. The base strength of the reconstructed hydrotalcite containing OH^- ions is stronger than the original hydrotalcite containing CO_3^{2-} ions. Figueras and co-workers found that the reconstructed materials were very useful catalysts for aldol condensation [123,212] and Michael addition [141]. The OH^- ions in the interlayers are believed to be active sites for these reactions.

The hydrotalcite-type structure and the formation process of the hydrotalcite-related materials are presented in Scheme 5.1 [207,209].



Scheme 5.1 The hydrotalcite-type structure (up) and formation process of the hydrotalcite-related materials (down)

Hydrotalcites are commercially available, cheap solid bases. As mentioned above, hydrotalcites as well as calcined hydrotalcites are highly active, selective catalysts and play an important role in many base-catalyzed reactions, e.g., Claisen-Schmidt condensations [131] and Knoevenagel condensations [213]. Their surface base sites were characterized by temperature programmed desorption (TPD) after adsorption of CO_2 [214,215], FTIR spectroscopy with CO_2 [216,217,218], and gas-phase microcalorimetry (with CO_2 and SO_2)

[216,219,220,221]. In addition to the base sites, acid sites or acid-base pairs on these materials also influence catalytic performance. Acid-base sites on mixed oxides are highly active sites for many reactions: Meerwein-Ponndorf-Verley reactions [222], cycloadditions of carbon dioxide to epoxides [223], and aldol condensations to form 2-nonenal [224]. Acid-base properties of Mg-Al mixed oxides are governed by the Mg/Al molar ratio [215,216,217,218], calcination temperature [219], and preparation condition [214,218,225,226]. While the acid-base properties are important for understanding catalytic activity and selectivity, the relation between catalytic behavior in Michael additions, the acid-base properties, and the composition of hydrotalcite and calcined hydrotalcites is still poorly understood.

Thus, the aim of this chapter was to a) find efficient, selective catalyst that is easily acquired or prepared for further Michael additions and b) study the influence of its acid-base properties and chemical composition on the catalytic performance of the calcined hydrotalcites [227]. The Michael additions of 1,3-diones with different pK_a values to methyl vinyl ketone were examined on calcined commercial Mg-Al hydrotalcites including an Al-rich (Mg/Al = 0.6) sample. MgO and Al₂O₃ were also involved for comparison. Acid-base properties of the catalysts were investigated by gaseous probe molecules with FTIR spectroscopy and microcalorimetry. Microcalorimetric measurements with benzoic acid were carried out for the study of catalyst basicity under similar liquid-phase reaction conditions.

5.2 Preparation and characterization of calcined Mg-Al hydrotalcites

5.2.1 Catalyst preparation

Hydrotalcites (PURAL MG 30, 50, 61, 70 from SASOL Germany GmbH) [228] were calcined at 550 °C in air for 3 h. Al₂O₃ was obtained by calcination of the AlO(OH) (Pural SB, SASOL Germany GmbH) [228] under the same conditions. Calcination of dried Mg(OH)₂ at 600 °C in air for 4 h produced MgO. The hydroxide was precipitated from Mg(NO₃)₂ with KOH and dried at 110 °C (see chapter 3). In this chapter, the following sample codes are used: HT0.6 or CHT0.6 for the sample with a bulk Mg/Al molar ratio of 0.6; the C in the sample code indicates that the sample has been calcined (Table 5.1).

5.2.2 Characterization of calcined hydrotalcites

Physical properties

The physical properties of hydrotalcites (HT), calcined hydrotalcites (CHT), MgO and Al₂O₃ are given in Table 5.1. N₂ adsorption experiments at 77 K show that the HT samples have low specific surface areas, S_{BET} (13–20 m²/g) and high average pore diameter, d_p (167–205 Å) with the exception of Al-rich HT0.6, which has a much higher specific surface area of 163 m²/g and pore diameter of 76 Å, which may be due to the existence of boehmit (Fig. 5.1A: d). Sample calcination increases S_{BET} independent of composition; the CHT samples have significantly higher surface areas (>200 m²/g) with exception of CHT2.2 (114 m²/g). The average pore diameter (d_p) are similar (45–52 Å) with the exception of 81 Å for CHT0.6 (Table 5.1). It is interesting to note that the surface areas of the CHT samples decreased dramatically when the fresh calcined samples were kept for several days even in closed containers prior to adsorption experiments. The reference compounds, MgO and Al₂O₃, have surface areas of 75 and 234 cm²/g and pore diameters of 258 and 45 Å, respectively. The pore volumes (V_p) are the highest for these two samples with values of 0.96 (MgO) and 0.54 cm³/g (Al₂O₃).

Table 5.1Textural properties of hydrotalcites, calcined hydrotalcites, MgO and Al₂O₃

Sample	Mg/Al molar ratio			S_{BET} (m ² /g)	V_p^a (cm ³ /g)	d_p^b (Å)	C^c (wt%)	Weight Loss ^d (wt%)
	Theor.	Bulk (ICP)	Surface (XPS)					
HT0.6	0.5	0.6	n.d.	163	0.32	76	1.42	31
HT1.4	1.25	1.4	n.d.	13	0.05	167	1.19	36
HT2.2	2.0	2.2	n.d.	15	0.05	128	2.42	42
HT3.0	3.0	3.0	n.d.	20	0.10	205	2.27	44
CHT0.6	0.5	0.6	0.8	257	0.52	81	-	-
CHT1.4	1.25	1.4	1.4	201	0.23	45	-	-
CHT2.2	2.0	2.2	2.0	114	0.13	46	-	-
CHT3.0	3.0	3.0	2.0	203	0.22	52	-	-
MgO	-	-	-	75	0.96	258	-	-
Al ₂ O ₃	-	-	-	234	0.54	45	-	-

a: BJH desorption cumulative pore volume of pores between 17.0 and 3000.0 Å diameter

b: Average pore diameter by BET

c: Carbon content

d: Based on the weights before and after calcination in air at 550 °C

ICP-OES results show that the Mg/Al molar ratios of the corresponding HT and CHT samples are identical and, thus, independent of the samples' thermal treatment. In comparison, the surface Mg/Al molar ratios (XPS measurements) deviate from the bulk ratios depending on the composition (Mg/Al molar ratio) of the CHT samples. The surface Mg/Al ratio for CHT0.6 of 0.8 is slightly higher than the bulk ratio (Mg-enriched surface, $Al_{\text{surface}} < Al_{\text{bulk}}$), whereas the identical surface Mg/Al molar ratios of CHT2.2 and CHT3.0 are lower in value (both 2.0) than that of the bulks (Al-enriched surfaces, $Al_{\text{surface}} > Al_{\text{bulk}}$). The bulk and surface Mg/Al ratios of CHT1.4 are identical ($Al_{\text{surface}} = Al_{\text{bulk}}$). If XPS is considered a pure surface method independent of surface area [214,215], the ICP and XPS results confirm the homogeneity of CHT1.4. This homogeneity suggests that smaller Al^{3+} cations are more easily incorporated into the main Mg oxygen network ($Mg/Al > 1$) than the larger Mg^{2+} cations into the main Al oxygen network ($Mg/Al < 1$: CHT0.6). The “nonincorporation” effect becomes more significant (Al-enriched surfaces) the higher the Mg/Al ratio ($>> 1$); the degree of Al enrichment of the CHT3.0 surface is higher than that of CHT2.2. Al-enriched surfaces were also found with XPS ($Mg/Al = 1.5$ and 2.4) for calcined Mg-Al hydrotalcites with Mg/Al molar ratios of 1.87 and 4.57, respectively [214].

XRD

The XRD patterns of the HT samples show that crystallinity of the HT samples increases with Mg content (Fig. 5.1A: a–d) and that the HT samples have a hydrotalcite-like structure similar to those presented in [225,226,229,230]. Additional weak peaks at 28° and 49° in the HT0.6 pattern (Fig. 5.1A: d) can be assigned to boehmit (cf. Fig. 5.1A: e for Pural SB, $AlO(OH)$, PDF No. 49-133). Calcination of the HT samples (CHT3.0–1.4) results in the destruction of the hydrotalcite-like structure and the formation of a periclase MgO (PDF No. 45-946, Fig. 5.1B: a, b, c) also found for the pure MgO sample (Fig. 5.1B: f). The MgO peaks (at about 43° and 63°) of the CHT samples including CHT0.6 (Fig. 5.1B: a, b, c and d) have higher 2θ values than those of pure MgO; this is caused by the incorporation of smaller Al^{3+} cations in the bulk lattice of all four CHT samples [14,18,29,30]. These peaks shift from higher to lower 2θ values as the Mg/Al ratio increases, which shows that the amount of Al^{3+} cations incorporated decreases accordingly. These results agree with the XPS results: CHT0.6 ($Al_{\text{surface}} < Al_{\text{bulk}}$) and CHT3.0 ($Al_{\text{surface}} > Al_{\text{bulk}}$). The $AlO(OH)$ reference material forms $\gamma-Al_2O_3$ after calcination (PDF No. 29-63, Fig. 5.1B: e). In the pattern of the homogeneous CHT1.4 sample ($Al_{\text{surface}} = Al_{\text{bulk}}$, Fig. 5.1B: c), weak broad peaks for $MgAl_2O_4$ (35° , PDF No. 21-1152) and $\gamma-Al_2O_3$ (66°) are

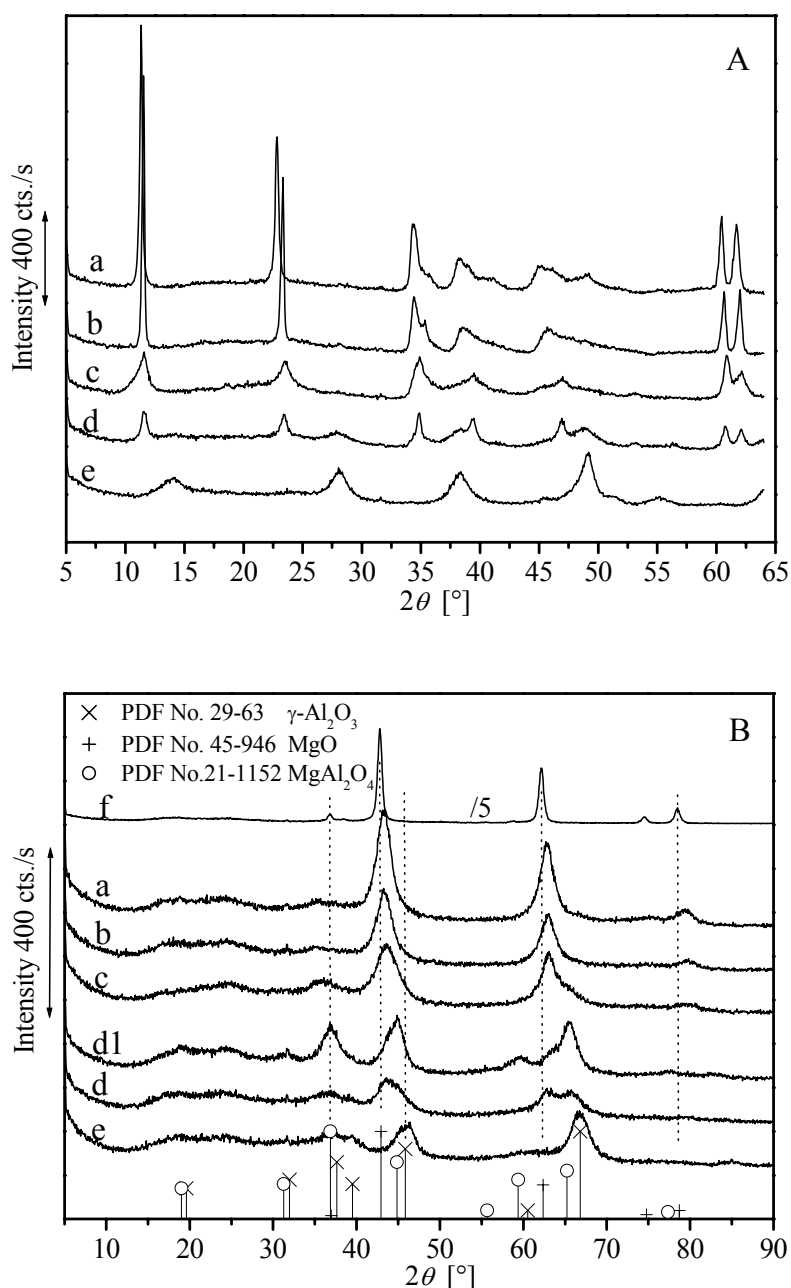


Fig. 5.1 XRD patterns of hydrotalcites (A) and hydrotalcites calcined at 550 °C (B) with Mg/Al molar ratios of 3.0 (a), 2.2 (b), 1.4 (c), and 0.6 (d). The sample in A: d was further calcined at 700 °C to give the XRD pattern B: d1. The MgO reference material is shown after calcination in B: f. The Al₂O₃ reference oxide is shown before (boehmite in A: e) and after calcination (γ-Al₂O₃ in B: e).

observed. The intensity decrease of the MgAl₂O₄ and γ-Al₂O₃ peaks from CHT0.6 to CHT3.0 also indicates finely dispersed Al³⁺ cations in the bulk MgO network [219]. In the pattern of the very amorphous CHT0.6 sample, the broad peak at ca. 43° (Fig. 5.1B: d) may be attributed to regions of MgO, γ-Al₂O₃, and an additional spinel phase of MgAl₂O₄ in this sample [215]. Its maximum narrows, sharpens, and shifts to a slightly higher 2θ

value (45°) as a separate spinel phase forms during further calcination at 700°C (Fig. 5.1B: d1); weak, broad peaks for MgO at ca. 43 and 63° (Fig. 5.1B: b) decrease in intensity after calcination at 700°C , whereas the peaks for MgAl_2O_4 at 37 , 45 , 59 , and 65° become stronger (Fig. 5.1B: d1). Thus, the increased calcination temperature of 700°C causes a separate phase of MgAl_2O_4 to form [219,231]. With higher Mg contents (higher Mg/Al ratios), MgO is the main phase (strong peak at ca. 63° in Fig. 5.1A: a), and the spinel peak disappears ($2\theta = 37^\circ$).

²⁷Al MAS NMR

The ²⁷Al MAS NMR spectra of $\gamma\text{-Al}_2\text{O}_3$ and calcined hydrotalcites are shown in Fig. 5.2. Two broad signals at about 5 and 64 ppm are observed in the spectra of both pure Al_2O_3 and the CHT samples for octahedrally and tetrahedrally coordinated aluminum cations (Al_O and Al_T), respectively [214,217,219,229,231]. The identical spectra of $\gamma\text{-Al}_2\text{O}_3$ and CHT0.6 (highest Al content) regarding signal shapes, in particular that of the 64-ppm signal, indicate a similar Al coordination in these two samples and explains the weak, broad peaks in the XRD patterns (Fig. 5.1B: b and d). The maximum of the signal at 5 ppm shifts slightly to lower fields (from ca. 2 to 6.5 ppm) with increasing Mg/Al ratio, which indicates increased bonding of the AlO_6 octahedra in the bulk to a less electronegative element (Mg): Mg-O-Al_O [217,219]. A lack of signal splitting [219] suggests that distinct Al coordination sites do not exist in the samples. CHT1.4 has a relatively narrow signal (at 5 ppm) compared to other samples, which indicates a low degree of disorder of the AlO_6 octahedra and may be related to the homogeneity of this sample confirmed by ICP-OES and XPS ($\text{Al}_\text{bulk} = \text{Al}_\text{surface}$).

The $\text{Al}_\text{T}/\text{Al}_\text{O}$ ratio calculated from the integrated signals for Al_2O_3 is 0.38 (or 28% Al_T) and is close to the value 0.4 of alumina given in [214]. The 28% Al_T observed here is somewhat lower than that found in cubic aluminas (31–33%), but higher than the amount of Al_T found in hexagonal alumina (15–25%) [232]. The samples, CHT0.6, CHT1.4, and CHT2.2, all have a $\text{Al}_\text{T}/\text{Al}_\text{O}$ ratio identical to that of Al_2O_3 (0.38); however, CHT3.0 has a much higher ratio of 0.59 (37% Al_T). This indicates that the octahedral coordination Al_O is predominant in the structure of all the samples, yet tetrahedral Al_T cations are more common in CHT3.0 possibly by forming inverse spinel-like domains: Mg-O-Al_T [217]. AlO_4 tetrahedra are generally formed during calcination [231, 233] (pre-calcination: exclusively AlO_6 octahedra); the preparation method [214] and Al content [214,217] can also influence the $\text{Al}_\text{T}/\text{Al}_\text{O}$ ratio. The CHT samples were all prepared and calcined under

the same conditions; thus, the higher Al_T/Al_O ratio in CHT3.0 ($Al_{surface} \gg Al_{bulk}$) can only be the result of the strong difference in Al content between the bulk and surface not observed in the other samples. The influence of surface Al on the Al_T/Al_O ratio has been suggested before [214].

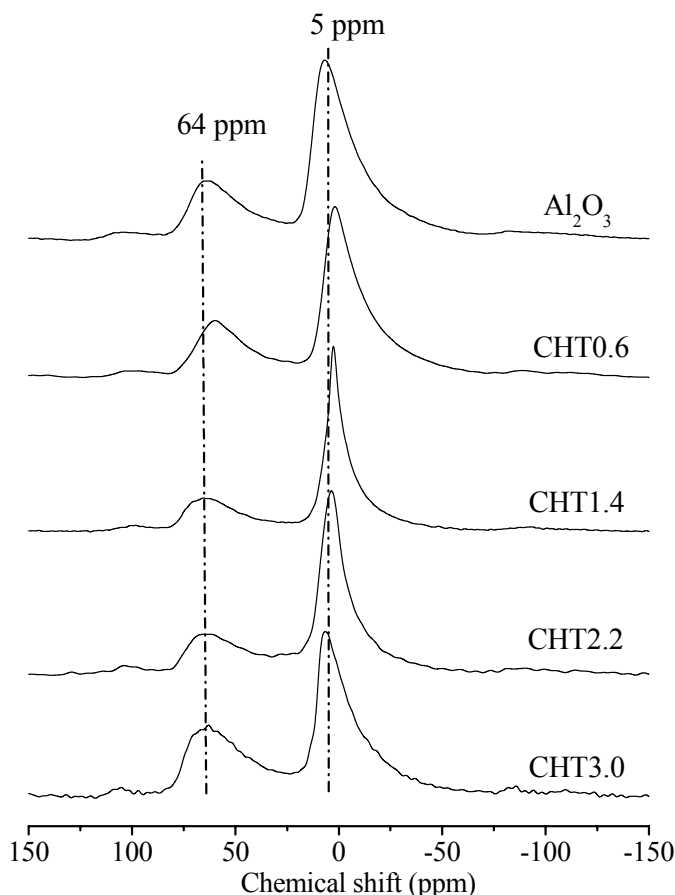


Fig. 5.2 ^{27}Al MAS NMR spectra of Al_2O_3 and calcined hydrotalcites

TG-DTA

The TG-DTA curves of HT0.6 and HT3.0 are shown in Fig. 5.3. In the TG-DTA curves of HT0.6 (Fig. 5.3a) and HT3.0 (Fig. 5.3b), gradual weight loss is observed from about 60 to approximately 600 °C with two main endothermic effects at about 250 and 416 (432) °C; a broad, weak endothermic peak is found at 90 °C for HT0.6. The first large endothermic effect at about 250 °C may be attributable to the loss of inter-layer water [225,234]; the second endothermic effect of HT3.0 signifying the loss of OH^- groups and the decomposition of the CO_3^{2-} anion in the brucite-like layers of hydrotalcites [225,234] occurs at 432 °C. The total weight loss observed for HT0.6 and HT3.0 (ca. 33.5 and 42.5%, respectively) is similar to that given in Table 5.1 measured pre- and post-calcination at 550 °C (31 and 44%, respectively).

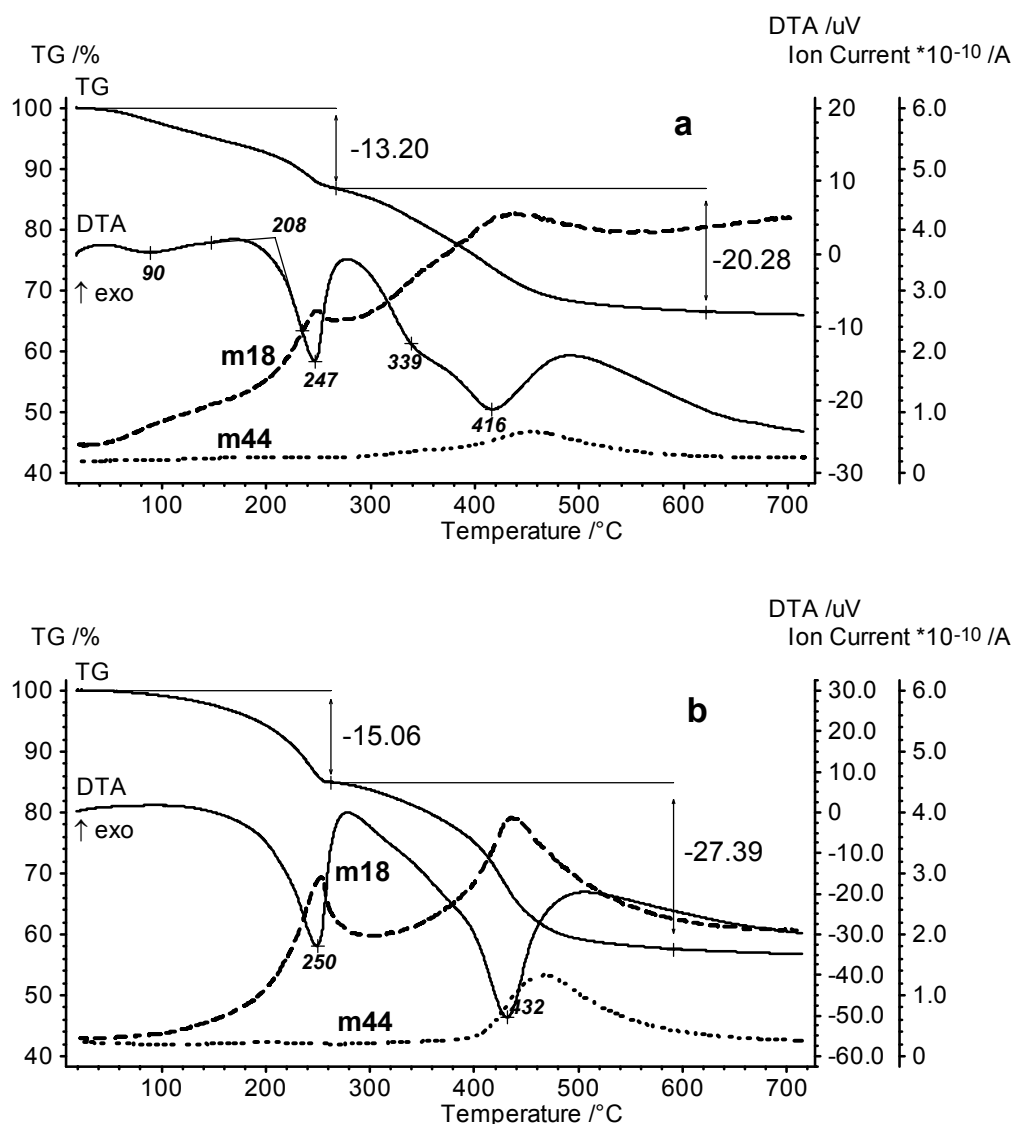


Fig. 5.3 TG-DTA profiles of hydrotalcites with Mg/Al molar ratios of 0.6 (a) and 3.0 (b)

The monitored m/z peak at 18 (H_2O^+) for H_2O or OH^- shows an immediate, continuous increase in intensity upon heating up to 416 $^{\circ}\text{C}$ with slight maxima at 247 and 416 $^{\circ}\text{C}$ (Fig. 5.3a) and 250 and 432 $^{\circ}\text{C}$ (Fig. 5.3b) for HT0.6 and HT3.0, respectively. The shape of these curves confirms the release of water and OH^- groups as the main cause of weight loss. Intensity increases of the mass peak, $m/z = 44$ (CO_2^+), are only observed during the second main step of weight loss from 300 (HT0.6) or 400 (HT3.0) to 600 $^{\circ}\text{C}$ (both) with maxima at around 460 $^{\circ}\text{C}$ [231]. This increase is also gradual for HT0.6 at temperatures higher than 300 $^{\circ}\text{C}$, but immediate and more defined for HT3.0 at 410 $^{\circ}\text{C}$. The intensity differences of the $m/z = 44$ maxima are a direct result of the varying carbon contents (1.42 for HT0.6 < 2.27 for HT3.0, Table 5.1) and are less significant to the samples' overall weight loss (1 mole CO_3^{2-} vs. 16 moles OH^- and 4 moles crystal water). Due to the removal of water and

dehydroxylation, as well as the decomposition of carbonate anions observed by the thermal analysis, surface areas and pore volumes increased after calcination (Table 5.1).

5.3 Catalytic behavior of calcined Mg-Al hydrotalcites

Michael addition of 2-methylcyclohexane-1,3-dione to methyl vinyl ketone – comparison of hydrotalcites and calcined hydrotalcites

A comparative catalytic study of the HT and CHT samples is shown in Fig. 5.4A and 5.4B, respectively. Both types of samples (HT and CHT) are very active and produce the target product with 100% selectivity. In contrast, the calcined hydrotalcite studied in [141] exhibited no catalytic activity in 1,4-Michael additions. This could not be confirmed here. The catalytic activity of the sample was evaluated from the yield of the Michael adduct as a function of reaction time. After a reaction time of 24 h, the final catalytic yields decreased in the following order regardless of sample calcination: (C)HT0.6 > (C)HT3.0 > (C)HT1.4 > (C)HT2.2 ($> \text{Al}_2\text{O}_3 > \text{MgO} \approx 0$ in Fig. 5.4B). A linear correlation between Mg/Al molar ratio and catalytic activity was not found; samples with the highest and lowest Mg content, (C)HT0.6 and (C)HT3.0, respectively, achieved the highest yields. HT0.6 and CHT0.6 gave respective target product yields of 98 and 100% after 24 h; the use of HT3.0 and CHT3.0 resulted in yields of 82 and 94%, respectively. The sample with a Mg/Al ratio of 2.2 (HT2.2 and CHT2.2) was the least active of these samples. The catalytic yield a) remained more or less the same (Mg/Al = 1.4 and 0.6), b) decreased from 69 to 49% (Mg/Al = 2.2), or c) increased significantly from 82 to 94% (Mg/Al = 3.0) after calcination of the corresponding hydrotalcite at 550 °C. Due to weight loss during calcination, i.e., amount of catalyst (0.225 g) used was weighed out prior to calcination, CHT0.6 and CHT3.0 showed enhanced yields. This weight loss could also explain the drastic decrease in the catalytic activity of CHT2.2; however, HT2.2 also gave the lowest catalytic yield suggesting that other factors may be involved in the low yield of CHT2.2.

In the case of the pure oxides (Al_2O_3 and MgO), the catalytic activity of Al_2O_3 was lower than that of the CHT samples (final yield of 23% after 24 h, Fig. 5.4B), whereas MgO was found to have a considerably different, less selective behavior. In the case of MgO , 65% of the target product was formed within 30 min, but the amount of the Michael adduct in the reaction mixture dropped to 6% in a reaction time of 24 h. In the ^1H NMR spectra of the reaction mixtures, additional CH_3 signals (0.97 and 1.23 ppm) were found for 6-hydroxy-1,6-dimethyl-2,9-dioxobicyclo[3.3.1]nonane formed by the aldol cyclization

of 2-methyl-2-(3-oxo-butyl)-cyclohexane-1,3-dione. In our experiments, when $\text{Mg}(\text{OH})_2$ or different MgO catalysts were used, cyclization under the same conditions also took place (see chapter 3).

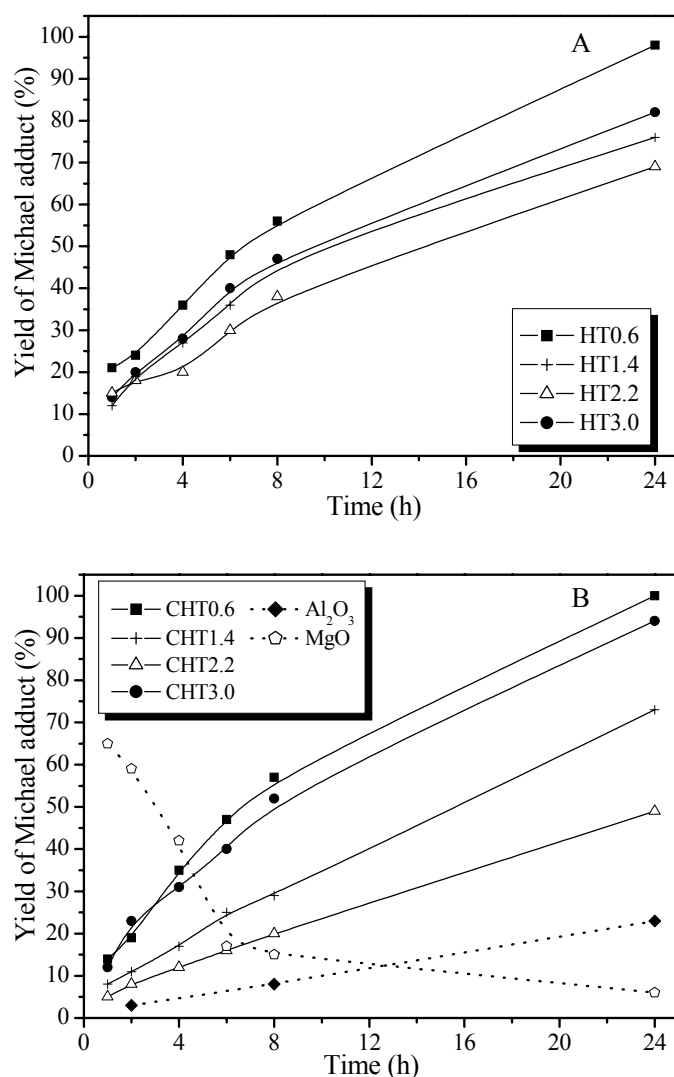


Fig. 5.4 Results of the Michael addition of 2-methylcyclohexane-1,3-dione (15 mmol) to methyl vinyl ketone (22.5 mmol) in 10 mL methanol over the hydrotalcites (A) and over the calcined hydrotalcites, Al_2O_3 and MgO (B). Catalyst amounts were 0.225 g for the hydrotalcites, Al_2O_3 , and MgO and the amount remaining after calcination of 0.225 g hydrotalcite at 550 °C

Michael addition of 2-acetylcyclopentanone and 2-acetylcyclohexanone to methyl vinyl ketone over calcined hydrotalcites

The Michael addition of 2-acetylcyclopentanone ($\text{pK}_a = 7.8$) and 2-acetylcyclohexanone ($\text{pK}_a = 10.1$) to methyl vinyl ketone was performed (Fig. 5.5A and 5.5B, respectively) to investigate possible further applications and compare the basic site strengths and numbers of CHT samples.

The catalytic results (Fig. 5.5) using these liquid diones can not be compared directly to those in Fig. 5.4B (2-methylcyclohexane-1,3-dione, a solid, is only slightly soluble in methanol at room temperature). A similar decreasing order of catalytic activity ($\text{CHT0.6} > \text{CHT3.0} > \text{CHT2.2} > \text{CHT1.4} > \text{Al}_2\text{O}_3 > \text{MgO}$) was found in these two Michael additions after 24 h. Note, CHT1.4 was the least active of the CHT samples for these reactions in comparison to the results of the reaction with the 1,3-dione.

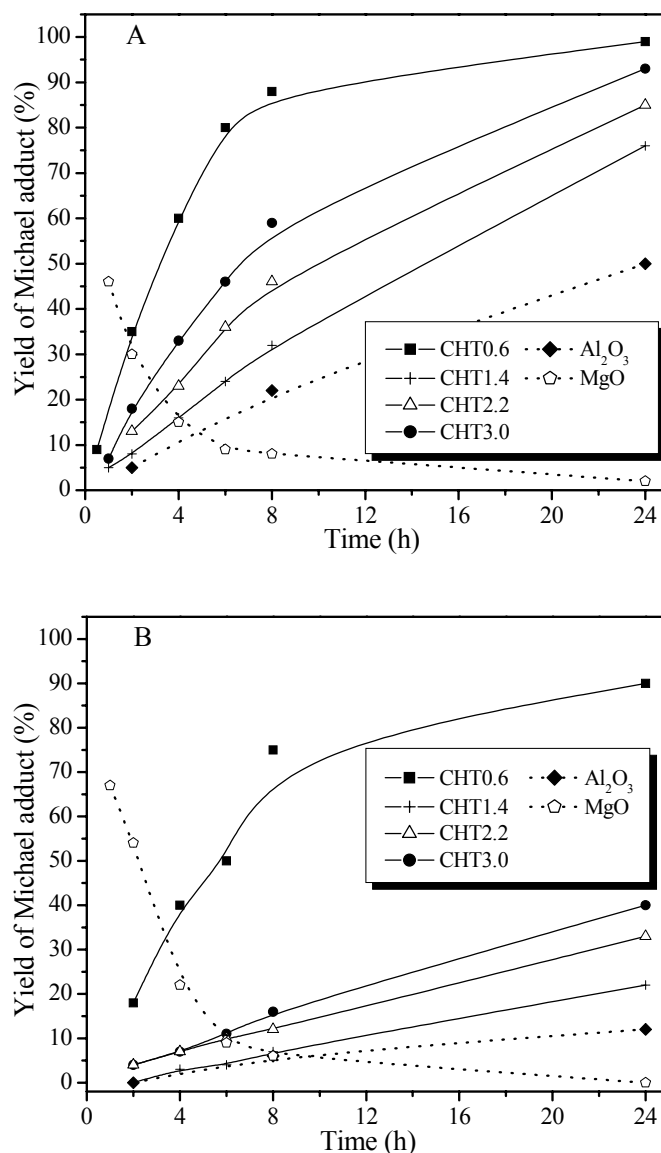


Fig. 5.5 Results of the Michael additions of 2-acetylcyclopentanone (15 mmol) (A) and 2-acetylcyclohexanone (15 mmol) (B) to methyl vinyl ketone (22.5 mmol) in 10 mL methanol over calcined hydrotalcites (0.225 g)

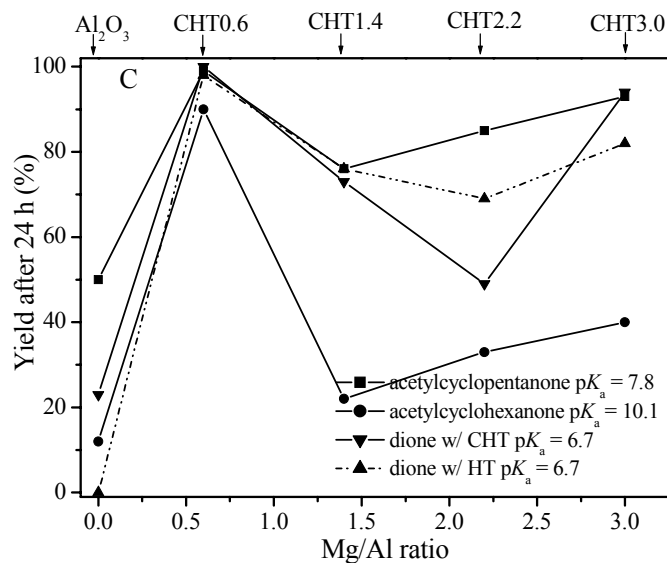


Fig. 5.6 Dependence of Michael adduct yield on Mg/Al ratio of catalyst after 24 h

The correlation between catalytic activity and the Mg/Al molar ratio was again nonlinear (Fig. 5.6) and identical for both reactions. Independent of the sample used (CHT, MgO, or Al₂O₃), the addition of 2-acetylcyclopentanone to methyl vinyl ketone proceeds faster than that of 2-acetylcyclohexanone (i.e., slope of curves is higher in Fig. 5.5A than in Fig. 5.5B up to a reaction time of 8 h). The higher slopes (Fig. 5.5A) and final yields reached after 24 h (Fig. 5.6) are both easily explained by the higher acidity of 2-acetylcyclopentanone (lower pK_a, deprotonation ease). In the case of the less acidic 2-acetylcyclohexanone, CHT0.6 exhibited a much higher activity than that of the other catalysts (Fig. 5.5B and Fig. 5.6). It has been suggested that a decrease in Al contents results in a decrease of the total basic sites, but the fraction of stronger ones increases [213]. The high activity observed for CHT0.6 could also be caused by strong Lewis acid sites discussed below. It was also suggested that the catalytic performance of Mg_yAlO_x catalysts is related not only to the surface density of active sites but also to the nature of the bulk structure and transformations in the cation (Mg²⁺ or Al³⁺) environment induced by a change in the chemical composition [217]. The higher initial yield after 1 h for MgO in the cyclohexanone addition reaction (cf. Fig. 5.5A and 5.5B) indicates a slowed (consecutive) reaction.

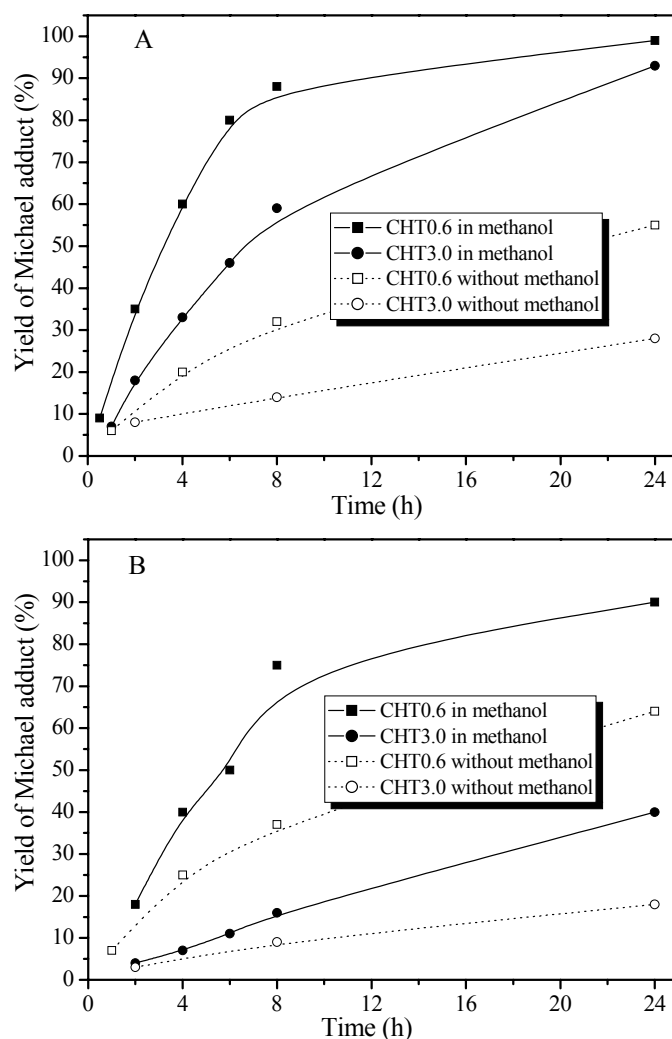


Fig. 5.7 Results of the solvent-free Michael additions of 2-acetylcyclopentanone (15 mmol) (A) and 2-acetylcyclohexanone (15 mmol) (B) to methyl vinyl ketone (22.5 mmol) on CHT0.6 and CHT3.0 (0.225 g)

Solvent-free Michael additions were carried out to examine the possibility of this type of environmentally friendly implementation of the reaction. This was checked with the most active samples, CHT0.6 and CHT3.0, in the Michael additions with 2-acetylcyclopentanone (Penta) and 2-acetylcyclohexanone (Hex) (Fig. 5.7). The reactions were catalyzed without the presence of a solvent, and CHT0.6 is again the more active catalyst; however, yields are decreased for both catalysts: from 99 (Penta) and 90% (Hex) to 55 (Penta) and 64% (Hex) for CHT0.6 and from 93 (Penta) and 40% (Hex) to 28 (Penta) and 18% (Hex) for CHT3.0 after 24 h. Moreover, in the case of CHT0.6, the solvent-free addition of 2-acetylcyclopentanone ($pK_a = 7.8$) to methyl vinyl ketone proceeded slightly slower than that of 2-acetylcyclohexanone ($pK_a = 10.1$). This result of CHT0.6 was

unexpected since the pK_a value of the former 1,3-dione is lower; the addition of former 1,3-dione should proceed faster. However, for CHT0.6, the reactions seem to be independent of the pK_a values of the reactants that are normally determined in water or methanol. The similar result was also observed in base-catalyzed Knoevenagel condensation before [235] and could be explained by the role of the level of stabilization of the carbanionic intermediate throughout the particular interactions between reactant and the catalyst [235]. In contrast, the reaction with cyclopentanone proceeded slightly faster than the latter in the case of CHT3.0. Meanwhile, yields of the target products were lower than those found when a solvent was used for both catalysts after 24 h. The low (delayed) product formation may be related to the absence of solvation necessary to stabilize the carbanion generated from the CH-acid compound for the addition to methyl vinyl ketone. Nonetheless, the investigated heterogeneously catalyzed Michael-additions can be performed under solvent-free conditions with only slightly longer reaction times.

In summary, although the reaction rates and product yields of solvent-free Michael additions were, respectively, slower and lower than those observed in methanol, the solvent-free results are promising regarding their environmental impact.

5.4 Acid-base properties of calcined hydrotalcites

To understand the catalytic behavior of the catalysts, the acid-base properties were characterized by FTIR studies after pyridine and CO_2 adsorption. Temperature programmed desorption (TPD) of the adsorbed probe molecules was used to study the strength of the acid and base sites. Microcalorimetric measurements were also involved in the investigation.

5.4.1 FTIR study of pyridine adsorption

The spectra measured after pyridine adsorption at 40 °C on Al_2O_3 , MgO and CHT samples are shown in Fig. 5.8. The spectra of all the samples show bands for stretching vibrations of pyridine molecules coordinatively bonded to Lewis acid sites between 1630 and 1600 cm^{-1} (ν_{8a} mode) and between 1450 and 1440 cm^{-1} (ν_{19b} mode). Protonation of pyridine on Brønsted acid sites (bands at 1640 and 1540 cm^{-1}) [236,237] was not observed on any of the samples studied here.

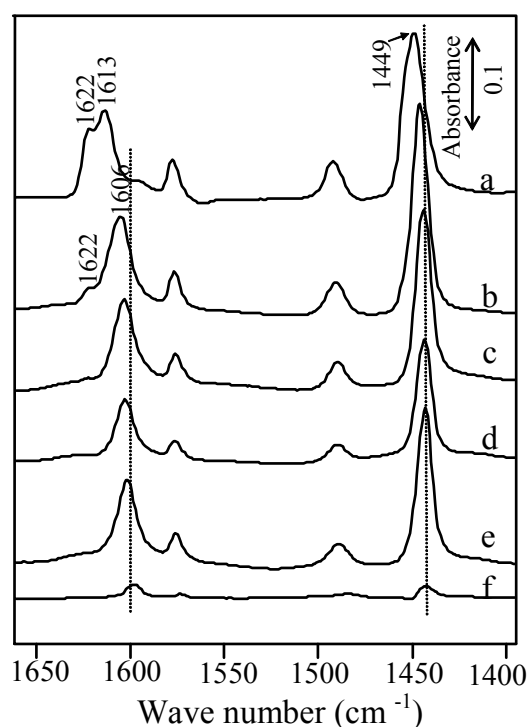


Fig. 5.8 Pyridine adsorption on Al_2O_3 (a), calcined hydrotalcites with Mg/Al molar ratios of 0.6 (b), 1.4 (c), 2.2 (d) and 3.0 (e) and MgO (f). Spectra were measured after adsorption and evacuation at 40 °C

The negligible Lewis acidity of MgO (Fig. 5.8f) indicated by weak bands at 1600 and 1440 cm^{-1} corresponds to coordinatively unsaturated Mg^{2+} cations [237]. The shift of the ν_{8a} band distinguishes the strength of the Lewis acid sites, whereas the intensity of the ν_{19b} band characterizes their number [238]. With increasing aluminum content, the ν_{8a} band shifts to higher wave numbers from 1601 (CHT3.0, Fig. 5.8e) to 1613 cm^{-1} Al_2O_3 (Fig. 5.8a). In general, bands at 1618–1612 and 1626–1620 cm^{-1} on Al_2O_3 are attributed to pyridine bonded to a pair of coordinatively unsaturated Al^{3+} ions in octahedral and tetrahedral positions and coordinatively unsaturated tetrahedral Al^{3+} , respectively [239,240,241,242]. In the spectrum of Al_2O_3 (Fig. 5.8a), an additional band at 1622 cm^{-1} can be ascribed to pyridine strongly adsorbed on Al^{3+} ions in tetrahedral positions, Al_T . A band similar in wave number, but of much lower intensity was observed for the CHT0.6 sample (Fig. 5.8b). These results indicate the presence of stronger Lewis acid sites (involving Al_T) on the surface of Al_2O_3 and CHT0.6, but that CHT0.6 has a much lower number of these sites. The XPS results show that the Mg/Al ratio on the surface of CHT0.6 is slightly higher than in the bulk. The presence of MgO domains probably leads to the decrease in the number of strong acid sites on the surface of CHT0.6. Although ^{27}Al MAS NMR showed that the bulk Al_T/Al_O ratio was identical for Al_2O_3 and CHT0.6–2.2 (0.38),

no band was observed at 1622 cm^{-1} in the IR spectra of CHT1.4 and 2.2 after pyridine adsorption. The $\text{Al}_\text{T}/\text{Al}_\text{O}$ ratio of CHT3.0 was higher (0.59, i.e., octahedral coordination predominates, but the number of Al_T is higher for this sample than for other CHT samples), and the Mg/Al molar ratio was much lower on the surface of CHT3.0 than in the bulk. This would suggest that more Al tetrahedra are on the surface of CHT3.0 and can easily adsorb pyridine. Although this may be the case, it does not lead to the formation of strongly bonded pyridine adsorbate complexes (absence of band at 1622 cm^{-1} in Fig. 5.8e). The presence of the band in Fig. 5.8a and b may have a structural origin. When comparing the CHT patterns, that of CHT0.6 (Fig. 5.1B: d) is the only one with peaks for $\gamma\text{-Al}_2\text{O}_3$ (e.g., at 66°). The presence of the $\gamma\text{-Al}_2\text{O}_3$ structure in CHT0.6 could be of significance in the formation of strong acid sites. No indication of $\gamma\text{-Al}_2\text{O}_3$ is seen in the pattern of CHT3.0 (Fig. 5.1B: a). The influence of increasing Al contents and consequent structural changes on the catalytic activity of Mg-Al mixed oxides has been mentioned before [215,217].

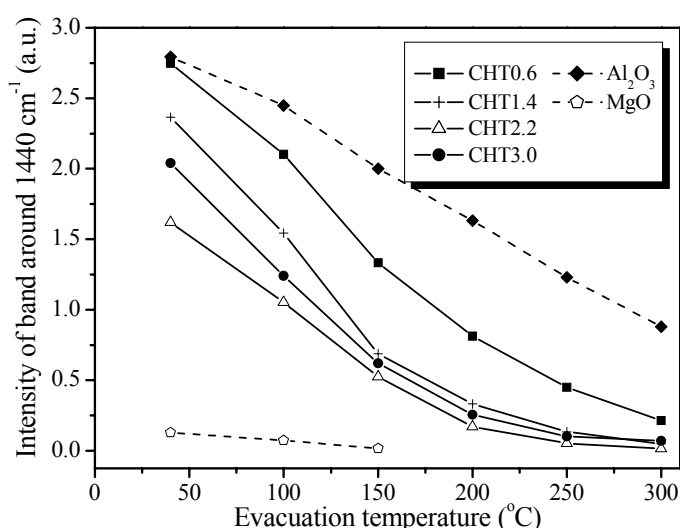


Fig. 5.9 Temperature programmed desorption of pyridine. Effect of the evacuation temperature on the intensity of the band of adsorbed pyridine around 1440 cm^{-1}

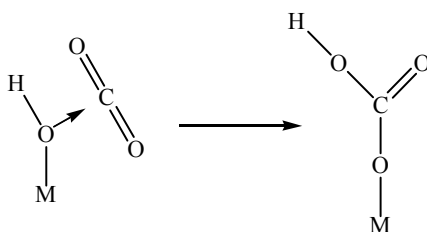
The total amount of absorbed pyridine molecules was estimated by the integration of the band (ν_{19b} mode) around 1440 cm^{-1} . The value calculated after evacuation at different temperatures is plotted against the evacuation temperature in Fig. 5.9. The total number of Lewis acid sites is highest for Al_2O_3 and CHT0.6 (practically identical band intensities at 40°C) and decreases with Al content in the following order: $\text{CHT1.4} > \text{CHT3.0} > \text{CHT2.2}$. Few Lewis acid sites were detected on the surface of MgO, which agrees with weak bands found in Fig. 5.8f. As the evacuation (desorption) temperature was increased, the

integrated intensity, i.e., number of pyridine molecules still adsorbed, decreased. At an evacuation temperature of 200 °C, most of the pyridine on CHT1.4–3.0 had desorbed; higher intensities (> 0.5 a.u.) are only observed for Al_2O_3 and CHT0.6. After evacuation at 300 °C, Al_2O_3 is the only sample with a band intensity over 0.5 a.u. These experiments show that while the CHT1.4–3.0 have varying amounts of acid sites (different band intensities after evacuation at 40 °C), they have a similar number of stronger acid sites (similar intensities after evacuation at temperatures higher than 150 °C). Thus, the amount of weaker acid sites increases from CHT2.2 to CHT3.0 to CHT1.4, which may explain the slightly lower activity of this sample (CHT1.4) in the Michael addition with 2-methylcyclohexane-1,3-dione in comparison to that of the other CHT samples.

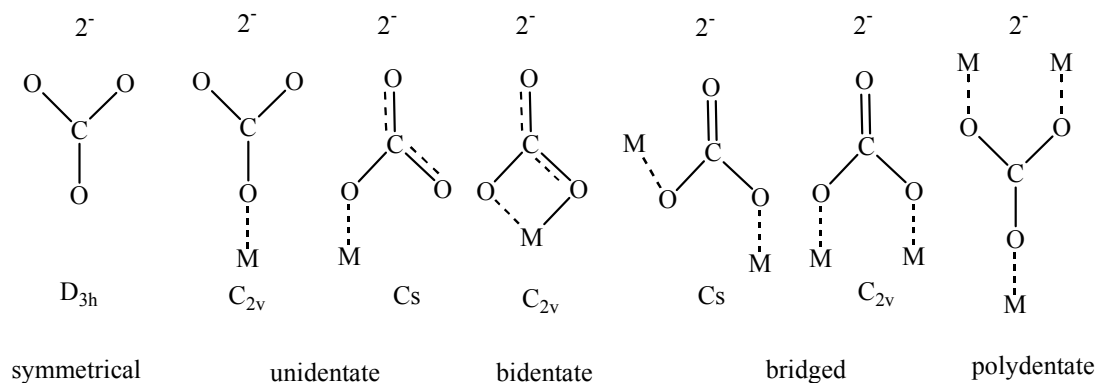
In summary, CHT0.6 has the highest acidity among the CHT samples with respect to the number and strength of acid sites. The total amount of acid sites on the other CHT samples (CHT1.4–3.0) is much lower. The Al-rich sample (CHT0.6) and Al_2O_3 have the same total amount of acid sites (identical intensities at 40 °C), yet the stronger the sites are (the higher the evacuation temperature) the lower their numbers (amount of pyridine still adsorbed) for CHT0.6 compared to that for Al_2O_3 . This may begin to explain the drastic difference in the activity of a) CHT0.6 and Al_2O_3 and b) CHT0.6 and CHT1.4–3.0.

5.4.2 FTIR study of CO_2 adsorption

Because CO_2 is acidic, it adsorbs specifically on basic sites. However, a lot of species can be formed. CO_2 reacts with **basic hydroxyl groups** forming hydrogen carbonate (bicarbonate) species (Scheme 5.1) and with **basic oxygen ions** forming different kinds of carbonate species (Scheme 5.2) [243,244].



Scheme 5.1 Bicarbonate species



Scheme 5.2 Carbonate species

In the infrared spectra of bulk alkaline bicarbonates, which are present in dimer form in solid state, bands are observed at 2620-2450 cm^{-1} ($\nu_{\text{OH}\cdots\text{O}}$), 1655-15 (asym $\nu_{\text{C=O}}$), 1430-1370 (sym $\nu_{\text{C=O}}$) and 1300 cm^{-1} ($\delta_{\text{OH}\cdots\text{O}}$).

The **free carbonate ion** (D_{3h} symmetry) has three IR active vibrations:

ν_3 (E)	asymmetric ν_{CO} vibration:	1415 cm^{-1}
ν_2 (A_2')	out of plane π (CO_3) deformation:	879 cm^{-1}
ν_4 (E)	in plane δ (CO_3) deformation:	680 cm^{-1}
and one Raman active vibration:		
ν_1 (A_1')	symmetric ν_{CO} vibration:	1063 cm^{-1} .

In the adsorbed state, the symmetry is lowered (Scheme 5.2) and the doubly degenerate ν_3 and ν_4 vibrations are splitted and the ν_1 vibration becomes IR active. The splitting of the ν_3 mode is related to the structure of the carbonate (the angular distortion from D_{3h} symmetry within the carbonate ligand) [244]:

$\Delta\nu_3$ ca. 100 cm^{-1}	monodentate
$\Delta\nu_3$ ca. 300 cm^{-1}	bidentate
$\Delta\nu_3$ ca. 400 cm^{-1}	bridged

However, much smaller values (50–150 cm^{-1}) also have been observed for bridging carbonates. The thermal stability of surface carbonates should also be taken into account [5]. For instance, monodentate carbonates are usually less stable than the corresponding bidentate carbonates.

The FTIR spectra (1100–1800 cm^{-1}) of Al_2O_3 , MgO and CHT samples after CO_2 adsorption at 40 °C are shown in Fig. 5.10. The thermal stability of the surface species was studied by desorption experiments at temperatures up to 300 °C (Fig. 5.11, 5.12 and 5.13). Analysis of the spectra allows us to distinguish two different types of surface basic sites on all catalysts, Brønsted base sites (basic OH^- groups) and Lewis base sites (basic O^{2-} ions), and to estimate the respective amount and strength of the basic sites.

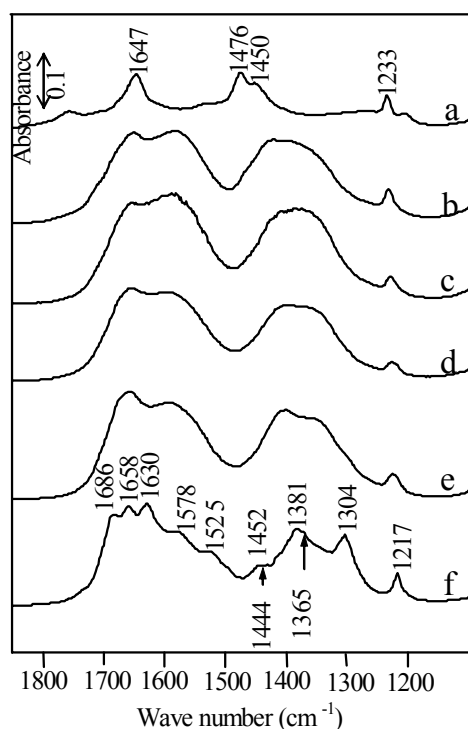


Fig. 5.10 CO_2 adsorption on Al_2O_3 (a), calcined hydrotalcites with Mg/Al ratios of 0.6 (b), 1.4 (c), 2.2 (d) and 3.0 (e), and MgO (f). Spectra were measured after adsorption and evacuation at 40 °C

FTIR study of CO_2 adsorption on Al_2O_3

The predominant species observed on Al_2O_3 (Fig. 5.10a and Fig. 5.11) is bicarbonate (HCO_3^-) with bands at 3609 (ν_{OH}), 1647 (asym $\nu_{\text{C=O}}$), 1476 (sym $\nu_{\text{C=O}}$) and 1233 cm^{-1} (δ_{OH}), which forms on surface basic OH^- groups. Bands at 1756, 1704, 1537, 1265, and 1204 cm^{-1} (Fig. 5.11) and the one at 1450 cm^{-1} can be attributed to surface carbonate species, CO_3^{2-} . The adsorption of CO_2 on surface oxygen atoms can form different types of carbonates, monodentate, bidentate, bridged or polydentate, as mentioned above, depending on the environment of the oxygen atom [243,244]. One of the three IR active vibrations of the free carbonate ion, which possesses D_{3h} symmetry, is the doubly degenerate ν_3 (E) mode at 1415 cm^{-1} . In the adsorbed state, the symmetry of the CO_3^{2-} ion is lowered, and the ν_3 vibration splits into two components ($\Delta\nu_3$) [243,244] dependent on

the structure of the surface carbonates. In the case of Al_2O_3 , this splitting leads to bands at 1756 and 1204 cm^{-1} ($\Delta\nu_3$ splitting = 552 cm^{-1}), which can be assigned to the $\nu_{\text{C=O}}$ vibrations of bridged “organic-like” complexes; the shoulders at 1704 and 1265 cm^{-1} ($\Delta\nu_3$ splitting = 439 cm^{-1}) can be assigned to bidentate carbonate species. The assignment of the bands at 1537 cm^{-1} and 1450 cm^{-1} is less clear, which could indicate the presence of non-coordinated symmetrical carbonate or monodentate carbonate.

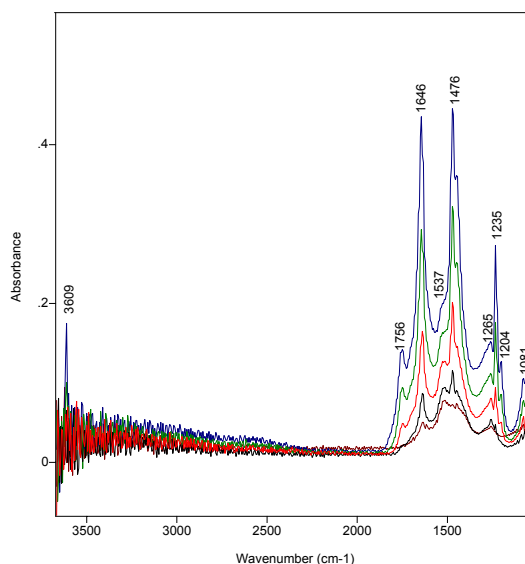


Fig. 5.11 TPD of CO_2 adsorbed on Al_2O_3 , spectra taken in vacuum at 40, 100, 150, 200 and 250 °C

FTIR study of CO_2 adsorption on MgO

The spectrum of MgO (Fig. 5.10f and Fig. 5.12) after CO_2 adsorption is complex with numerous bands between 1800 and 1100 cm^{-1} . The major bicarbonate species is indicated by the bands at 1630, 1452 and 1217 cm^{-1} . Weaker bands (shoulders) at 1600, 1448 and 1200 cm^{-1} (Fig. 5.12) could belong to another type of bicarbonate species. Pairs of bands at 1686/1365 and 1658/1304 cm^{-1} can be assigned to the ν_3 vibrations of two different bidentate carbonate structures. Based on desorption experiments (spectra not shown), the most thermally stable species on MgO have band pairs at 1578/1444 and 1525/1381 cm^{-1} . Based on their low $\Delta\nu_3$ splitting (134 and 144 cm^{-1} , respectively), these bands could be assigned to monodentate carbonate species [244,245,246]. However, since they are observed even at higher evacuation temperatures of 200 °C, i.e., high thermal stability of these corresponding species, they are probably caused by polydentate carbonates [243].

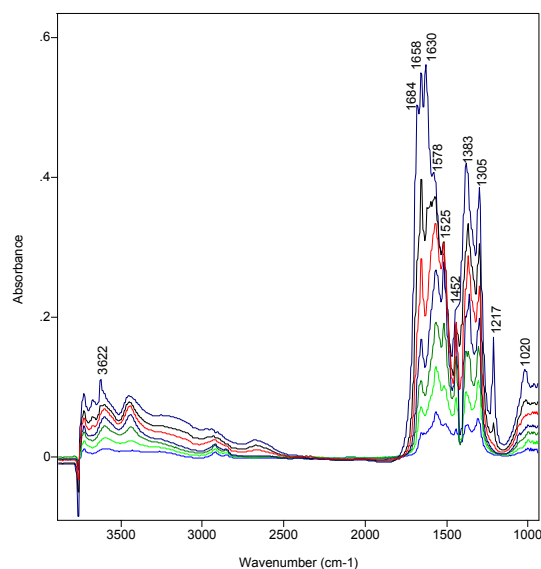


Fig. 5.12 TPD of CO₂ adsorbed on MgO, spectra taken in vacuum at 40, 100, 150, 200, 250 and 300 °C.

FTIR study of CO₂ adsorption on CHT samples

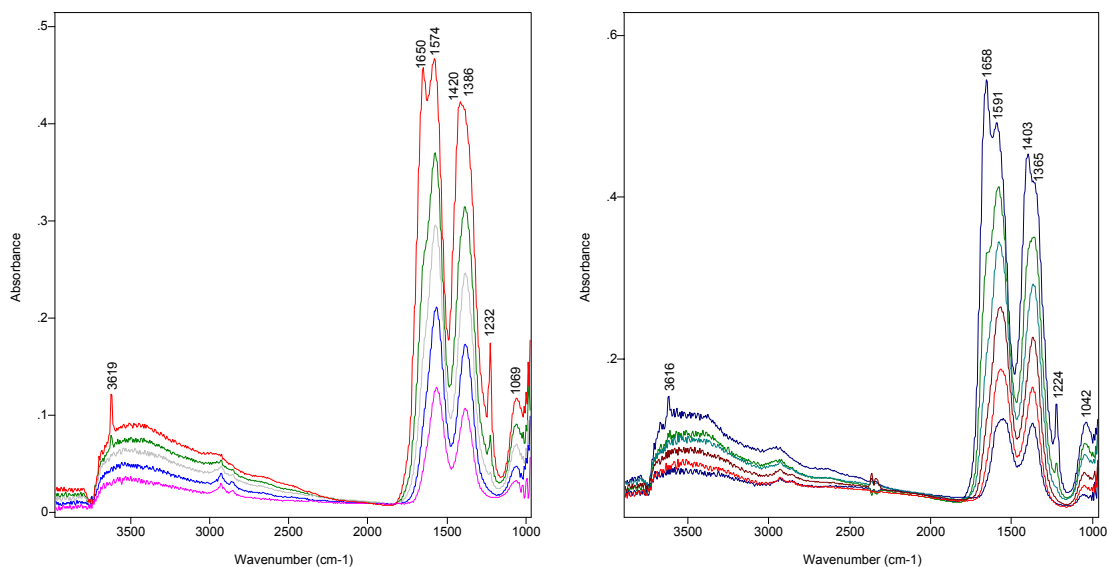


Fig. 5.13 TPD of CO₂ adsorbed on CHT0.6 (left) and CHT3.0 (right), spectra taken in vacuum at 40, 100, 150, 200, 250 and 300 °C

Compared with MgO, a lower structural variety of the carbonates was formed on the surface of CHT samples (Fig. 5.10b–e and Fig. 5.13). Very broad bands are seen in two regions, 1750 to 1500 and 1500 to 1250 cm⁻¹, with a single band between 1233 and 1217 cm⁻¹; the general band shape in these regions closely resembles that found in the spectrum

of MgO without the distinct maxima. The band for bicarbonates formed on the surface broadens and shifts to lower wave numbers (from 1233 cm^{-1} for CHT0.6 in Fig. 10b to 1220 cm^{-1} for CHT3.0 in Fig. 5.10e) as the Mg/Al ratio increases; its intensity also gives information about the number of OH^- species and compares the basicities of surface hydroxyl groups [243,244]. Based on the $\Delta\nu_3$ splittings between 188 and 226 cm^{-1} , the maxima at $1591\text{--}74$ and $1386\text{--}65\text{ cm}^{-1}$ could be assigned to monodentate surface carbonates. On the other hand, the thermal stability of these species is rather high. The bands are observed even after evacuation at $300\text{ }^\circ\text{C}$. Thus, as in the case of MgO, the formation of polydentate structures is likely, similar to that of bulk species [244].

The strength and the amount of base sites

According to Davydov et al. [246], the formation of different types of carbonates is related to the basicity of the surface oxygen atoms. It was postulated that the structural nonuniformity of oxygen ions on the catalyst surface leads to differences in the effective negative charge of the oxygen ions, i.e., their basicity, and that this causes the formation of different carbonate structures. The spectral parameter, $\Delta\nu_3$, was proposed as a measure of the relative strength of surface basic sites [246]: the smaller the $\Delta\nu_3$ value, the stronger the surface basic site is involved in the interaction with CO_2 .

Based on the ν_3 splittings, the following conclusions can be drawn. Al_2O_3 exhibits the weakest Lewis basicity with $\Delta\nu_3$ values of 552 and 439 cm^{-1} for the bridged and bidentate carbonate species, respectively. The strongest basicity was observed for MgO, which formed monodentate species with CO_2 and exhibits the smallest $\Delta\nu_3$ of 134 cm^{-1} . The calcined hydrotalcites are less basic than MgO, but more basic than Al_2O_3 . Here, the strength of basic sites (decrease in $\Delta\nu_3$) of the CHT samples decreases with increasing magnesium content in the following order: CHT0.6 (188 cm^{-1}) > CHT1.4 (209 cm^{-1}) > CHT2.2 (225 cm^{-1}) \approx CHT3.0 (226 cm^{-1}). The relative amount of surface, basic oxygen atoms (Lewis base sites) was estimated by the integration of the carbonate bands (1572 , 1444 , 1517 and 1388 cm^{-1} for MgO, and bands at $1574\text{--}1581$ and $1368\text{--}1386\text{ cm}^{-1}$ for CHT samples) after evacuation at $150\text{ }^\circ\text{C}$, i.e., after removal of bicarbonate species (spectra not shown). When the amount of Lewis base sites is normalized by weight, intensities decreased for the samples in the following order: CHT3.0 \sim CHT1.4 \sim MgO > CHT2.2 > CHT0.6 \gg Al_2O_3 . CHT3.0 has the highest number of weakest Lewis base sites (higher splitting), whose strengths are similar to those found on CHT2.2; Lewis base sites on CHT0.6, the most catalytically active sample, are the strongest, but few in number.

These findings agree with results of Corma et al. who observed that the total amount of basic sites increases, but the proportion of stronger basic sites decreases with increasing Mg/Al molar ratio of calcined hydrotalcites [229].

Finally, the intensity of the OH^- deformation band (around 1230 cm^{-1}) for surface bicarbonates after evacuation at $40\text{ }^\circ\text{C}$ has been used to quantitatively determine the number of basic OH^- species [245]. The amount of basic OH^- groups (Brønsted base sites) on the surface of the calcined hydrotalcites does not correlate linearly with an increase in the Mg/Al ratio (Fig. 5.14). Interestingly enough, however, the decrease in the band intensities (amount of OH^- species), $\text{CHT0.6} > \text{CHT3.0} > \text{CHT1.4} > \text{CHT2.2}$ (Fig. 5.14), does correlate with catalytic activities found for the CHT samples in the Michael addition of 2-methyl-cyclohexane-1,3-dione. This is not true of the Michael addition with the cyclopentanone and cyclohexanone, in which CHT1.4 was less active than CHT2.2. The shift of the 1230-cm^{-1} band to lower wave number indicates that the strengths increase with Mg content from CHT0.6 to MgO. Thus, CHT0.6 has a high number of Brønsted base sites; the Brønsted base sites on CHT3.0 are lower in number, but stronger. This may explain why both of these samples achieved the highest catalytic yields.

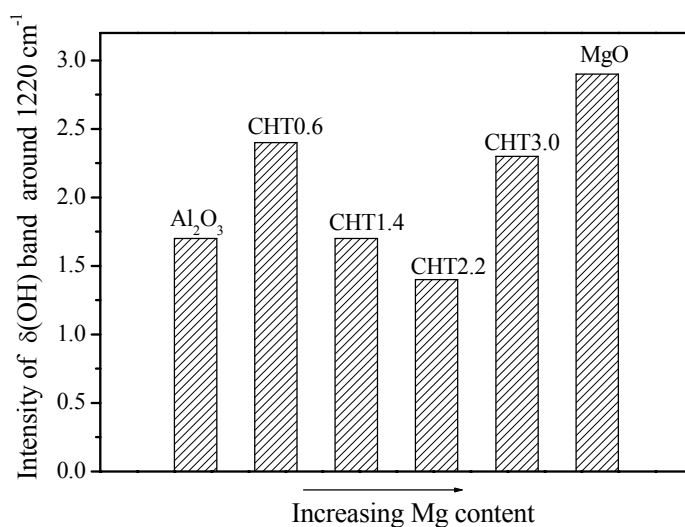


Fig. 5.14 Intensity of band around 1220 cm^{-1} after evacuation at $40\text{ }^\circ\text{C}$

5.4.3 Microcalorimetric measurements

The base sites were further characterized by a series of microcalorimetric measurements using a gaseous probe molecule, CO_2 , and a liquid probe molecule, benzoic acid, to gain new insights into and supplementary information on the basic sites and differences in their behavior in gas atmosphere and in solution.

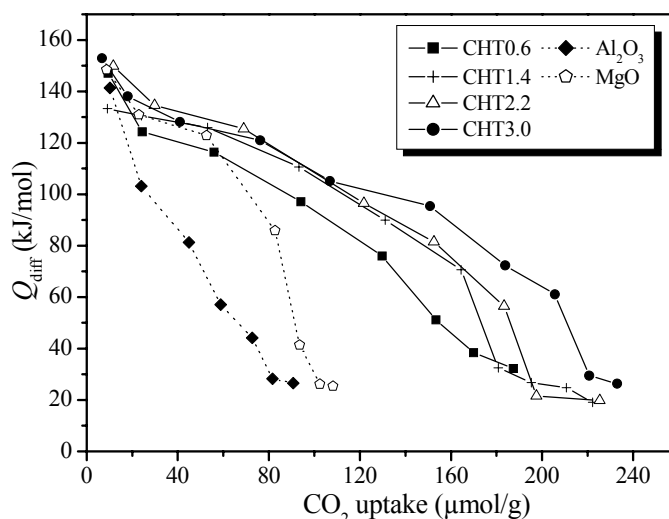


Fig. 5.15 Differential heat of CO₂ adsorption at 40 °C as a function of CO₂ uptake

The curves of the differential heat of CO₂ adsorption as function of CO₂ uptake on calcined hydrotalcites, Al₂O₃ and MgO at 40 °C are shown in Fig. 5.15. The curves for CHT samples are similar in shape; however, MgO and Al₂O₃ do not adsorb CO₂ at high uptakes in comparison to the CHT samples. All of the initial heats are between 130 and 155 kJ/mol. The absence of a plateau of the differential heats at lower uptakes, i.e., the heat of adsorption decreases immediately and continuously with the amount of adsorbed CO₂, indicates basic sites with different strengths exist on all the samples. Based on the differential heats in the entire range of CO₂ uptake (Fig. 5.15), it seems that the strength of basic sites on CHT samples increase with Mg content. In contrast, the FTIR studies of CO₂ adsorption at 150 °C showed that the strength of the Lewis basic sites was highest for MgO, increased with decreasing Mg content, and was the lowest for Al₂O₃: MgO > CHT0.6 > CHT 1.4 > CHT 2.2 ~ CHT3.0 > Al₂O₃ using the spectral splitting (Δv_3). Since the microcalorimetric measurements were performed at 40 °C [close to room (reaction) temperature] instead of 150 °C (FTIR measurements), nonspecific adsorption of CO₂ on basic sites of varying strength can not be excluded from the differential heats measured [247]. Therefore, the differential heat of adsorption of calcined hydrotalcites measured at 40 °C does not accurately determine the strength of the base sites. The measured differential heats may be average values for the sites that the molecules adsorb on; differences among these sites may not be detectable.

To further understand the specific catalytic sites, the amounts of totally and irreversibly adsorbed CO₂ were determined from the adsorption and re-adsorption isotherms at 0.2 Torr;

this pressure was chosen because the level of irreversible adsorption is practically constant above it. The quantitative results are shown in Table 5.2.

Table 5.2

Total and irreversible adsorption of CO₂ at $p = 0.2$ Torr at 40°C

Catalyst	V_{tot} (μmol/g)	V_{irr} (μmol/g)	$V_{\text{irr}}/V_{\text{tot}}$
CHT0.6	155.6	110.3	0.71
CHT1.4	189.4	154.6	0.82
CHT2.2	184.9	140.5	0.76
CHT3.0	201.4	166.5	0.83
Al ₂ O ₃	70.2	44.0	0.63
MgO	97.0	75.1	0.77

The total amount of adsorbed CO₂ including reversible and irreversible adsorption decreases in the following order: CHT3.0 > CHT 2.2 ~ CHT 1.4 > CHT 0.6 > MgO > Al₂O₃. The CO₂ amount decreases with a decrease in Mg content except for MgO. Reversible adsorption involves weak interactions and is ascribed mainly to physisorption. The irreversibly adsorbed CO₂ corresponds to the chemisorption of CO₂; the amount of chemisorbed CO₂ (V_{irr}) decreases in the following way: CHT3.0 > CHT1.4 > CHT2.2 > CHT0.6 > MgO > Al₂O₃. The portion of CO₂ chemisorbed on Al₂O₃ of 0.63 is slightly lower than that of the other samples: 0.71–0.83. MgO has a lower total CO₂ uptake (97.0 μmol/g) and a lower amount of chemisorbed CO₂ (75.1 μmol/g) than those of the calcined hydrotalcites. This may result from the formation of bulk carbonates on strong basic sites on MgO, which are then blocked and inaccessible to CO₂. Species (CO₂) with high thermal stability that exhibit a rather low $\Delta\nu_3$ splitting (134 cm⁻¹ for MgO is smallest observed here), can have a polydentate structure similar to that of bulk species. The intensity of the bands, which corresponds to the amount of Lewis basic sites, decreases similarly to V_{irr} values observed: CHT3.0 ~ CHT1.4 ~ MgO > CHT2.2 > CHT0.6 > Al₂O₃ with exception of MgO (FTIR). This suggests the results of microcalorimetric gas-phase CO₂ adsorption under our conditions do give some information about the amount of basic sites, but are not accurate in regard to strength.

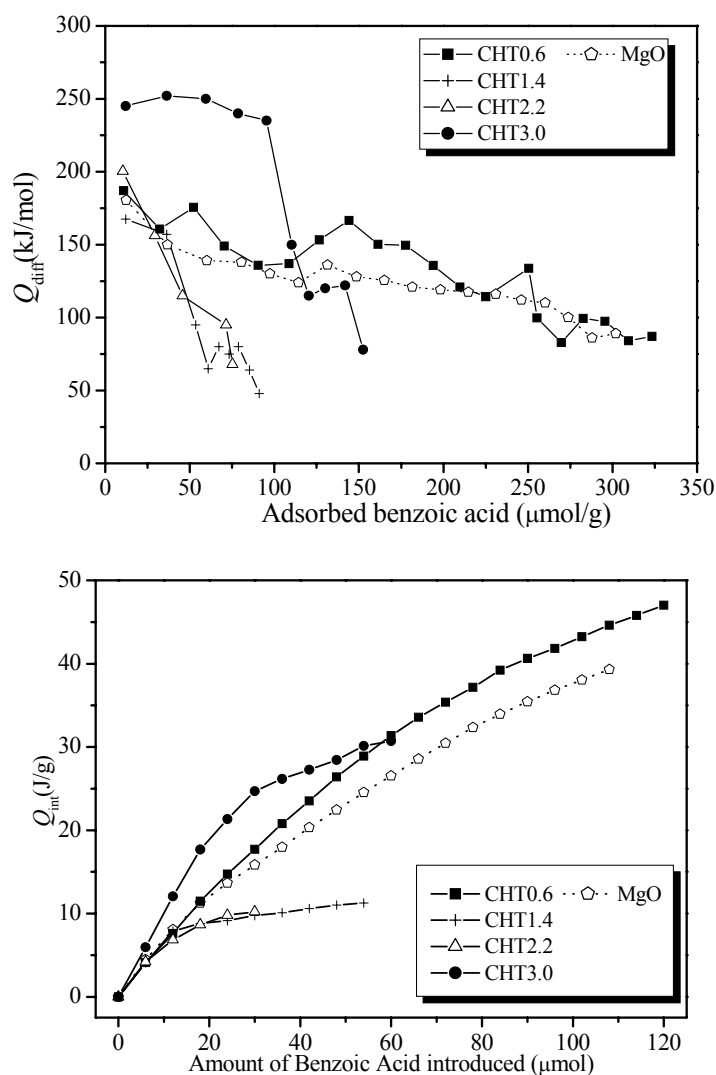


Fig. 5.16 Differential heat (up) and integral heats (down) of adsorption of benzoic acid in toluene measured by microcalorimetry at 70 °C, except for that of MgO (at 40 °C)

Benzoic acid is used for the measurement of the strength and amount of basic sites by indicator titration [11]. Microcalorimetric measurements with benzoic acid in toluene were also performed here to measure basicity under liquid phase conditions identical to that of the catalytic test reactions studied here. The curves of the differential heat and integral heat of adsorption are shown in Fig. 5.16 for MgO and CHT0.6–2.2. The number of base sites (amount of benzoic acid uptake) differs from that found using CO_2 and decreases in the following order: $\text{CHT0.6} > \text{MgO} > \text{CHT3.0} > \text{CHT2.2} \sim \text{CHT1.4}$; in this case, not CHT3.0, but CHT0.6 has the most base sites and MgO has more sites using the benzoic acid probe molecule than the rest of the CHT samples. Based on the integral heats measured, the following order of decreasing strength was observed: $\text{CHT3.0} > \text{CHT0.6} > \text{MgO} > \text{CHT1.4} \approx \text{CHT2.2}$. The change in the order of decreasing amounts of acid sites, i.e., MgO after

CHT0.6 has the second highest amount of base sites found using benzoic acid, could be a direct effect of the absence of site blocking by the probe molecule.

Since chemisorption of CO₂ occurs on the catalytically active base sites, the amount of chemisorbed CO₂ should correlate with the catalytic results. However, here, the gas phase microcalorimetric results do not agree with the activities found for the liquid phase Michael reactions. In contrast, the activities of CHT samples in the Michael additions directly relate to the amount of the base sites determined by liquid phase microcalorimetric measurements. This reflects the difference in behavior of base sites in the gas and liquid phase. Differences in the base site properties of MgO with the probe molecules, however, also suggest that the chemistry of the probe molecule may influence their number and strength. Interestingly enough, the base sites of CHT1.4 and 2.2 were similar in strength and number using the probe molecule, benzoic acid; these sites were also similar in number based on gas phase microcalorimetry experiments, but CHT1.4 chemisorbed more CO₂ than CHT2.2. These gas phase result indicate some differences between CHT1.4 and 2.2 and may begin to explain the reactant-dependent catalytic behavior of these two samples.

5.5 Correlation of catalytic behavior and the acid-base properties

Information regarding the nature, strength and number of the acid-base sites obtained from the FTIR and microcalorimetric measurements is crucial to understanding the relationship between acid-base properties and catalytic activities. To clarify this relationship the results of these measurements and findings are discussed here by answering several questions.

Is the acidity responsible for the activity?

Michael additions can be catalyzed by not only base catalysts, but also acid catalysts. Acid-catalyzed Michael additions have been reported for such catalysts as acetic acid [159] (homogeneous catalyst) and metal complexes [146] or TS-1 molecular sieve [147] (both heterogeneous catalysts). However, among the oxide catalysts studied here, Al₂O₃, which has the strongest and highest amount of Lewis acid sites (IR, pyridine adsorption), as well as the weakest and lowest amount of base sites compared with CHT samples (IR, CO₂ adsorption) was the least active in the Michael additions. Moreover, when HS-AlF₃ [248], a very strong Lewis acid, was used as a catalyst for the Michael addition with 1,3-dione,

no obvious activity was observed. These results suggest that the acid sites are not the main ones responsible for catalytic activity and that they cannot catalyze the Michael additions independently of base sites. Interestingly enough, Al_2O_3 does show a considerable activity (50% catalytic yield) in the Michael addition of 2-acetylcyclopentanone ($\text{p}K_{\text{a}} = 7.8$) (Fig. 5.5A). The presence of weak base sites combined with mild acid sites on Al_2O_3 can catalyze the Michael addition to some extent. In other words, the important active sites determining the catalytic activity for Michael additions investigated here are base sites. However, the cooperation of the acid sites with the base sites can not be excluded. This is indicated by the very high activity of CHT0.6, the only sample to exhibit acid sites similar to those found in Al_2O_3 , but much lower in number (IR, pyridine adsorption). These acid sites are much stronger than those in the other CHT samples.

Which base sites contribute to the Michael additions, Brønsted base or Lewis base sites or both?

For hydrotalcites, Brønsted base sites (OH^- groups) are the main base sites. However, Lewis and Brønsted base sites (O^{2-} anions) are present on the surface of MgO and the calcined hydrotalcites (CHT samples). As demonstrated in the Michael additions of 1,3-diones, both kinds of sites catalyze the reaction. This result is very different from that of Choudary et al.[141], who observed that Brønsted base sites exclusively catalyzed the Michael additions. Moreover, it is interesting that the amount of Brønsted base sites (Fig. 5.14) on the CHT samples correlates with the catalytic yields; CHT0.6 and CHT3.0, which have the highest number of OH^- groups (Brønsted base sites, Fig. 5.14), achieved the highest catalytic yields. However, this does not prove that the Brønsted base sites are the only active sites for the reactions. Lewis base sites on the CHT samples predominate with respect to their amount and the strength in comparison to those of the Brønsted base sites; this suggests that OH^- groups enhance catalytic activity, but by no means exclusively cause it.

Does the base strength influence the selectivity?

MgO did not selectively produce the target Michael adducts. This could be attributed to the very strong Lewis basic character of MgO , which is demonstrated by FTIR; the reaction pathway of the resulting consecutive reaction is shown in chapter 3. $\text{Mg}(\text{OH})_2$ exhibits the same poor selectivity as MgO in the reaction with the 1,3-dione because of its expected strong Brønsted basicity, yet the reaction was much faster with $\text{Mg}(\text{OH})_2$ (4 h).

This indicates that the reaction time needed decreases with an increasing number of Brønsted base sites. It seems clear that Michael additions investigated here are selectively catalyzed by moderate strength base sites, Brønsted base or Lewis base sites ($\Delta\nu_3$), in methanol. The strength of the base sites that is lower than those on MgO prevents consecutive reactions and yields high selectivities.

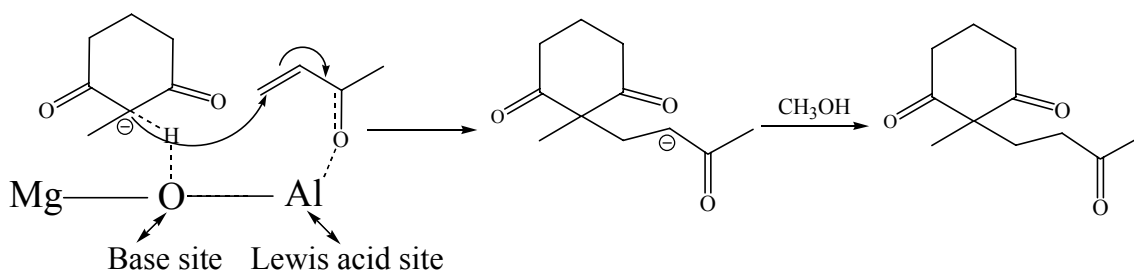
What is more important: the strength or the amount of moderate basic sites?

And what is the possible mechanism of reaction?

For the Michael additions, the performance of the calcined hydrotalcites in the reactions depended on the Mg/Al molar ratios and the acidity of the Michael donors. The general activity of the catalysts has following order: CHT0.6 > CHT3.0 > CHT2.2 ~ CHT1.4. A direct (linear) correlation between the Mg/Al molar ratios and the catalytic behavior was not observed. However, based on the catalytic behaviors, the four CHT catalysts can be divided into two groups. One is the Al-rich sample CHT0.6, which showed the highest activity in all three reactions. High yields (90–99%) were obtained after 24 h for all three Michael additions. The second group includes the Mg-rich samples (Mg/Al > 1.0). Why CHT0.6 is the most efficient catalyst should be related to its special acid-base properties. Regarding strength, CHT0.6 ($\Delta\nu_3 = 188 \text{ cm}^{-1}$) has the strongest Lewis base sites after those on MgO ($\Delta\nu_3 = 134 \text{ cm}^{-1}$) and medium-strength Lewis acid sites comparable to strength of those on Al_2O_3 . Regarding amount of base sites, CHT0.6 has the most Brønsted base sites and highest total number of base sites determined by IR and liquid phase microcalorimetric measurement, respectively. It is interesting to point out that the activity directly correlates with the amount of the base sites determined by the liquid phase microcalorimetric measurements. However, as mentioned above, the acid sites may participate in and enhance the catalytic process, because the difference in the amount of the Lewis base sites between CHT0.6 and the other three samples does not completely explain its outstanding behavior in the Michael addition of 1,3-dione, especially with 2-acetylcyclohexanone with a high $\text{p}K_{\text{a}}$ value.

Therefore, a plausible mechanism based on the cooperation of the acid sites with the basic sites (synergy) is presented in Scheme 5.3. Initially, the 1,3-dione is exclusively activated by deprotonation of the α -C atom between the two ketone groups by base site on the surface of the catalyst to produce a carbanion. At the same time, methyl vinyl ketone via its O atom is bonded to the surface of the adjacent Lewis acid site. Then, the carbanion attacks the carbon atom at β -position of methyl vinyl ketone to form the product anion. The

product anion picks up a proton from the catalyst surface or from solvent to yield product. Basic and acidic sites located close to each other cooperate to yield high activities. A similar synergy on Mg-Al oxide has also been suggested by Yamaguchi et al. for the cycloaddition of carbon dioxide to epoxides [223]. Climent et al. also observed a cooperative effect between weak acid and base sites in aldol condensations on solid catalysts [249]. Indeed, if the appropriate strength of the active site is one of the keys in the catalytic cycle, an important aspect is the stabilization of the reaction intermediates [90]. When the methyl vinyl ketone is bonded to the adjacent Lewis acid sites, which exist on CHT samples and Al_2O_3 , the intermediates are stabilized and the methyl vinyl ketone becomes more reactive. In fact, for CHT0.6, the acid sites are stronger and higher in number than those of the Mg-rich samples; these acid sites make the cooperative effect between base and acid sites more apparent and distinct in the Michael addition of 1,3-dione, especially with 2-acetylcyclohexanone with a high $\text{p}K_{\text{a}}$ value.



Scheme 5.3 Plausible mechanism of Michael addition of 1,3-dione to methyl vinyl ketone over acid-base pairs on calcined hydrotalcites

In the absence of moderate-strength acid sites for the first step of the reaction, although there is slight difference in the strength of base sites on CHT samples depending on the Mg/Al molar ratio, the strengths of the base sites of the Mg-rich CHT samples are all strong enough to activate the 1,3-dione. Thus, the amount of base sites, *normalized to the same weight of the catalyst*, may determine the rate of the reactions and the yields of Michael adduct in the same reaction time. In this case, the behavior $\text{CHT3.0} > \text{CHT2.2} \sim \text{CHT1.4}$ also directly correlates the results of the FTIR and microcalorimetric measurements; the amount of base sites decreases in the following order: $\text{CHT3.0} > \text{CHT2.2} \sim \text{CHT1.4}$. Both the intermediate stabilization by acid sites and the strength of the base sites decreases with increasing Mg/Al ratio, whereas the amount of basic sites

increases with higher Mg/Al ratios; this “compensation” explains the V-like (first decrease then increase, Fig. 5.6) catalytic behavior of the CHT samples with increasing Mg/Al ratio.

In conclusion, the optimal balance of acid-base properties compared to that of Al_2O_3 and MgO makes the Al-rich calcined hydrotalcite an excellent catalyst in the Michael addition of numerous 1,3-diones independent of their $\text{p}K_{\text{a}}$ values.

5.6 Conclusions

Calcined hydrotalcites exhibit Lewis acid, Brønsted base, and Lewis base sites. The Al-rich sample (Mg/Al molar ratio of 0.6) possesses Lewis acid sites similar in strength to those found on Al_2O_3 , but stronger than those found on the Mg-rich hydrotalcites.

Hydrotalcites and calcined hydrotalcites catalyze the Michael additions of 2-methylcyclohexane-1,3-dione, 2-acetylcyclopentanone, and 2-acetylcyclohexanone to methyl vinyl ketone with high selectivity (no side product formation). These heterogeneously catalyzed Michael additions in methanol proceeded faster than the solvent-free reactions.

Pure Al_2O_3 was the least active among the investigated catalysts. Both the Al-rich hydrotalcite and calcined hydrotalcite (Mg/Al molar ratio of 0.6) gave product yields above 95% within 24 h.

A nonlinear correlation between the Mg content and catalytic activity suggested the activity of pure MgO surpasses that of the calcined hydrotalcites, but causes consecutive reactions of the Michael addition products, which reduce the product selectivities and yields.

Catalytic activity correlates with the amount of the base sites determined by benzoic acid microcalorimetry dependent on the Mg/Al molar ratio.

An optimal balance of acid-base properties may make the Al-rich calcined hydrotalcite an excellent catalyst in the Michael addition of numerous 1,3-diones independent of their $\text{p}K_{\text{a}}$ values.

Chapter 6

*Sol-gel preparation, characterization and
catalytic behavior of Mg(O,F)*

6.1 Introduction

Sol-gel preparation of catalytic materials has the ability to change physical characteristics such as surface area, pore size distribution and pore volume, and vary compositional homogeneity at a molecular level. Moreover, during sol-gel step, it is possible to introduce several components into solution to prepare multi-component oxides and bimetallic catalysts. A promoter or an active species can also be introduced to catalysts by sol-gel process. With its versatility and excellent control on a product's characteristics, sol-gel method has played an important role in catalyst preparation and will continue to do so [250].

In chapter 3, MgO catalysts were found too strong solid base to catalyze Michael addition selectively; in contrast, in chapter 5 calcined Mg-Al hydrotalcites (mixed oxides) with suitable acid-base properties are highly efficient and selective catalysts for Michael additions. F^- and O^{2-} are similar "basic" anions; however, MgF_2 is neutral and catalytically inactive, while MgO is a strong base. Thus, the question was if by sol-gel method OH^- or O^{2-} groups can be introduced into the MgF_2 framework and obtain new compounds and tune the acid-base properties of the resulting materials.

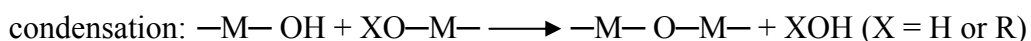
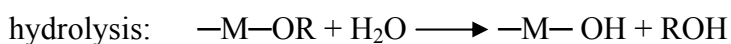
Recently, a novel facile sol-gel synthesis route was reported to prepare high-surface-area X-ray amorphous metal fluorides [248,251], such as AlF_3 and MgF_2 . The resulting high-surface-area AlF_3 (HS- AlF_3) has not only a very high surface area but also an extremely strong Lewis acid [248]. More recently, the first aluminum alkoxide fluoride was prepared by a sol-gel fluorination method and the process of fluorination was presented in detail [252]. As in the case of oxides, the sol-gel process was proved an efficient method to prepare fluoride compound with special properties. Meanwhile, "F-anion-doped" metal oxo/hydroxidefluorides prepared by fluorination of metal oxides [253,254,255], aluminum chloride fluoride [256] and aluminum bromide fluoride [257] were proved to have some special structure and catalytic properties in many acid-catalyzed reactions. Acidic Al(III), Cr(III), Fe(III) oxyhydroxy-fluorides were also synthesized by Demourgue et al. [258]. A review about fluorinated metal oxides and metal fluorides as heterogeneous catalysts is also available [259].

Therefore, in this chapter, an amorphous-like magnesium oxide/hydroxidefluoride, $Mg(O,F)$, with high surface area was prepared by soft sol-gel fluorination-hydrolysis method for the first time and the structure properties are studied by XRD, FTIR, XPS, ^{19}F

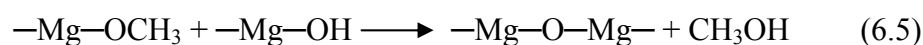
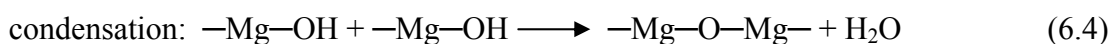
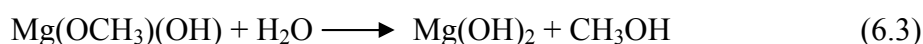
MAS NMR. Magnesium oxide/hydroxidefluoride catalysts were also tested in Michael additions of CH-acid compounds with methyl vinyl ketone.

6.2 Sol-gel preparation

Sol-gel method is widely used to prepare materials with high surface areas, such as ZrO_2 [260], Al_2O_3 [261] and MgO [177,262]. Generally, at its simplest level, sol-gel process can be achieved through the hydrolysis and condensation of a metal alkoxide.



However, using $Mg(OCH_3)_2$, the sol-gel process may involve following reactions:



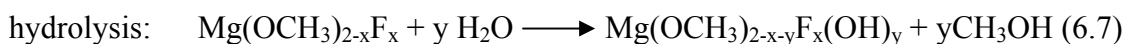
The formation of gel from the hydrolysis of alkoxides involves simultaneous hydrolysis and polycondensation reactions. It is found the hydrolysis does not complete according to Eq.(6.1) even an adequate amount of water is added. Instead, a stepwise hydrolysis according to Eq.(6.2) and Eq.(6.3) are suggested [263]. Eq.(6.3) is also suggested to be reversible reaction, therefore, the hydrolysis may proceed to completion as shown in Eq.(6.2), but not complete according to Eq.(6.3). Moreover, condensation reactions [Eq.(6.4) and Eq.(6.5)] are simultaneous to hydrolysis, which may be the reason why the hydrolysis step does not complete. Finally, an intimate gel of $MgO-Mg(OH)_2-Mg(OCH_3)(OH)$ may be obtained.

In our case of preparation of magnesium oxide/hydroxidefluoride, before the hydrolysis step, $Mg(OCH_3)_2$ is first partial fluorinated with anhydrous HF/Et_2O solution via following reaction [Eq.(6.6)]:

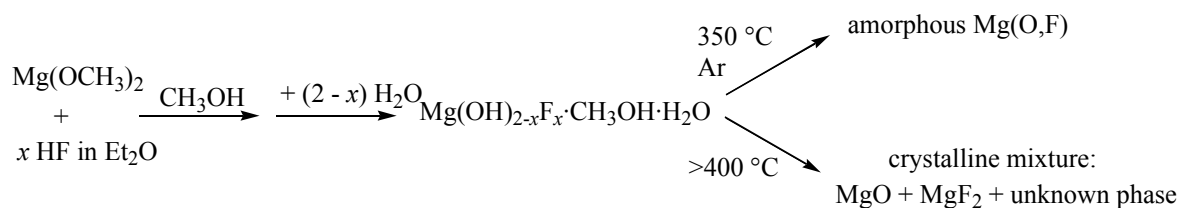


If stoichiometric amount of HF is used, it is supposed to obtain pure MgF_2 . Since MgF_2 is a neutral material, which is of less interest, our aim is not to prepare MgF_2 . Moreover, in

the case of preparation of high-surface-area AlF_3 , under non-aqueous conditions, it was found only aluminum alkoxide fluoride was obtained even stoichiometric amount of HF was used. Thus, a second gas phase fluorination step was applied to get the pure high-surface-area of AlF_3 [248]. However, here, after fluorination, further hydrolysis is used to introduce $-\text{OH}$ groups into the framework of the final product via following reaction [Eq.(6.7)].



Consequently, the sol-gel process for the preparation of magnesium oxide/hydroxidefluoride with different F contents (see Table 6.1, MOF-0.4–MOF-2.0) involved two steps (scheme 6.1): (1) Synthesis of fluoride precursor gel under non-aqueous conditions by partial fluorination of magnesium methoxide with anhydrous HF/ Et_2O solution (*HF is dangerous, which must be handled with care*); 2) one-pot hydrolysis of the precursors by adding moderate excess of water to the gel. By this soft sol-gel method, fluoride and hydroxide groups can be simultaneously introduced into the network of the final product. Typically, dried CH_3OH (100 mL) was added to magnesium metal (5.0 g, small turnings, 99.98%, Aldrich) in a round-bottom flask with a reflux condenser. After the mixture reacted for about 1–2 h, the $\text{Mg}(\text{OCH}_3)_2$ solution was transferred to a PTFE (polytetrafluoroethylene) bottle. Then a certain amount of HF/ Et_2O (17.4 mol/L) was added to $\text{Mg}(\text{OCH}_3)_2$ drop by drop at 0 °C in an ice bath and the resulting mixture was stirred for 4–6 h in the tightly closed PTFE bottle. After that, certain amount (a two-fold stoichiometric amount) of distilled water was then added and the reaction mixture was stirred overnight. The final gel was evaporated under vacuum at around 50 °C to produce dry powder. The dry powder was calcined in a flow-through tube furnace at 350 °C under Ar for 3 h to get the catalyst for Michael addition. The detailed preparation conditions were shown in Table 6.1.



Scheme 6.1 Sol-gel preparation of the Mg(O,F) samples

Samples MgO-s and MgF₂-s (Table 6.1) were also prepared by only hydrolysis step with four-fold stoichiometric amount of H₂O (MgO-s) and only fluorination step with 2.5-fold stoichiometric amount of HF (MgF₂-s), respectively. Meanwhile, the precursor samples were also prepared by only partial fluorination step (i.e. without hydrolysis step, see Table 6.1, MF-1.0–MF-2.0) as reference materials.

The series of samples (MOF and MF) are denoted in the following way: MOF-1.6 for the magnesium oxyfluoride [Mg(O,F)] fluorinated with a preparation F/Mg ratio of 1.6 and hydrolyzed; MF-1.6 for the magnesium oxyfluoride precursor fluorinated with a F/Mg ratio of 1.6 without hydrolysis; MgO-s and MgF₂-s are MgO and MgF₂ prepared by sol-gel method, respectively. MgF₂-c is a commercially available MgF₂ (Aldrich, 99%).

Table 6.1

Preparation conditions, elemental analysis results and texture properties of the samples

Sample	HF/Mg (mol ratio)	H ₂ O/Mg (mol ratio)	C (wt%) ^a	X (wt%) after calcination ^b			F/Mg ^e	O/Mg ^e
				C	H	F		
MgO-s	0	4.0	5.19	1.34	1.18	-	-	1.1
MOF-0.4	0.4	3.2	5.86	3.15	2.12	10.19	0.3	1.0
MOF-0.8	0.8	2.4	7.85	3.94	2.26	23.36	0.5	0.9
MOF-1.2	1.2	1.6	5.93	2.86	1.57	28.10	0.8	0.7
MOF-1.6	1.6	0.8	5.01	1.51	1.02	40.60	0.9	0.5
MOF-2.0	2.0	0.8	3.12	0.20	0.23	49.19	-	-
MF-1.0	1.0	0	17.87	11.67	3.02	23.99	-	-
MF-1.6	1.6	0	10.00	2.95 ^f	1.20 ^f	n.d.	-	-
MF-2.0	2.0	0	8.47	n.d.	n.d.	n.d.	-	-
MgF ₂ -s	2.5	0	0.58	0.05	0.04	56.17	-	-
MgF ₂ -c ^c	-	-	-	0.03 ^c	0 ^c	59.52 ^c (62 ^d)	-	-

a: before calcination

b: after calcination in Ar at 350 °C

c: commercial product without further calcination

d: calculated value

e: determined by XPS

f: after calcination in air at 350 °C

6.3 Characterization of Mg(O,F) samples

Elemental analysis

The elemental analysis results of samples are summarized in Table 6.1. High carbon contents (3–8 wt%) on the as-prepared samples could be attributed to remaining –OCH₃

groups [263,264] or adsorbed organic compounds. The remaining $-\text{OCH}_3$ groups could not even totally substituted by the second hydrolysis step. The carbon contents of dried precursor gels (MF-1.0, MF-1.6 and MF-2.0, prepared without further hydrolysis step) are much higher than that of corresponding final dried $\text{Mg}(\text{O},\text{F})$ samples after hydrolysis (e.g. 10 wt% carbon content for MF-1.6 and only 5 wt% carbon content for MOF-1.6). Compared the carbon contents, it indicates the second hydrolysis completed around 50% during the sol-gel process. Thus, the hydrolysis step seems to be critical to the substitution of alkoxy groups with hydroxy groups, yet the carbon contents indicates that the hydrolysis step does not result in complete replacement of the methoxy groups with hydroxy groups despite the two-fold stoichiometric amount of water used, which is same as the previous results [263]. Hence, in our case, $\text{Mg}(\text{OCH}_3)_{2-x-y}\text{F}_x(\text{OH})_y$ (x and y depended on the HF/Mg and $\text{H}_2\text{O}/\text{Mg}$ ratios) was probably formed after the fluorination and hydrolysis of the solution of $\text{Mg}(\text{OCH}_3)_2$ in methanol.

After calcination, the carbon contents decrease more or less due to the remove of residual organics. However, the remaining $-\text{OCH}_3$ groups could not even totally removed by calcination at $350\text{ }^\circ\text{C}$ in Ar (Table 6.1), which agrees with the results in literature [265]. When the nominal ratio of HF/Mg was increased, the final carbon contents after calcination decreased to some extent; the experimental fluorine contents increased linearly with the amount of HF added (MOF series). It is interesting to note that the carbon content of MgF_2 -s prepared by this method was only 0.58% and 0.05%, respectively, before and after calcination. The low carbon contents found for MgF_2 -s suggests that the addition of excess HF does lead to the complete removal of $-\text{OCH}_3$ groups. On the other hand, the fluorine content of this sample (56.17 wt%) indicates incomplete fluorination (MgF_2 : 62 wt%). Oxygen as either O^{2-} or OH^- must be present in the network. Compared the nominal F contents, it was found that the F contents were less than the corresponding theoretical values, even for MgF_2 -s, because HF could not completely react with $\text{Mg}(\text{OCH}_3)_2$ under the conditions. The measured and calculated F content of commercial MgF_2 are 59.52% and 62%, respectively. The difference comes from the measurement.

Textural properties

The $\text{Mg}(\text{O},\text{F})$ samples after calcination at $350\text{ }^\circ\text{C}$ in Ar have very high surface areas ($270\text{--}390\text{ m}^2/\text{g}$, Table 6.2) with high pore volumes ($0.37\text{--}0.56\text{ cm}^3/\text{g}$, Table 6.2) except that MOF-2.0 has a relative lower surface area of $104\text{ m}^2/\text{g}$ with pore volume of $0.38\text{ cm}^3/\text{g}$. However, the surface area of MgF_2 -s is only $27\text{ m}^2/\text{g}$, which is similar to that of MgF_2

prepared by normal methods [266]. Commercially available MgF_2 has only surface area of $0.4 \text{ m}^2/\text{g}$. The surface areas of the fluorinated MOF samples (MOF-0.4–1.6) may be roughly related to the carbon ($-\text{OCH}_3$) contents (high C, high S_{BET}), whereas MgO-s has a low carbon content (1.5 wt%) but an incredibly large surface area ($373 \text{ m}^2/\text{g}$). This suggests a different relationship between the carbon content and surface area in systems containing only magnesium and oxygen.

Table 6.2

Texture properties of the samples

Sample	$S_{\text{BET}} (\text{m}^2/\text{g})$	$V_{\text{BJH-d}} (\text{cm}^3/\text{g})^b$	$d_{\text{avg}} (\text{\AA})^c$
MgO-s	373	0.58	62
MOF-0.4	327	0.37	46
MOF-0.8	387	0.45	48
MOF-1.2	363	0.56	62
MOF-1.6	278	0.46	66
MOF-2.0	104	0.38	146
$\text{MgF}_2\text{-s}$	27	0.16	230
$\text{MgF}_2\text{-c}^a$	0.4	0.005	427

a: commercial product without further calcination

b: BJH desorption cumulative pore volume of pores between 17.0 and 3000.0 Å diameter

c: Average pore diameter by BET

The adsorption/desorption isotherms of all the samples are of type IV, which are obtained for mesoporous adsorbents. The isotherms and hysteresis loops are slightly different depending on the F contents (Fig. 6.1). Combination of the isotherm shape with the analysis of the shape and the width of the hysteresis loop can give the main information on the texture characteristics of a solid [267]. Small mesopores in MgO-s and MOF-0.4–1.6 are indicated by a closing of the hysteresis loop at P/P_o values of ca. 0.4. Larger mesopores are found in the samples with higher fluorine contents, MOF-2.0 and $\text{MgF}_2\text{-s}$, whose loops close at around 0.6 and 0.7, respectively. All the samples exhibit a limited amount of macroporosity (i.e., slight increase in adsorption between 0.95 and 1.00), which can be attributed to N_2 adsorption between particles. The observed loops in Fig. 6.1 indicate that the types of pore formed depend on the fluorine content from small cone-shaped pores (MgO-s) to ink-bottle pores (MOF-0.4 and MOF-0.8) to cylinder-shaped pores and parallel plates (MOF-2.0 and $\text{MgF}_2\text{-s}$, respectively) [267]. MOF-1.2 and MOF-1.6 exhibit two

desorption steps but it is unclear if this is due to two different types of pores or to pores with two different cross sections [268].

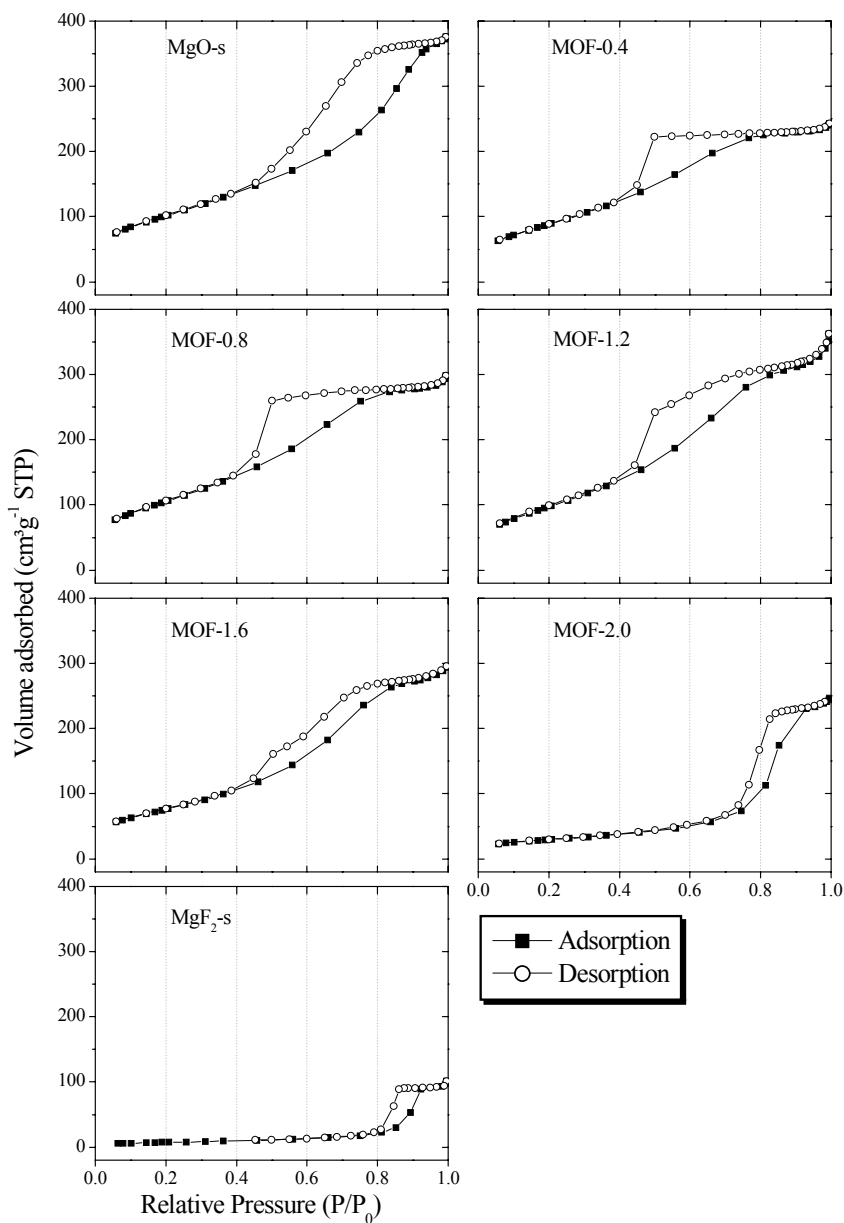


Fig. 6.1 N₂ adsorption/desorption isotherms of calcined Mg(O,F) samples

The pore size distributions of calcined Mg(O,F) samples are shown in Fig.6.2. The pore size distributions of MOF-0.4–MOF-1.6 have maxima at 35 Å, except that MOF-1.6 has an additional maximum at about 55 Å. However, MOF-2.0, MgO-s and MgF₂-s exhibit broader pore size distributions with maxima at higher values about 90, 60 and 135 Å, respectively.

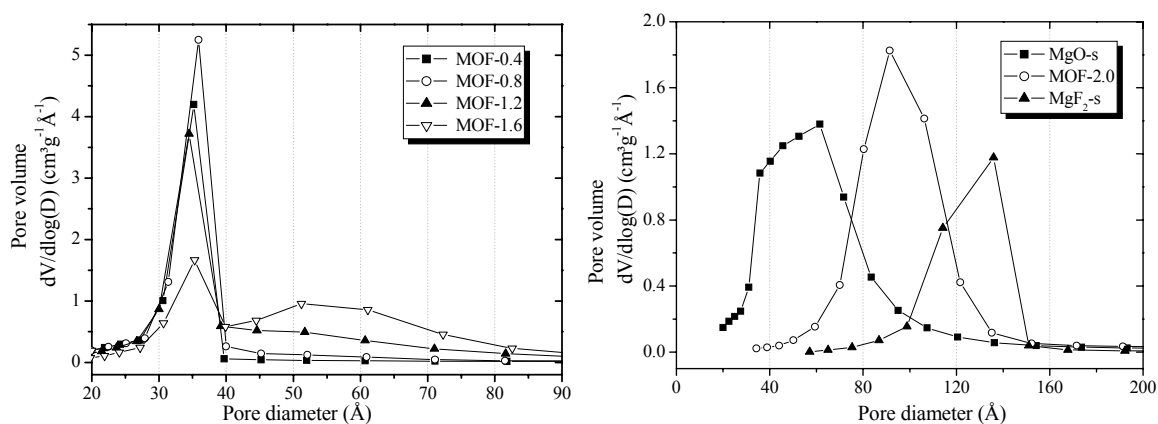


Fig. 6.2 Pore size distributions of calcined Mg(O,F) samples

XRD study

Before calcination, all the dried samples are X-ray amorphous-like materials (Fig. 6.3A). However, broad peaks around 2θ of 11° and 61° and the decaying peak at 2θ of 33.5° (Fig. 6.3A: a,b,c,d) indicate the presence of $\text{Mg}(\text{OH})_x(\text{OCH}_3)_y$ or $\text{Mg}(\text{OH})_x(\text{OCH}_3)_y\text{F}_z$ (i.e. the hydrolysis of $-\text{OCH}_3$ groups is not totally completed) [263]. The XRD pattern is similar to that of $\text{Mg}(\text{OCH}_3)_{1.3}(\text{OH})_{0.7}$ (PDF No.22-1788). This is also the reason why the dried products have high carbon contents (3–8 wt%, Table 6.1). Broad characteristic peaks around 2θ of 40° and 53° with very low intensity are observed in the patterns of MOF-1.6 (Fig. 6.3A:e) and MOF-2.0 (Fig. 6.3A:f), the samples with high F contents. Reference MgF_2 -s prepared by this sol-gel method has all the characteristic peaks from MgF_2 (PDF No. 41-1443) and these peaks are all broad.

After calcination at 350°C in Ar, MgO-s (Fig. 6.3B:a) and MgF_2 -s (Fig. 6.3B:g) show the patterns of MgO (PDF No. 45-946) and MgF_2 (PDF No. 72-1150), respectively. However, the Mg(O,F) samples (MOF-0.4 to MOF-2.0) are still amorphous-like materials. Characteristic peaks from $\text{Mg}(\text{OH})_x(\text{OCH}_3)_y\text{F}_z$ disappear more or less in the patterns of MOF-0.4, MOF-0.8 and MOF-1.2 (Fig. 2B: b,c,d). Broad peaks for MgF_2 in the patterns of sample MOF-1.6 and MOF-2.0 (Fig. 6.3A: e,f) become a little sharper (Fig. 6.3B: e,f), still with low intensities. In contrast, good crystalline MgF_2 is formed (Fig. 6.3B: g) after calcining the reference material MgF_2 -s under the same conditions. These results indicate that crystallization process promoted by calcination is not obvious for Mg(O,F) samples. Some special species formed during hydrolysis preserved the distortion during the calcination. Further calcination at 550°C led to the formation of separated crystalline phases MgO and MgF_2 (Fig. 6.3C: c,d,e,f). Further calcination at 550°C led to separate, crystalline phases of MgO and MgF_2 . The main phase was MgF_2 for the samples with

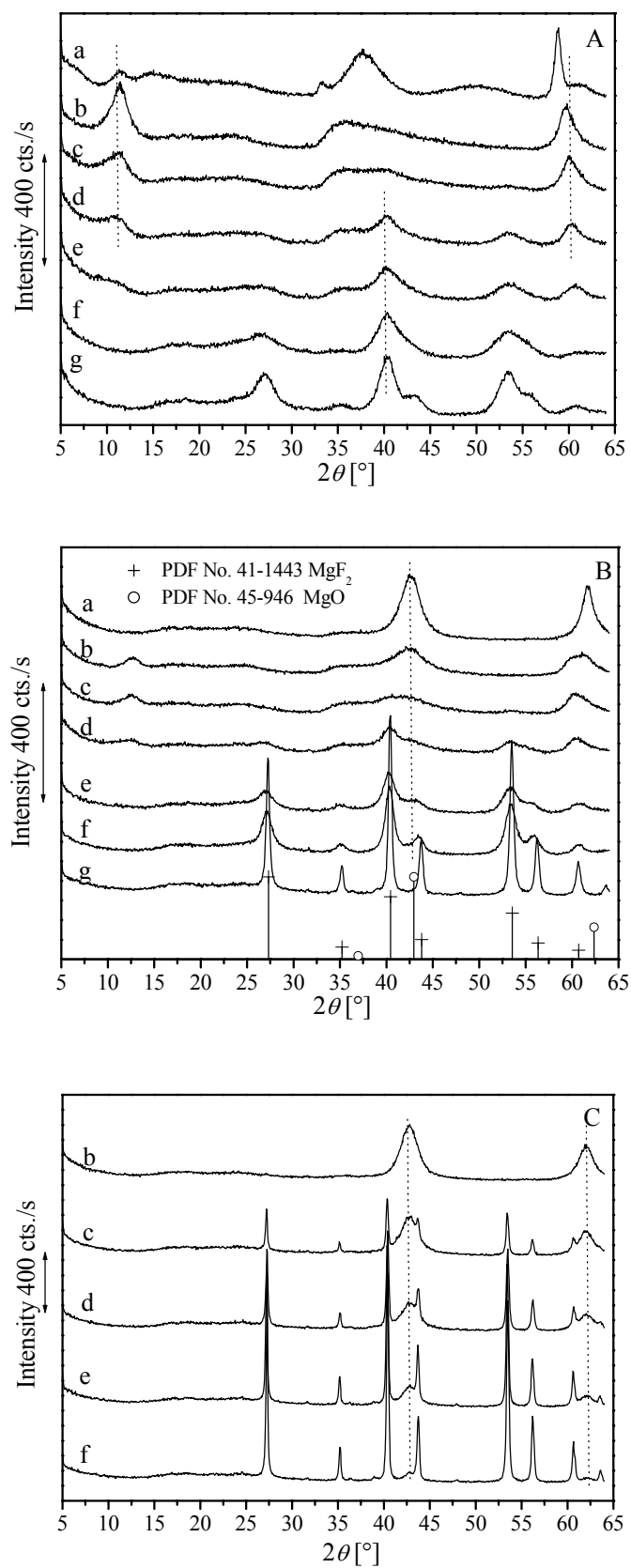


Fig. 6.3 XRD patterns of Mg(O,F) samples (b-f) and reference materials MgO-s (a) and MgF₂-s (g) before calcination (A) and after calcination at 350 °C (B) and 550 °C (C) in Ar

F/Mg ratios higher than 1.0. Peaks for both MgF_2 and MgO indicated a mixture of these phases in MOF-0.8, whereas the pattern of MOF-0.4 (Fig. 6.3C: b) with 10.2 wt% F exhibited a pure MgO showing two broad MgO peaks and no MgF_2 peaks, which can be explained by that small amount of MgF_2 is covered by MgO and can not be detected by XRD.

Thermal analysis

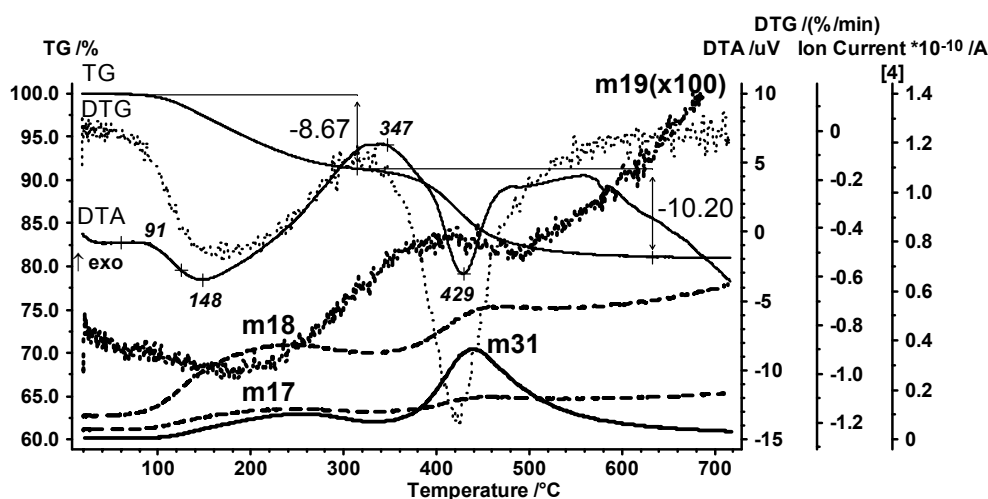


Fig. 6.4 TG- DTA profiles of uncalcined MOF-1.6

The presence of $-\text{OH}$ and $-\text{OCH}_3$ in the framework was confirmed by simultaneous thermal analysis (performed using a TA-MS device). TG-DTA profiles of the uncalcined samples, MOF-1.6 (5.0 wt% C) is shown in Fig. 6.4. The TG curve (under N_2) of MOF-1.6 shows an initial weight loss of about 8.7% below 320 °C mainly due to the desorption of water [$m/z = 17$ (OH^+), 18 (H_2O^+)]. The corresponding differential thermal analysis (DTA) peak and endothermic effect are around 148 °C. However, the condensation of some unstable $-\text{OH}$ groups cannot be excluded completely in this case. The weight loss (10.2%) from 320 to 600 °C corresponds to the loss of $-\text{OH}$ and also some $-\text{OCH}_3$ species. The corresponding DTA curve with a strong endothermic peak with T_{on} 347 °C and T_{p} 429 °C has to be attributed to the condensation reactions of $-\text{OH}$ groups to produce H_2O or condensation reactions of $-\text{OH}$ and $-\text{OCH}_3$ groups to produce CH_3OH , which is confirmed by the ionic current signal for $m/z = 18$ (H_2O^+) and $m/z = 32$ (CH_3OH^+), respectively. The thermal behavior of the sample after calcination at 350 °C in Ar is similar (not shown),

which indicates the presence of $-\text{OH}$ and $-\text{OCH}_3$ even after calcination at $350\text{ }^\circ\text{C}$ in Ar. The weight losses of two steps are slightly lower, 3.4 and 7.7%, respectively.

FTIR

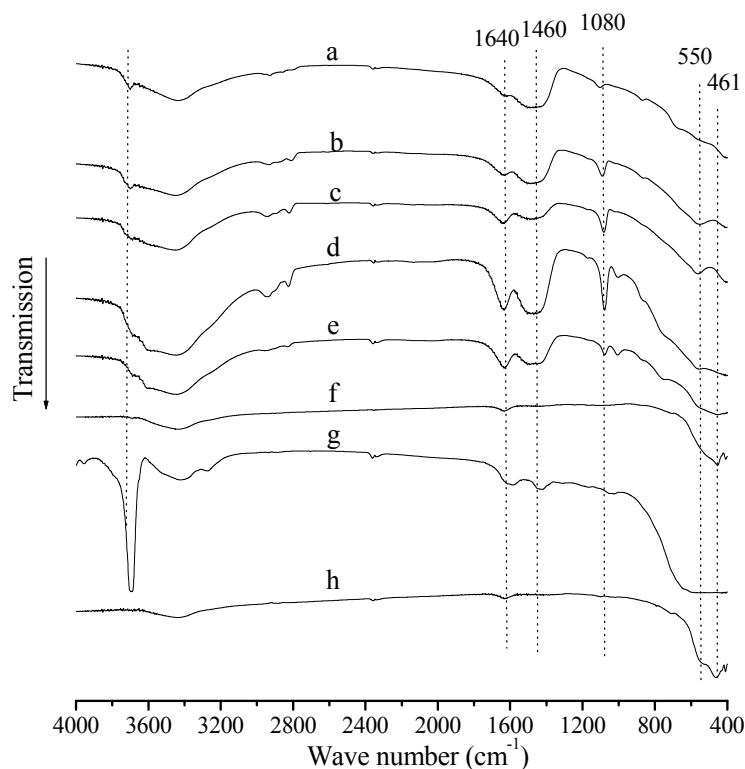


Fig. 6.5 FTIR spectra of calcined MOF-0.4–MOF-1.6 (b–e), MgO-s (a), MgF₂-s (f), and commercial Mg(OH)₂ (g) and MgF₂-c (h)

To further investigate the framework of the Mg(O,F) samples, FTIR of calcined samples was performed to clarify whether OH^- or $(\text{OCH}_3)^-$ or O^{2-} or all are present in the network. FTIR was also carried out on MgO-s, MgF₂-s, commercially available Mg(OH)₂ and MgF₂ (MgF₂-c) reference samples (Fig. 6.5g and h). The FTIR spectra of KBr pellets of calcined Mg(O,F) samples are shown in Fig. 6.5 and the assignment based on [265] is shown in Table 6.3. The very strong, broad band at 1460 cm^{-1} can be attributed to not only $\delta_{\text{asC-H}}$, but also bicarbonates formed by adsorbed carbonate on the basic surface (see chapter 5). This explains the large intensity differences between the $\nu_{\text{C-H}}$ and $\delta_{\text{asC-H}}$ bands. The 1640-cm^{-1} ($\delta_{\text{H-OH}}$) band and a broad band between 3675 and 3290 cm^{-1} ($\nu_{\text{O-H}}$) could correspond to adsorbed water on the sample surface and is found in all of the spectra (Fig. 6.5a–h). In [269], absorption at 1620 cm^{-1} was attributed to bridging hydroxy or oxy

groups in intermediate alkoxy/hydroxy compounds. A very weak band at 872 cm^{-1} ($\nu_{\text{C-O}}$) could indicate a negligible amount of methanol in the sample.

Table 6.3

Assignment of the FTIR absorption bands

Wave number (cm^{-1})	Mode assigned	Group or compound
3700	$\nu_{\text{O-H}}$	Hydroxyl group
3630 (3750–3000)	$\nu_{\text{O-H}}$	Adsorbed water
2750–2970	$\nu_{\text{C-H}}$	Alkoxy group
1630–1650	$\delta_{\text{H-OH}}$	Adsorbed water
1400–1500	$\nu_{\text{C-O}}$	Carbonate ion
1050–1130	$\nu_{\text{C-O}}$	Alkoxy group
500–600	$\nu_{\text{Mg-O}}$	Mg–OR
400–500	$\nu_{\text{Mg-F}}$	Mg–F

The spectrum of MgO-s (Fig. 6.5a) shows a band at 3700 cm^{-1} for isolated OH groups. Very weak vibrations observed between 3000 and about 2750 cm^{-1} ($\nu_{\text{C-H}}$) and 1087 cm^{-1} ($\nu_{\text{C-H}}$ or $\nu_{\text{C-O}}$) suggests the presence of very few methoxy groups in this sample. The spectra of the MOF samples and MgO-s vary in their band intensities except for the band(s) at 1087 cm^{-1} (and 1001 cm^{-1} in Fig. 6.5e) and the region above 3000 cm^{-1} and below 600 cm^{-1} . The following changes are observed in the MOF spectra with increasing fluorine contents: the OH-band at 3700 cm^{-1} decreases in intensity and shifts to lower wave number; a second band at 3609 cm^{-1} appears (Fig. 6.5d) and increases in intensity (Fig. 6.5e); the 1080-cm^{-1} band becomes stronger (Fig. 6.5b–d) and then decreases in intensity (Fig. 6.5e), while a weaker band appears at 1000 cm^{-1} (Fig. 6.5e); bands below 600 cm^{-1} are shifted. It seems the isolated OH groups become bridged when higher amounts of fluorine are present in the network. The spectrum of $\text{Mg}(\text{OH})_2$ (Fig. 6.5g) has a very strong band at 3700 cm^{-1} for the isolated OH group characteristic. Carbonates are also found on the surface of $\text{Mg}(\text{OH})_2$ (1460 cm^{-1} band). Whereas adsorbed water is observed on the surface of the hydroxide, very little water is found on the surface of MgF_2 (MgF_2 -s and MgF_2 -s, Fig. 6.5f and h). The only strong bands for these two samples are observed below 600 cm^{-1} and can be attributed to $\nu_{\text{Mg-F}}$ [270]. The main band is at 460 cm^{-1} with a shoulder at 550 cm^{-1} and a sharp but weak band at 410 cm^{-1} . The crystal structure of MgF_2 (ICSD No. 56506, PDF No. 41-1443) contains two Mg–F bonds (2.012 and 1.988 Å).

In the range of $400\text{--}600\text{ cm}^{-1}$, the bands of calcined Mg(O,F) samples (Fig. 6.5b–e) are different with that of MgF_2 (Fig. 6.5f and 6.5e) and MgO-s (Fig. 6.5a). The band at 550

cm^{-1} (Mg–OR stretching [271]) are observed in the spectra (Fig. 6.5b and 6.3c) of calcined MOF-0.4 and MOF-0.8, which contain low F content ($< 25 \text{ wt\% F}$). However this band does not appear in the spectrum of calcined MgO-s. Meanwhile, the band of Mg–F stretching mode for MgF_2 ($\text{MgF}_2\text{-s}$ and $\text{MgF}_2\text{-c}$) around 460 cm^{-1} (Fig. 6.5f and 6.3h) is not observed in all the spectra of calcined Mg(O,F) samples (Fig. 6.5b–e). These results can be explained by the coexistence of Mg–O(R) and Mg–F in the different coordinated Mg spheres of calcined Mg(O,F) samples.

^{19}F MAS NMR

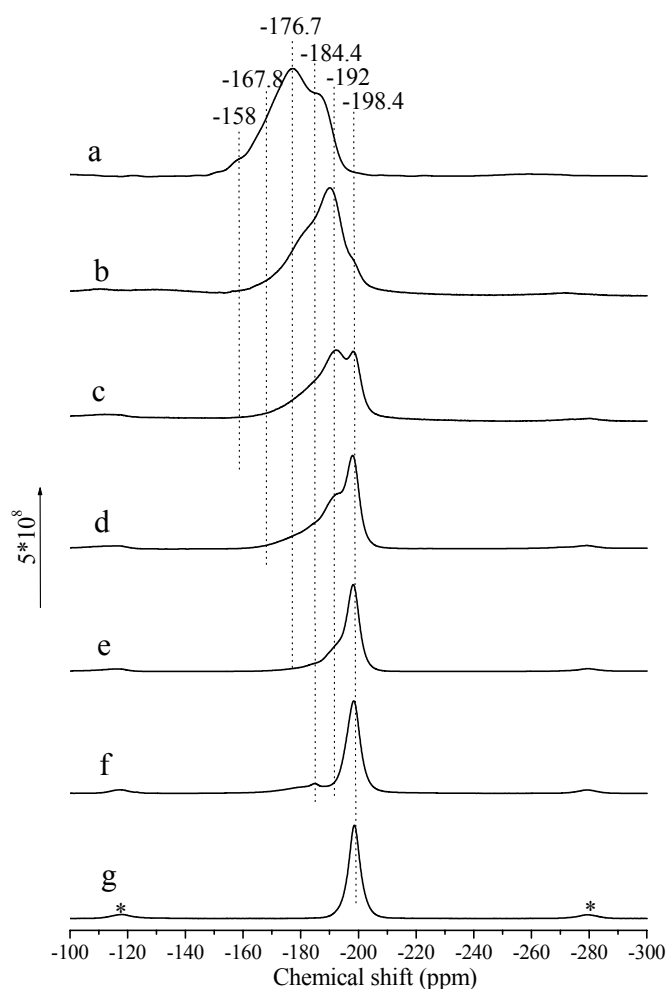


Fig. 6.6 ^{19}F MAS NMR spectra of MOF samples after calcination at $350 \text{ }^{\circ}\text{C}$: (a) MOF-0.4, (b) MOF-0.8, (c) MOF1.2, (d) MOF-1.6, (e) MOF-2.0, (f) $\text{MgF}_2\text{-s}$, and (g) $\text{MgF}_2\text{-c}$

From the structure of the crystal solvate of magnesium methoxide with methanol, Mg atom is octahedrally coordinated [272]. During the fluorination-hydrolysis process, F and

OH could substitute for $-\text{OCH}_3$ groups to form $\text{MgO}_x\text{F}_{6-x}$ octahedrally coordinated units. The coordinative state depends on the relative F and O contents.

High-resolution solid-state ^{19}F MAS NMR was used to study the fluorine coordination species in calcined $\text{Mg}(\text{O},\text{F})$ samples. The spectra of the samples with different fluoride contents and the commercial MgF_2 ($\text{MgF}_2\text{-c}$, without further treatment) are shown in Fig. 6.6. For $\text{MgF}_2\text{-c}$ (Fig. 6.6f), only signal around -198 ppm is observed which corresponds to the bridging fluorine in octahedrally coordinated MgF_6 sphere [251,273]. Crystalline, tetragonal MgF_2 (ICSD 56506, PDF No. 41-1443) has only one crystallographically unique fluorine atom, which coordinates three Mg atoms (Mg–F lengths: 2.0119, 2.0119, and 1.9883 Å and Mg–F–Mg bond angles: 129.9, 129.9, and 100.2°). Calcined $\text{MgF}_2\text{-s}$ has similar spectrum as commercial MgF_2 with an additional small signal at -184 ppm, which suggests a second type of fluorine coordination species in this sample. After calcination of the same sample at 550 °C, a very weak peak in the XRD pattern (Fig.6.3C: f) indicated a separate and minor phase of MgO. Thus, it seems there are minor mixed lattice regions (MgO_xF_y) in the network, in which the fluorine coordination (Mg–F bond lengths and Mg–F–Mg angles) is different than that found in MgF_2 . With the decreasing fluorine concentrations of the $\text{Mg}(\text{O},\text{F})$ samples, the ^{19}F MAS NMR signals (Fig. 6.6d–a) become broader. MOF-2.0, MOF-1.6 and MOF-1.2 have the same maximum at around -198 ppm as $\text{MgF}_2\text{-c}$. Meanwhile MOF-1.6 has two shoulder signals at around -192 and -184 ppm, and MOF-1.2 has another maximum at -192 ppm. MOF-0.8 and MOF-0.4 have much broader signals. Maximums at around -192 and -177 ppm with shoulders are observed, respectively. The dominant fluorine species in these samples has a different coordination compared to that in MgF_2 . Based on the spectra of all the samples, six resonance positions from high to low field may be distinguished at about the chemical shifts of about -158 , -168 , -177 , -184 , -192 , and -198 ppm, which are supposed to be MgO_5F , MgO_4F_2 , MgO_3F_3 , MgO_2F_4 , MgOF_5 , MgF_6 (oxygen may come from oxo or hydroxyl group, fluorine may come from bridge or terminal coordinated fluorine specie) coordination species in the first octahedrally coordinated Mg sphere. The number of fluorine atoms coordinated to Mg increases with fluorine chemical shift decreasing from high to low chemical shift field. A similar trend between the number of fluoride atoms coordinated to aluminum and the fluorine chemical shift was also observed in hydroxyl/oxyfluorides aluminum before (see Fig.6.7) [274]. In this case, the broad signals may be ascribed to the coexistence of some different fluorine coordination species. Meanwhile, the high disorder structure of $\text{Mg}(\text{O},\text{F})$ samples indicated by XRD may be another reason for the broad signals. The former

interpretation is preferred because two maxima are observed in the spectrum of MOF-1.2 (Fig. 6.6c), which cannot simply be explained by the degree of the disorder of the sample.

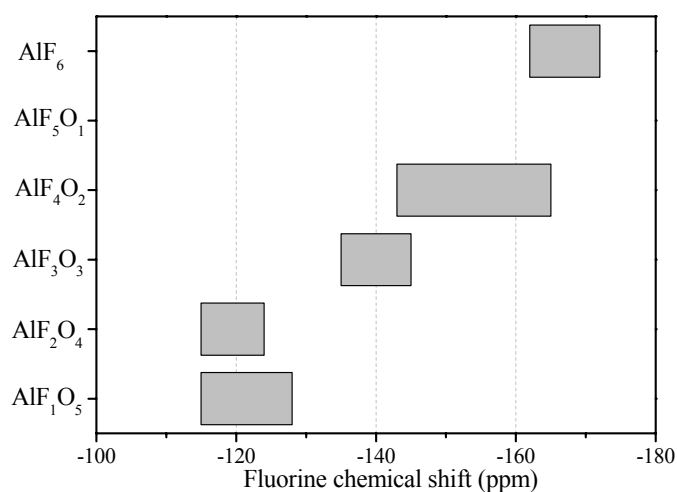


Fig. 6.7 Typical ^{19}F chemical shifts of octahedral aluminum environments with oxygen and fluorine in the first coordination sphere, $\text{AlO}_{6-x}\text{F}_x$, versus x [274]

In ^{19}F MAS NMR spectrum of MOF-1.6 calcined at $550\text{ }^{\circ}\text{C}$ (Fig. 6.8) the signal around -198 ppm with some weak signals (-150 to -190 ppm) appeared instead of the broad signal with a maximum at -198 ppm of the sample calcined at $350\text{ }^{\circ}\text{C}$ (Fig. 6.6d). This indicates high temperature calcination can destroy the framework of $\text{Mg}(\text{O},\text{F})$ and result in crystalline MgF_2 . This result also agrees with the presence of crystalline MgF_2 in XRD patterns of the samples calcined at $550\text{ }^{\circ}\text{C}$ (Fig. 6.3C). However, the weak signals demonstrate negligible amount of certain or some unknown fluorine species were formed during high temperature calcination, which can not be detected by XRD.

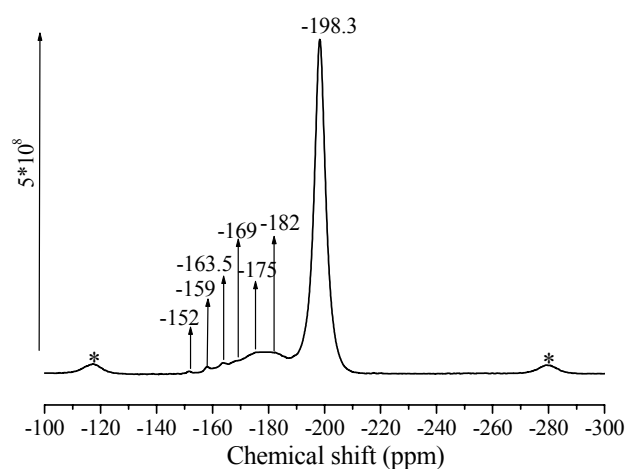


Fig. 6.8 ^{19}F MAS NMR spectra of MOF-1.6 after calcination at $550\text{ }^{\circ}\text{C}$

XPS

The XPS (Mg 1s, F 1s, O 1s) results of selected calcined Mg(O,F) samples and commercially available MgF_2 are shown in Fig. 6.9. The surface atomic ratios, F/Mg and O/Mg, for the MOF samples were determined by integration of the XPS peaks in Fig. 6.9 and are given in Table 1. The XPS spectra of commercially available MgF_2 ($\text{MgF}_2\text{-c}$) was measured and discussed in [251].

From the surface atomic ratio F/Mg and O/Mg, with the nominal F/Mg ratio increase, the surface F/Mg increases and the O/Mg decreases. The O/Mg of MgO-s is 1.1, which indicates that the surface species is MgO . This is consistent with the XRD result. For calcined MOF-0.4, MOF-0.8 and MOF-1.2, the values of $(2\text{O}/\text{Mg}+\text{F}/\text{Mg})$ are more than 2.0, which indicates that besides O^{2-} species on the surface there is OH^- or $(\text{OCH}_3)^-$ species. This result agrees with the FTIR result. However, on the surface of calcined MOF-1.6, the oxygen species is more likely O^{2-} since the value of $(2\text{O}/\text{Mg}+\text{F}/\text{Mg})$ is almost equal to 2.0, which means this sample seems to be a true magnesium fluoride exclusively with O^{2-} species.

Changes in the chemical environment of an atom may be followed by changes in the photoelectron energies. From the binding energy (BE) of Mg 1s, it seems that when more F is bonded to Mg from MgO-s to MOF-1.6, the Mg 1s BE shift to high value from 1302.7 to 1304.0 eV. This means the introduction of F does change the chemical environment of Mg. The BEs of F 1s varied from sample to sample as shown in Fig.6.9, while there is not a direct correlation between the BE and the F content. It is surprising to note that in the F 1s spectrum of calcined MOF-1.2, there is an additional peak at around 687.6 eV besides the peak at around 684.6 eV, which may be ascribed to the significantly different F chemical environment. From the ^{19}F MAS NMR spectra, obviously, calcined MOF-1.2 is the only sample that has two separated peaks. It is the same case for calcined MOF-1.2 in the O 1s spectra. Calcined MOF-1.2 has two peaks at around 530.8 and 533.5 eV, respectively. Again, there is no direct correlation between the BE and the O content. The BE varies from 530.8 to 533.5 eV.

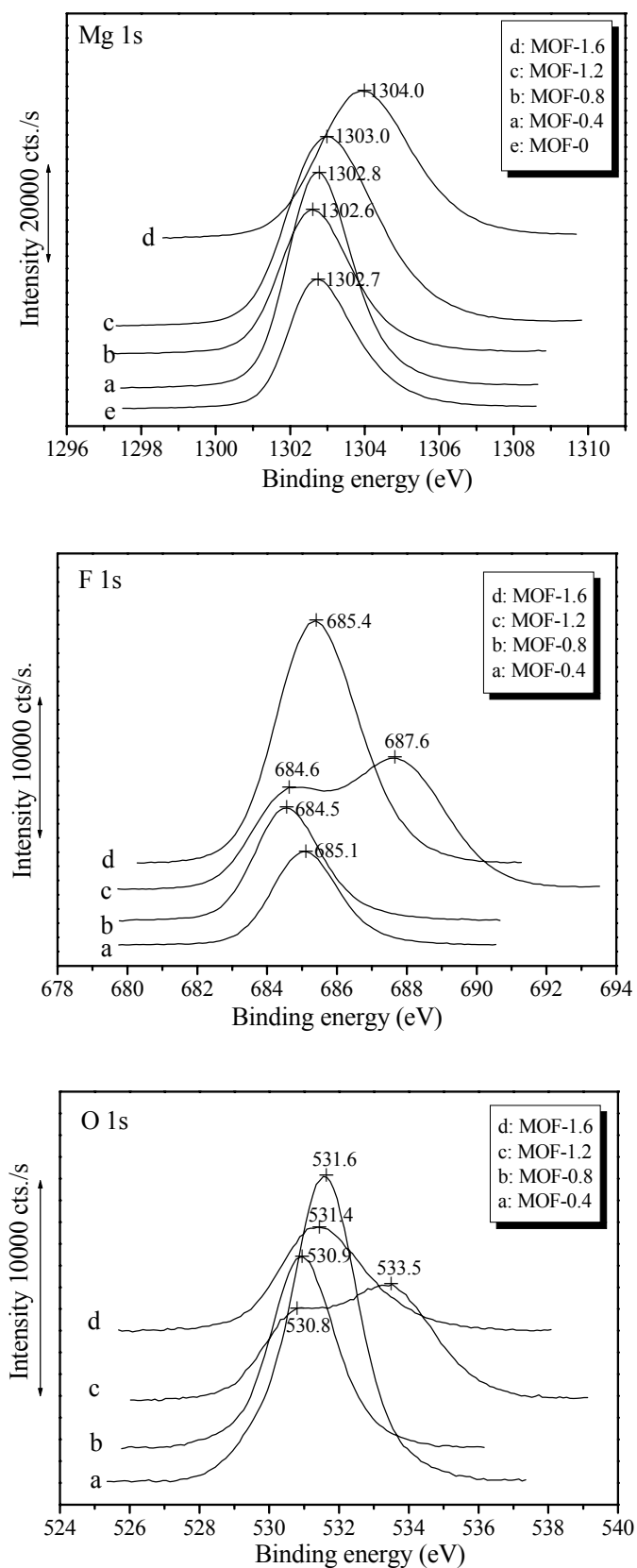


Fig. 6.9 XPS results of Mg(O,F) samples after calcination at 350 °C in Ar

TEM

TEM was used to study the morphology of calcined Mg(O,F) sample. The TEM of calcined MOF-1.6 at 350 °C in Ar is shown in Fig. 6.10. Irregular shapes of particles (around 10 nm) are observed, which has low contrast and are probably agglomerates of much smaller particles. The selected-area electron diffraction patterns of the particles are not very diffused, which indicates the particles are somehow crystalline. Because the particles are very small, in XRD pattern of this sample, only broad peaks are observed. According to the lattice distances measured from the diffraction rings, the predominant phase may be MgF_2 and some isolated particles may be MgO . Probably, MgO particles also coalesce with MgF_2 particles since very broad diffraction rings are also observed. Because of the very close lattice distances (d values) of MgF_2 and MgO , O atom partially incorporation in the lattice of MgF_2 may not change the structure and only slightly changes lattice distances. Thus, lattice distances measured from the diffraction rings can not be distinguished with that of MgF_2 and can not indicate the existence of the Mg(O,F) compound in this case. In contrast, the coexistence of O and F in the frameworks of Mg(O,F) samples has been proved by FTIR, ^{19}F MAS NMR and XPS. Energy-dispersive X-ray spectroscopy (EDX) confirmed qualitatively that calcined MOF-1.6 consists of Mg, F and O.

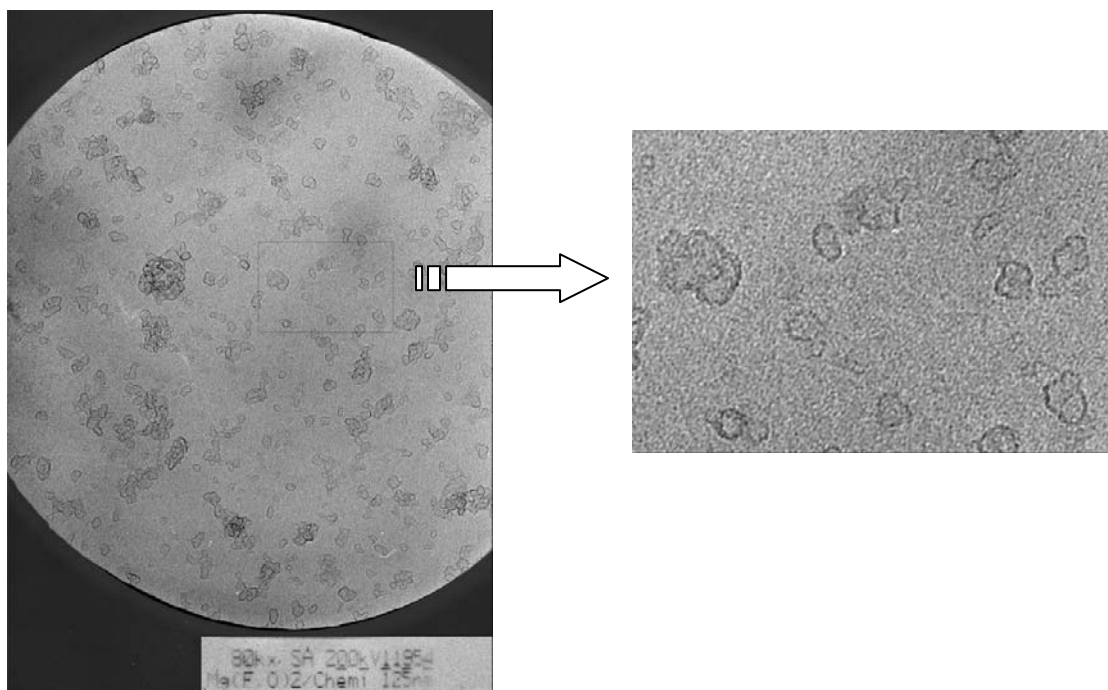


Fig. 6.10 TEM of calcined MOF-1.6

6.4 Catalytic behavior of Mg(O,F)

Catalytic behaviour of Mg(O,F) in Michael addition of 2-methylcyclohexane-1,3-dione to methyl vinyl ketone

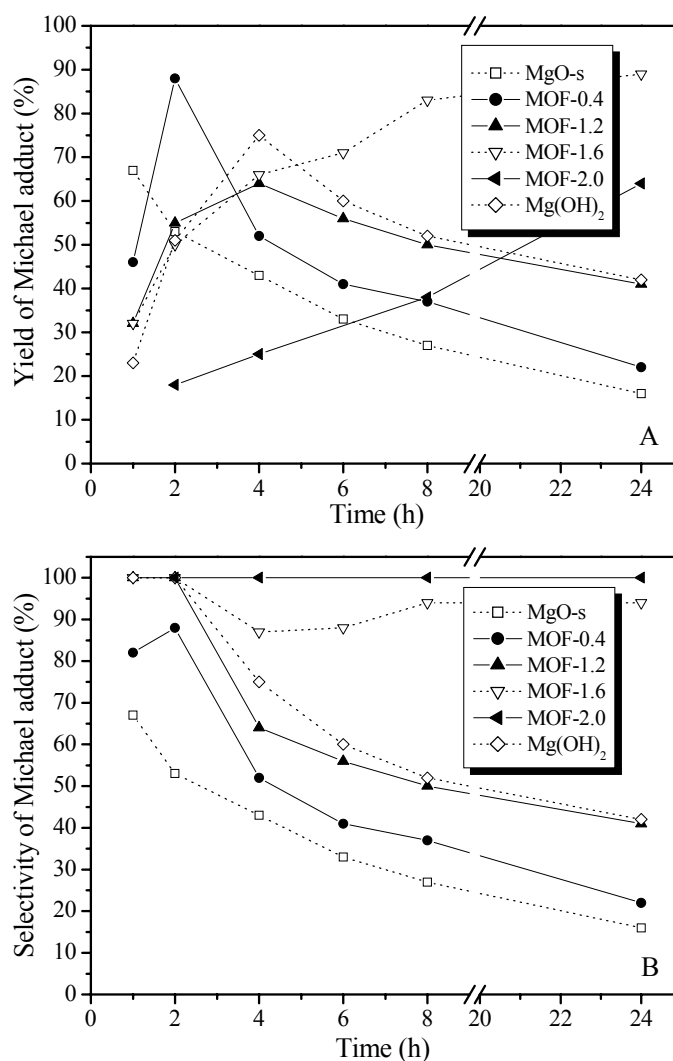


Fig. 6.11 Michael addition of 2-methyl-cyclohexane-1,3-dione to methyl vinyl ketone with the MOF samples calcined at 350 °C. Yield (A) and selectivity (B) of Michael adduct versus reaction time. Reaction temperature: room temperature (RT)

The catalytic activity of the MOF samples was first screened for the Michael addition of 2-methylcyclohexane-1,3-dione to methyl vinyl ketone at room temperature; these results are shown in Fig. 6.11. Although supported fluoride ion (e.g. KF/Al₂O₃) as a solid base shows very good activities in many reactions [93], including Michael additions, the pure, crystalline MgF₂ samples, MgF₂-c and MgF₂-s, were totally inactive. The MOF samples, MOF-0.4–MOF-2.0, MgO-s and commercially available Mg(OH)₂ exhibited diverse

catalytic activities. MgO-s (Fig. 6.11) shows a very unselective catalytic activity similar to that found for MgO synthesized in aqueous medium in chapter 3: high initial yield (ca. 70%, 1 h) with a decrease to below 20% over 24 h caused by a consecutive intramolecular aldol cyclization (see chapter 3). The product yield achieved with commercial $\text{Mg}(\text{OH})_2$ went through a maximum of over 70% yield after 4 h but did not decrease as drastically as in the case of MgO (final yield: 45%, not 20%). In chapter 5, the activity and selectivity of the catalyst were attributed to the type of base site and presence of Lewis acid sites. MgO had a low amount of Brønsted base sites (OH^-), but more and stronger Lewis base sites (O^{2-}), whereas $\text{Mg}(\text{OH})_2$ only has Brønsted base sites (strong absorption at 3700 cm^{-1} for isolate OH groups in IR spectrum). This could indicate that not only Brønsted base sites but also Lewis base sites can catalyze the reaction, however, the presence of acid sites may be important for high reaction selectivity.

The different F contents of the MOF-0.4–MOF-2.0 samples also have a direct effect on catalytic activity. The sample with the lowest fluorine contents (MOF-0.4, 10.2 wt% F) exhibits the highest initial yield of about 90% after 2 h, after which the yield decreases parallel to that of MgO-s giving a final yield of ca. 25%. In the case of MOF-1.2, maximum yield was reached at a longer reaction time (4 h) and was lower (65%). The decrease in yield for this sample thereafter resembles that of $\text{Mg}(\text{OH})_2$ and not MgO (final yield: 45%). The yields of the samples with higher fluorine contents (MOF-1.6, 40 wt% F and MOF-2.0, 49.2 wt% F) no longer went through a maximum of yield; a consecutive reaction did not occur. Both of these samples demonstrated the most selective activities and achieved the highest final yields: 65% for MOF-2.0 and 90% for MOF-1.6. Thus, a preliminary conclusion is that the combination of Brønsted base sites, Lewis base sites, and Lewis acid sites is optimal in these two samples. Reaction with MOF-2.0 is however significantly slower than with MOF-1.6. Fig. 6.11B shows that the reaction selectivity achieved with MOF-0.4 and MOF-1.2 are in between that of MgO-s (MgO) and $\text{Mg}(\text{OH})_2$. Based on the results of calcined hydrotalcite (chapter 5), it is assumed that optimum acid–base properties, compared to MgO and $\text{Mg}(\text{OH})_2$, could make MOF-1.6 and MOF-2.0 more selective catalyst in the reaction. On the other hand, the results indicate that the acid–base properties on $\text{Mg}(\text{O},\text{F})$ can be adjusted by adjusting the F. From the catalysis results, it is shown that the acid–base property of the material may be modified by varying the relative ratio of the anions.

Catalytic behaviour of MOF-1.6 in Michael addition of 2-methylcyclohexane-1,3-dione to methyl vinyl ketone at different temperatures

The Michael addition of 2-methylcyclohexane-1,3-dione to methyl vinyl ketone was performed using MOF-1.6 as catalyst at 50 and 75 °C. The results were shown in Fig. 6.12. With the reaction temperature increase, the yield of Michael adduct went through a maximum of over 90% yield after 2 h at reaction temperature of 50 °C and over 85% after 1 h at 75 °C. The yield of Michael adduct decreased to 76% and 35%; and the yield of bridged ketol increased to 20% and 57% after 8 h at 50 °C and 75 °C, respectively because of the consecutive reaction described in chapter 3. These results indicated that at higher reaction temperature, the behavior of MOF-1.6 became similar to that of MgO at room temperature.

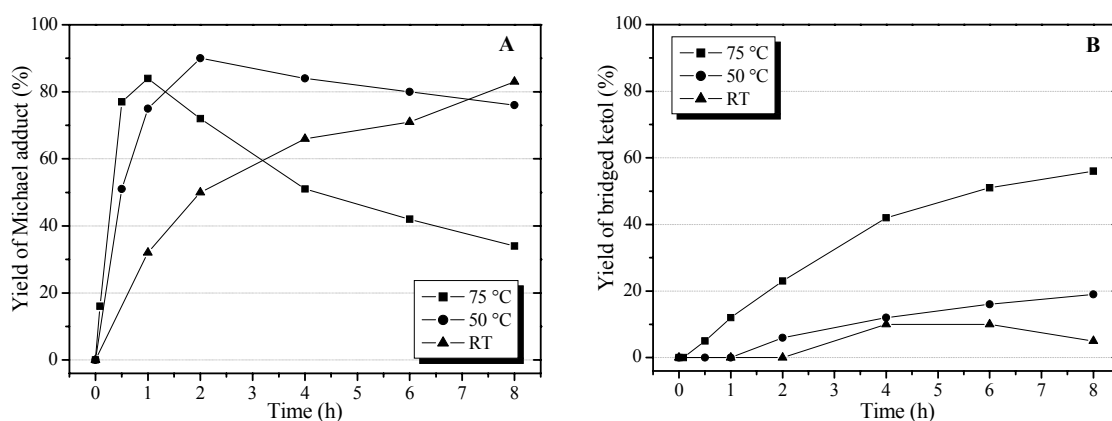
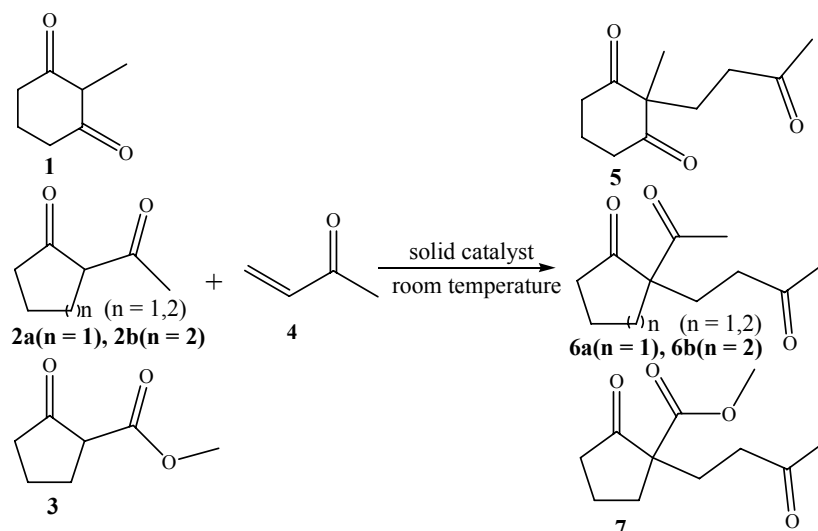


Fig. 6.12 Michael addition of 2-methyl-cyclohexane-1,3-dione to methyl vinyl ketone with the MOF-1.6 at RT, 50 and 75 °C. Yield of Michael adduct (A) and bridged ketol (B) versus reaction time

Michael addition of 2-acetylcyclopentanone, 2-acetylcyclohexanone and 2-methoxycarbonyl cyclopentanone to methyl vinyl ketone over MOF-1.6

Based on its high activity and selectivity, MOF-1.6 was chosen to test in three Michael additions (see Scheme 6.2) with liquid CH-acids of different strengths (pK_a values): 2-acetylcyclopentanone (7.8), 2-acetylcyclohexanone (10.1), and 2-methoxycarbonyl cyclopentanone (10.3) at room temperature. The result was shown in Fig. 6.13. As in the reaction with 2-methyl-cyclohexane-1,3-dione to methyl vinyl ketone, high product yields (75–90% after 24 h) with 100% selectivities were obtained successfully with MOF-1.6 that were directly dependent on the pK_a of the CH-acid. The addition of reactant with lower pK_a

to methyl vinyl ketone proceeds faster. Interesting enough, MOF-1.6 had a similar catalytic behavior as the most active calcined hydrotalcite catalyst CHT0.6 (see chapter 5). It means by fluorination-hydrolysis sol-gel process, it was successful to design a new efficient catalyst system for Michael additions.



Scheme 6.2 Michael additions of 2-methylcyclohexane-1,3-dione (**1**), 2-acetylcyclopentanone (**2a**), 2-acetylcyclohexanone (**2b**) and 2-methoxycarbonyl cyclopentanone (**3**) to methyl vinyl ketone (**4**). Michael adduct: 2-methyl-2-(3-oxo-butyl)-cyclohexane-1,3-dione (**5**), 2-acetyl-2-(3-oxo-butyl)-cyclopentanone (**6a**), 2-acetyl-2-(3-oxo-butyl)-cyclohexanone (**6b**) and 2-oxo-1-(3-oxo-butyl)-cyclopentanecarboxylic acid methyl ester (**7**)

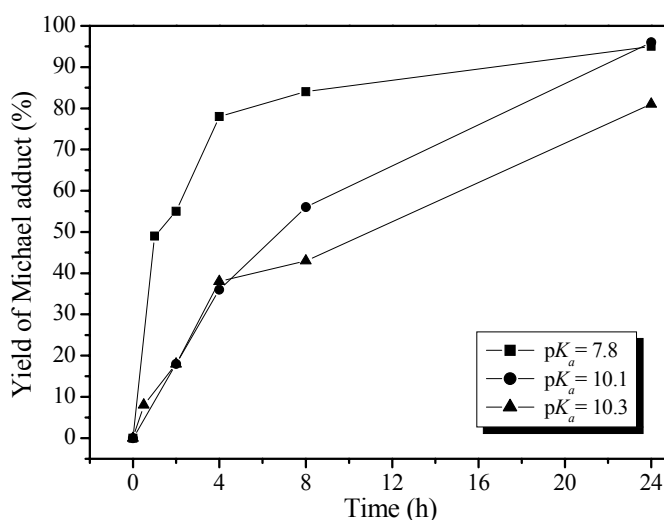


Fig. 6.13 Michael addition of 2-acetylcyclopentanone ($pK_a = 7.8$), 2-acetylcyclohexanone ($pK_a = 10.1$) and 2-methoxycarbonyl cyclopentanone ($pK_a = 10.3$) to methyl vinyl ketone with calcined MOF-1.6. Yield of Michael adduct versus reaction time. Reaction temperature: room temperature (RT).

6.5 Conclusions

Amorphous-like material $\text{Mg}(\text{O},\text{F})$ with high surface area can be prepared by two-step soft fluorination-hydrolysis sol-gel process.

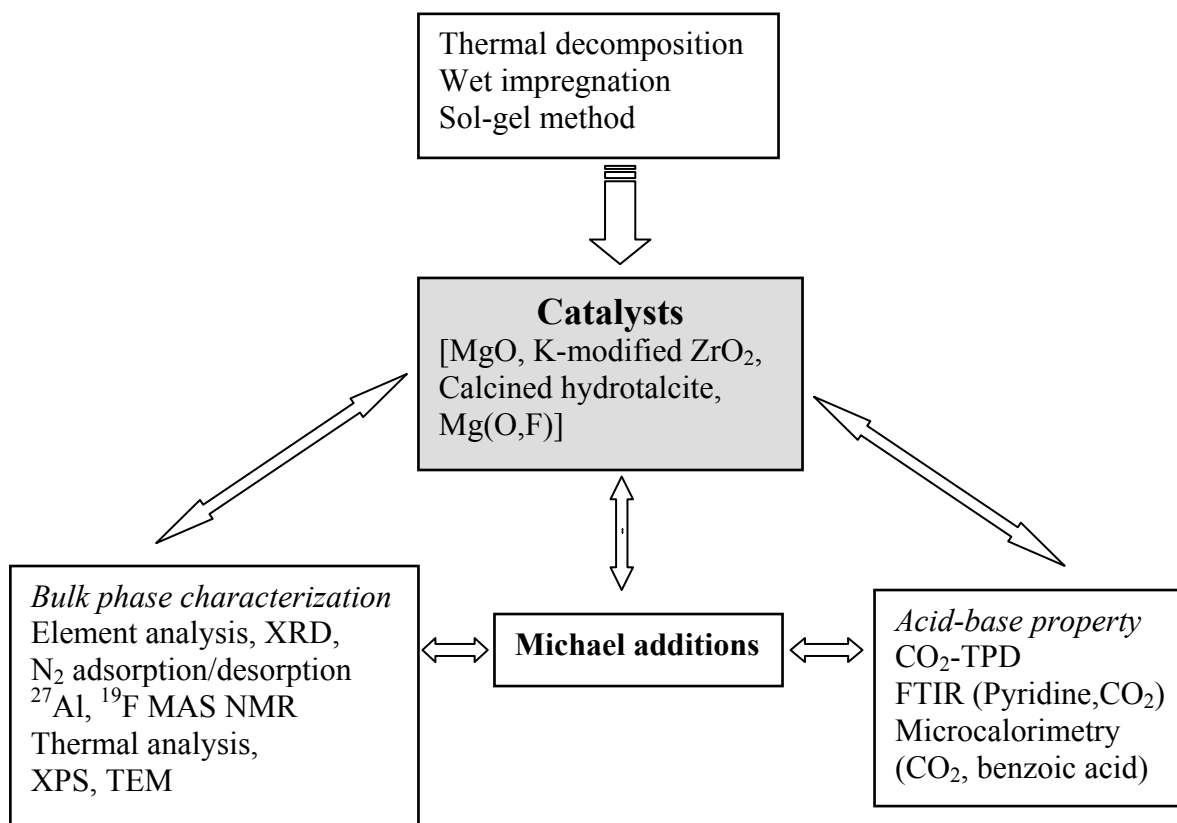
Different fluorine species in $\text{Mg}(\text{O},\text{F})$ are detected by ^{19}F MAS NMR and XPS. A periclase MgO or tetragonal MgF_2 structure is formed during low-temperature calcination at $350\text{ }^\circ\text{C}$ depending on the fluorine contents of sample. As the fluorine content decreases in the sample, the structural distortion of the fluorine coordination becomes greater. Low fluorine contents in the MgO network results in diverse fluorine coordinations. Two distinct fluorine coordinations are present in the mixed lattice of MgO and MgF_2 . As the fluorine content increases, the FMg_3 species becomes the dominant species. High-temperature calcination of $\text{Mg}(\text{O},\text{F})$ leads to the formation of separated crystalline MgO and MgF_2 phases.

Successfully controlled introduction of F into the MgO network makes it possible to tune the acid-base property of the resulting material. $\text{Mg}(\text{O},\text{F})$ with suitable F content can act as an efficient and selective catalyst for Michael additions. In the Michael addition of 2-methylcyclohexane-1,3-dione to methyl vinyl ketone. The catalyst with a F/Mg mol ratio of 1.6 achieved the best catalytic results producing the Michael addition product in a yield of 90% with a selectivity of 100% at room temperature within 24 h. This catalyst was successfully applied in other Michael additions of 2-acetylcyclopentanone, 2-acetylcyclohexanone, and 2-methoxycarbonylcyclopentanone as further CH-acids to methyl vinyl ketone to obtain high final yields and selectivities.

Chapter 7

Summary and conclusion

The research in this thesis concerns the design of highly active and selective heterogeneous base catalysts for liquid-phase Michael additions. MgO, potassium-modified ZrO₂, calcined Mg-Al hydrotalcite, and Mg(O,F) catalyst systems were prepared, characterized and tested in Michael additions. The research is simplified in scheme 7.1.



Scheme 7.1

Table 7.1 gives a brief summary of catalytic behavior of different catalysts.

Table 7.1

Summary of the behavior of catalysts in Michael addition

Catalysts	Active sites	Catalytic results in the reaction
MgO	Strong Lewis base	High activity, low selectivity
Mg(OH) ₂	Brønsted base	High activity, low selectivity
ZrO ₂	Amphoteric	No activity
Al ₂ O ₃	Amphoteric	No activity or low activity
K-modified ZrO ₂	Base	High activity, leaching of active sites
Calcined hydrotalcite	Base (main) + acid (weak)	High activity and high selectivity
Low F Mg(O,F)	Base	High activity and low selectivity
High F Mg(O,F)	Base (main) + acid (weak)	High activity and high selectivity

In **Chapter 3**, MgO prepared by different methods and conditions was first investigated in Michael additions of 2-methylcyclohexane-1,3-dione to methyl vinyl ketone. MgO can not catalyze the reaction selectively because of a consecutive aldol cyclization.

In **Chapter 4**, the properties and the activities of the catalysts can be influenced by a variety of parameters, such as the zirconia precursor and the potassium modifying agent. Modified hydrous zirconia forms the metastable, tetragonal ZrO_2 phase after calcination; the phase of modified anhydrous zirconia, on the other hand, is monoclinic. The specific surface areas of the modified samples are much lower than that of ZrO_2 . The potassium compounds on hydrous zirconia decompose in a broader temperature range than those on anhydrous zirconia. Stronger base catalysts were produced by potassium-modification of ZrO_2 . The modified anhydrous zirconia has a wider distribution of basic site strengths than modified hydrous zirconia. Potassium-modified zirconia give high yields and high *cis/trans* ratios of 2-butene in the double-bond isomerization of 1-butene. Although potassium-modified zirconia exhibit high activity and selectivity, it is less suitable as a solid base catalyst for liquid-phase Michael addition in methanol because of potassium leaching effects.

In **Chapter 5**, the influence of chemical composition and acid-base property on the catalytic performance of the calcined hydrotalcites was studied. Calcined hydrotalcites ($\text{Mg}/\text{Al} = 0.6, 1.4, 2.2, 3.0$) exhibit Lewis acid, Brønsted base, and Lewis base sites. The Al-rich sample (Mg/Al molar ratio of 0.6) possesses Lewis acid sites similar in strength to those found on Al_2O_3 , but stronger than those found on the Mg-rich hydrotalcites. Calcined hydrotalcites can catalyze the Michael additions of 2-methylcyclohexane-1,3-dione, 2-acetylcyclopentanone, and 2-acetylcyclohexanone to methyl vinyl ketone with 100% selectivity. A nonlinear correlation between the Mg content and catalytic activity was found. However, catalytic activity correlates with the amount of the base sites determined by benzoic acid microcalorimetry. An optimal balance of acid-base properties may make the Al-rich calcined hydrotalcite an excellent catalyst in the Michael addition of numerous 1,3-diones independent of their $\text{p}K_{\text{a}}$ values.

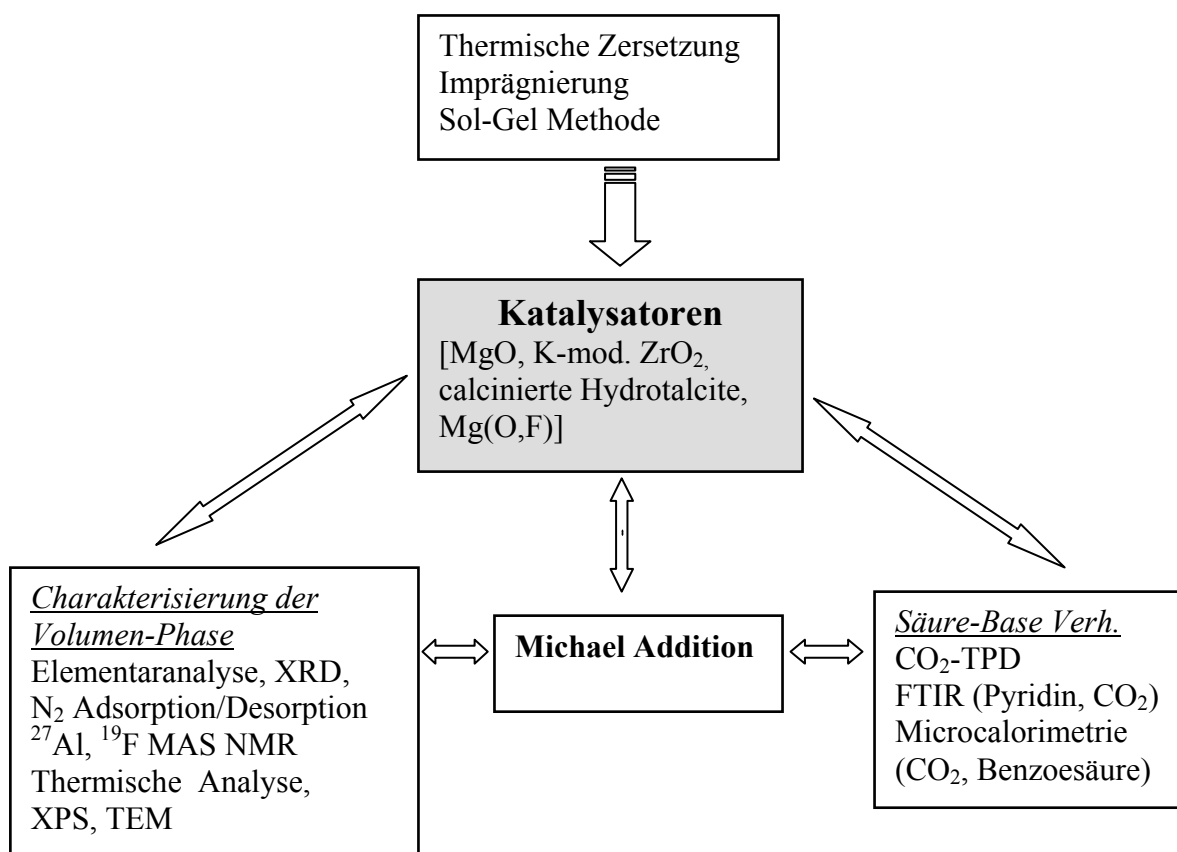
In **Chapter 6**, a novel catalyst system was prepared by sol-gel method. Amorphous-like material $\text{Mg}(\text{O},\text{F})$ with high surface area can be prepared by two-step soft fluorination-hydrolysis sol-gel process. Different fluorine species in $\text{Mg}(\text{O},\text{F})$ are detected by ^{19}F MAS NMR and XPS. $\text{Mg}(\text{O},\text{F})$ with suitable F content can act as an efficient and selective catalyst for Michael additions. The catalyst with a F/Mg mol ratio of 1.6 achieved the best catalytic results producing the Michael addition product in a yield of 90% with a selectivity

of 100% at room temperature within 24 h. Successfully controlled introduction of F and OH group into the MgO network makes it possible to tune the acid-base property of the resulting material. Therefore, this method enables the design of new bifunctional materials for catalytic reactions that have very specific requirements on the amount and type of base and acid sites necessary.

Zusammenfassung

Die Promotionsarbeit befasst sich mit der Herstellung und Untersuchung von hoch aktiven und selektiv wirkenden alkalischen Katalysatoren für Michael-Additionen in Flüssig-Phasen Reaktionen.

MgO, Kalium-modifiziertes ZrO_2 , calcinierte Mg-Al Hydrotalcite und Mg(O,F) basierte Katalysatoren mit basischen Zentren wurden hergestellt, charakterisiert und in Michael-Additionen getestet. Die Untersuchungen sind im Folgenden schematisch dargestellt.



Schema 7.1

Table 7.1

Zusammenfassung der katalytischen Eigenschaften verschiedener Katalysatoren

Katalysatoren	Aktive Zentren	Katalytische Ergebnisse
MgO	Starke Lewis Base	Sehr aktiv, geringe Selektivität
Mg(OH) ₂	Brønsted Base	Sehr aktiv, geringe Selektivität
ZrO ₂	Amphoter	Nicht aktiv
Al ₂ O ₃	Amphoter	Keine oder geringe Aktivität
K-mod. ZrO ₂	Base	Hohe Aktivität, Leaching
Calcinierte Hydrotalcite	Base (stark)+Säure (schwach)	Hohe Aktivität, geringe Selektivität
Mg(O,F) F↑	Base	Hohe Aktivität, geringe Selektivität
Mg(O,F) F↓	Base (stark)+Säure (schwach)	Hohe Aktivität, geringe Selektivität

Kapitel 3: MgO hergestellt nach unterschiedlichen Methoden wurde erstmalig in Michael-Additionen von 2-Methylcyclohexan-1,3-dion zu Methyl-vinyl Ketonen untersucht. MgO ist nicht in der Lage die Reaktion selektiv zu katalysieren, da sich eine Aldol-Cyclisierung als Folgereaktion anschließt.

Kapitel 4: Eigenschaften und Aktivitäten der Katalysatoren können durch eine Anzahl von Parametern beeinflusst werden wie z.B. im Fall des ZrO₂ –Precursors modifiziert durch Kalium-Dotierung. Modifiziertes wässriges Zirkonoxid bildet nach der Calcinierung eine metastabile tetragonale ZrO₂ Phase, während andererseits nichtwässriges Zirkonoxid monoklin ist. Die spezifischen Oberflächen der modifizierten Oberflächen sind viel kleiner als die von ZrO₂. Die Verbindung mit Kalium auf dem wässrigen ZrO₂ zersetzt sich thermisch in einem breiteren Temperaturbereich als das auf nichtwässrigem Wege erhaltene Zirkondioxid. Stärker basische Katalysatoren werden durch Modifizierung von ZrO₂ mit Kalium erhalten. Diese haben eine breitere Verteilung der Basenstärke als die modifizierten wässrigen ZrO₂ -Katalysatoren. Kalium modifiziertes ZrO₂ gibt hohe Ausbeuten und hohe *cis/trans* Verhältnisse in der Doppelbindungsisomerisierung von 1-Buten. Obwohl das Kalium modifizierte Zirconia hohe katalytische Aktivität und Selektivität aufweist, ist es als Basenkatalysator für die Michael Addition in der flüssigen Phase wenig geeignet, da es Leaching-Effekte zeigt.

Kapitel 5: Es wurde der Einfluss der chemischen Zusammensetzung und der Säure-Basen-Eigenschaften auf die katalytische Wirkung von calcinierten Hydrotalciten untersucht. Diese zeigen bei den Zusammensetzungen (Mg/Al = 0.6, 1.4, 2.2, 3.0) Lewis saure, Brønsted basische und Lewis basische Zentren. Die Al-reichen Proben (Mg/Al Verhältnis

0.6) besitzen Lewis saure Zentren in vergleichbarer Stärke wie im Al_2O_3 und jedoch stärkere als in den Mg-reichen Hydrotalciten. Calcinierte Hydrotalcite können Michael-Additionen wie 2-methylcyclohexan-1,3-dion, 2-acetylcyclopentanon, and 2-acetylcyclohexanon zu Methyl-vinyl keton mit 100% Selektivität katalysieren. Dabei hat sich eine nichtlineare Korrelation zwischen dem Mg-Gehalt und der katalytischen Aktivität ergeben. Die katalytische Aktivität korreliert dagegen jedoch mit der Anzahl der basischen Zentren, die mikrokolorimetrisch mit Benzoesäure bestimmt wurden. Ein optimales Säure-Base Gleichgewicht der Al-reichen Hydrotalcite macht diese zu ausgezeichneten Katalysatoren in Michael-Additionen von zahlreichen 1,3-Dionen, unabhängig von ihrem pK_a Wert.

Kapitel 6: Es wird ein neuartiges Katalysatorsystem beschrieben, dass nach einer Sol-Gel-Methode hergestellt wurde. Ein amorphes Material der allgemeinen Zusammensetzung von $\text{Mg}(\text{O},\text{F})$ mit einer aussergewöhnlich hohen Oberfläche kann nach einem 2-Stufenprozess in einer Fluorierungs-Hydrolyse-Reaktion vom Sol-Gel-Typ hergestellt werden. Verschiedene fluorierte Species in der allgemeinen Zusammensetzung $\text{Mg}(\text{O},\text{F})$ wurden durch ^{19}F MAS NMR und XPS nachgewiesen. $\text{Mg}(\text{O},\text{F})$ -Materialien mit einem geeigneten F Anteil können als effiziente und selektiv wirkende Katalysatoren in Michael-Additionen fungieren. Katalysatoren mit einem molaren Verhältnis von F/Mg wie 1.6 haben die besten Ergebnisse in diesen Reaktionen gezeigt mit einer Ausbeute von 90% und Selektivitäten von 100% bei Raumtemperatur in einer Reaktionszeit von 24 h. Die erfolgreiche kontrollierte Einführung von F und OH Gruppen in die MgO Strukturen erlaubt es die Säure-Basen-Eigenschaften des Katalysators in der gewünschten Weise einzustellen. Damit ermöglicht diese neuartige Methode die Herstellung von wirksamen bifunktionellen Materialien für katalytische Zwecke mit besonderen Anforderungen an Menge und Art der notwendigen Säure- und Basenzentren.

References

-
- [1] www.merriam-webster.com, merriam webster online dictionary.
 - [2] M.W. Roberts, *Catal. Lett.* 67 (2000) 1–73.
 - [3] B. Lindstrom, L.J. Pettersson, *Cattech* 7 (2003) 130–138.
 - [4] J. Wisniak, *Chem. Educator* 5 (2000) 343–350.
 - [5] *Catalysis from A to Z*, (eds. B. Cornils, W.A. Herrmann, R. Schlögl, C.-H. Wong), Wiley-Vch, 2003.
 - [6] www.nacatsoc.org, the homepage of the North American Catalysis Society and related www links.
 - [7] C. Adams, *Chemistry and Industry*, (1999) 740–743.
 - [8] G.-M. Schwab, in *Catalysis: Science and Technology* (eds. J.R. Anderson, M. Boudart), Springer-Verlag, Berlin, 1981, Vol.2, Chapt. 1 History of concepts in catalysis, 1–11.
 - [9] *Handbook of heterogeneous catalysis*, (eds. G. Ertl, H. Knözinger, J. Weitkamp), Wiley-VCH, 1997.
 - [10] J. Haber, in *Catalysis: Science and Technology* (eds. J.R. Anderson, M. Boudart), Springer-Verlag, Berlin, 1981, Vol.2, Chapt. 2 Crystallography of catalyst types, 13–95.
 - [11] K. Tanabe, M. Misono, Y. Ono, H. Hattori, *New solid acids and base*, Kodansha-Elsevier, Tokyo-Amsterdam, 1989.
 - [12] K. Tanabe, W.F. Hölderich, *Appl. Catal. A* 181 (1999) 399–434.
 - [13] H. Hattori, *Chem. Rev.* 95 (1995) 537–558.
 - [14] H. Pines, J.A. Veseley, V.N. Ipatieff, *J. Am. Chem. Soc.* 77 (1955) 6314–6321.
 - [15] D. Barthomeuf, *Catal. Rev.-Sci. Eng.* 38 (1996) 521–612.
 - [16] Y. Ono, T. Baba, *Catal. Today* 38 (1997) 321–337.
 - [17] R.J. Davis, *J. Catal.* 216 (2003) 396–405.
 - [18] Y. Ono, *J. Catal.* 216 (2003) 406–415.
 - [19] J. Weitkamp, M. Hunger, U. Ryma, *Micropor. Mesopor. Mater.* 48 (2001) 255–270.
 - [20] A. Corma, *Chem. Rev.* 95 (1995) 559–614.
 - [21] D. Barthomeuf, *J. Phys. Chem.* 88 (1984) 42–45.
 - [22] P.E. Hathaway, M.E. Davis, *J. Catal.* 116 (1989) 263–278.
 - [23] P.E. Hathaway, M.E. Davis, *J. Catal.* 116 (1989) 279–284.
 - [24] P.E. Hathaway, M.E. Davis, *J. Catal.* 119 (1989) 497–507.
 - [25] H. Tsuji, F. Yagi, H. Hattori, *Chem. Lett.* (1991) 1881–1884.
 - [26] F. Yagi, H. Tshji, H. Hattori, *Micropor. Mater.* 9 (1997) 237–245.
 - [27] Y. Wang, J.H. Zhu, J.M. Cao, Y. Chun, Q.H. Xu, *Micropor. Mesopor. Mater.* 26 (1998) 175–184.
 - [28] K. Arishtirova, P. Kovacheva, A. Predoeva, *Appl. Catal. A* 243 (2003) 191–196.
 - [29] L.R.M. Martens, P.J. Grobet, P.A. Jacobs, *Nature* 315 (1985) 568–570.
 - [30] L.R.M. Martens, P.J. Grobet, W.J.M. Vermeiren, P.A. Jacobs, *Stud. Surf. Sci. Catal.* 28 (1986) 935–941.
 - [31] B. Xu, L. Kevan, *J. Chem. Soc. Faraday Trans.* 87 (1991) 2843–2847.
 - [32] B. Xu, L. Kevan, *J. Phys. Chem.* 96 (1992) 2642–2645.
 - [33] T. Baba, G.J. Kim, Y. Ono, *J. Chem. Soc. Faraday Trans.* 88 (1992) 891–897.
-

-
- [34] T. Baba, S. Hikita, R. Koide, Y. Ono, T. Hanada, T. Tanaka, S. Yoshida, *J. Chem. Soc. Faraday Trans.* 89 (1993) 3177–3180.
- [35] A. Philippou, J. Rocha, M. Anderson, *Catal. Lett.* 57 (1999) 151–153.
- [36] A. Philippou, M. Anderson, *J. Catal.* 189 (2000) 395–400.
- [37] J.C. Lavalley, *Catal. Today* 27 (1996) 377–401.
- [38] M. Huang, S. Kaliaguine, *J. Chem. Soc. Faraday Trans.* 88 (1992) 751–758.
- [39] J. Xie, M. Huang, S. Kaliaguine, *React. Kinet. Catal. Lett.* 58 (1996) 217–227.
- [40] J.C. Kim, H.-X. Li, C.-Y. Chen, M.E. Davis, *Micropor. Mater.* 2 (1994) 413–423.
- [41] Y. Okamoto, M. Ogawa, A. Maezawa, T. Imanaka, *J. Catal.* 112 (1988) 427–436.
- [42] M. Huang, A. Adnot, S. Kaliaguine, *J. Catal.* 137 (1992) 322–332.
- [43] M. Huang, A. Adnot, S. Kaliaguine, *J. Am. Chem. Soc.* 114 (1992) 10005–10010.
- [44] S.Y. Choi, Y.S. Park, S.B. Hong, K.B. Yoon, *J. Am. Chem. Soc.* 118 (1996) 9377–9386.
- [45] E.J. Doskocil, S.V. Nordawekar, B.G. Kaya, R.J. Davis, *J. Phys. Chem. B* 103 (1999) 6277–6282.
- [46] M. Huang, S. Kaliaguine, M. Muscas, A. Auroux, *J. Catal.* 157 (1995) 266–269.
- [47] S.V. Bordawekar, R.J. Davis, *J. Catal.* 189 (2000) 79–90.
- [48] A.A. Kheir, J.F. Haw, *J. Am. Chem. Soc.* 116 (1994) 817–818.
- [49] M. Sánchez-Sánchez, T. Blasco, F. Rey, *Phy. Chem. Chem. Phys.* 1 (1999) 4529–4535.
- [50] V. Bosacek, R. Klik, F. Genoni, G. Spano, F. Rivetti, F. Figueras, *Magn. Reson. Chem.* 37 (1999) S135–S141.
- [51] J. Engelhardt, J. Szanyi, J. Valyon, *J. Catal.* 107 (1987) 296–306.
- [52] W.S. Wieland, R.J. Davis, J.M. Garces, *J. Catal.* 173 (1998) 490–500.
- [53] A. Corma, R.M. Martin-Aranda, F. Sanchez, *J. Catal.* 126 (1990) 192–198.
- [54] A. Corma, V. Fornes, R.M. Martin-Aranda, H. Garcia, J. Primo, *Appl. Catal.* 59 (1990) 237–248.
- [55] A. Corma, R.M. Martin-Aranda, F. Sanchez, *Stud. Surf. Sci. Catal.* 59 (1991) 503–511.
- [56] R. Ballini, F. Bigi, E. Gogni, R. Maggi, G. Sartori, *J. Catal.* 191 (2000) 348–353.
- [57] P.T. Wierchowski, L.W. Zatorski, *Catal. Lett.* 9 (1991) 411–414.
- [58] M. Tu, R.J. Davis, *J. Catal.* 199 (2001) 85–91.
- [59] C.T. Kresge, M.E. Leonowicz, W.J. Roth, J.C. Vartuli, J.S. Beck, *Nature* 359 (1992) 710–712.
- [60] D. Zhao, J. Feng, Q. Huo, N. Melosh, G.H. Fredrickson, B.F. Chmelka, G.D. Stucky, *Science* 279 (1998) 548–553.
- [61] K.R. Kloetstra, H. van Bekkum, *J. Chem. Soc. Chem. Commun.* (1995) 1005–1006.
- [62] K.R. Kloetstra, M. van Laren, H. van Bekkum, *J. Chem. Soc. Faraday Trans.* 93 (1997) 1211–1220.
- [63] K.R. Kloetstra, H. van Bekkum, *Stud. Surf. Sci. Catal.* 105 (1997) 431.
- [64] K.R. Kloetstra, J. van den Broek, H. van Bekkum, *Catal. Lett.* 47 (1997) 235–242.
- [65] Y.L. Wie, Y.M. Wang, J.H. Zhu, Z.Y. Wu, *Adv. Mater.* 15 (2003) 1943–1945.
- [66] D.J. Macquarrie, *Chem. Commun.* (1996) 1961–1962; (1997) 601–602.
- [67] D.J. Macquarrie, D.B. Jackson, *Chem. Commun.* (1997) 1781–1782.
- [68] A. Cauval, G. Renard, D. Brunel, *J. Org. Chem.* 62 (1997) 749–751.
- [69] M. Laspéras, T. Llorett, L. Chaves, I. Rodriguez, A. Cauvel, D. Brunel, *Stud. Surf. Sci. Catal.* 108 (1997) 75–82.
-

-
- [70] Y.V. Subba Rao, D.E. De Vos, P.A. Jacobs, *Angew. Chem. Int. Ed.* 36 (1997) 2661–2663.
- [71] I. Rodriguez, S. Iborra, A. Corma, F. Rey, J.L. Jorda, *Chem. Commun.* (1999) 593–594.
- [72] A. Corma, S. Iborra, I. Rodriguez, F. Sanchez, *J. Catal.* 211 (2002) 208–215.
- [73] X. Lin, G.K. Chuah, S. Jaenicke, *J. Mol. Catal. A* 150 (1999) 287–294.
- [74] B.M. Choudary, M.L. Kantam, P. Sreekanth, T. Bandopadhyay, F. Figueras, A. Tuel, *J. Mol. Catal. A* 142 (1999) 361–365.
- [75] S. Jaenicke, G.K. Chuah, X.H. Lin, X.C. Hu, *Micropor. Mesopor. Mater.* 35–36 (2000) 143–153.
- [76] A. Corma, S. Iborra, I. Rodriguez, M. Iglesia, F. Sanchez, *Cata. Lett.* 82 (2002) 237–242.
- [77] P.W. Lednor, R. de Ruiter, *J. Chem. Soc. Chem. Commun.* (1989) 320–321.
- [78] P.W. Lednor, R. de Ruiter, *J. Chem. Soc. Chem. Commun.* (1991) 1625–1626.
- [79] P.W. Lednor, *Catal. Today* 15 (1992) 243–261.
- [80] L.M. Gandia, R. Malm, R. Marchand, R. Conanec, Y. Laurent, M. Montes, *Appl. Catal. A* 114 (1994) L1–L7.
- [81] P. Grange, P. Bastians, R. Conanec, R. Marchand, Y. Laurent, *Appl. Catal. A* 114 (1994) L191–L196.
- [82] J.J. Benitez, J.A. Odriozola, R. Marchand, Y. Laurant, P. Grange, *J. Chem. Soc. Faraday Trans.* 91 (1995) 4477–4479.
- [83] A. Massinon, J.A. Odriozola, Ph. Bastians, R. Conanec, R. Marchand, Y. Laurant, P. Grange, *Appl. Catal. A* 137 (1996) 9–23.
- [84] M.J. Climent, A. Corma, V. Fornés, A. Frau, R. Guil-López, S. Iborra, J. Primo, *J. Catal.* 163 (1996) 392–398.
- [85] N. Fripiat, P. Grange, *Chem. Commun.* (1996) 1409–1410.
- [86] N. Fripiat, R. Conanec, A. Auroux, R. Marchand, Y. Laurent, P. Grange, *J. Catal.* 167 (1997) 543–549.
- [87] N. Fripiat, V. Parvulescu, V.I. Parvulescu, P. Grange, *Appl. Catal. A* 181 (1999) 331–346.
- [88] M.A. Centeno, S. Delsarte, P. Grange, *J. Phys. Chem. B* 103 (1999) 7214–7221.
- [89] D. Delsarte, A. Auroux, P. Grange, *Phys. Chem. Chem. Phys.* 2 (2000) 2821–2827.
- [90] H. Wiame, C. Cellier, P. Grange, *J. Catal.* 190 (2000) 406–418.
- [91] H. Wiame, C. Cellier, P. Grange, *J. Phys. Chem. B* 104 (2000) 591–596.
- [92] Y.D. Xia, R. Mokaya, *Angew. Chem.* 115 (2003) 2743–2748; *Angew. Chem. Int. Ed.* 42 (2003) 2639–2644.
- [93] J.H. Clark, *Chem. Rev.* 80 (1980) 429–452.
- [94] H. Tsuji, H. Kabashima, H. Kita, H. Hattori, *React. Kinet. Catal. Lett.* 56 (1995) 363–369.
- [95] H. Handa, T. Baba, Y. Ono, *J. Mol. Catal. A* 134 (1998) 171–177.
- [96] T. Baba, A. Kato, H. Takahashi, F. Toriyama, H. Handa, Y. Ono, H. Sugisawa, *J. Catal.* 176 (1998) 488–494.
- [97] H. Kabashima, H. Tsuji, S. Nakata, Y. Tanaka, H. Hattori, *Appl. Catal. A* 194–195 (2000) 227–240.
- [98] T. Ando, *Stud. Surf. Sci. Catal.* 85 (1994) 9–20.
- [99] T. Ando, J.H. Clark, D.G. Cork, T. Hanafusa, J. Ichihara, T. Kimura, *Tetrahedron Lett.* 28 (1987) 1421–1424.
- [100] T. Ando, S.J. Brown, J.H. Clark, D.G. Cork, T. Hanafusa, J. Ichihara, J.M. Miller, M.S. Robertson, *J. Chem. Soc. Perkin Trans. 2* (1986) 1133–1139.
-

-
- [101] J.-M. Clacens, D. Genuit, L. Delmotte, A. Garcia-Ruiz, G. Bergeret, R. Montiel, J. Lopez, F. Figueras, *J. Catal.* 221 (2004) 483–490.
- [102] J.-M. Clacens, D. Genuit, B. Veldurthy, G. Bergeret, L. Delmotte, A. Garcia-Ruiz, F. Figueras, *Appl. Catal. B* 53 (2004) 95–100.
- [103] A. Mitsutani, *Catal. Today* 73 (2002) 57–63.
- [104] T. Yamaguchi, Y. Wang, M. Komatsu, M. Ookawa, *Catal. Surveys Jpn.* 5 (2002) 81–89.
- [105] W.O. Haag, H. Pines, *J. Am. Chem. Soc.* 82 (1960) 387–391.
- [106] H. Pines, W.M. Stalick, *Base-catalyzed reactions of hydrocarbons and related compounds*, Academic press, New York, 1977, Chapt.2.
- [107] J. Kijenski, S. Malinowski, *Reac. Kinet. Catal. Lett.* 3 (1975) 343–347.
- [108] J. Kijenski, S. Malinowski, *Catalysis*, Vol. 4, R. Soc. Chem., London, 1981, 130.
- [109] T. Ushikubo, H. Hattori, K. Tanabe, *Chem. Lett.* (1984) 649–652.
- [110] N.J. Sun, K.J. Klabunde, *J. Catal.* 185 (1999) 506–512.
- [111] G. Suzukamo, M. Fukao, M. Minobe, *Chem. Lett.* (1987) 585–588.
- [112] G. Suzukamo, M. Fukao, T. Hibi, K. Chikaishi, *Acid-Base Catalysis*, 1989, 405.
- [113] T. Baba, H. Handa, Y. Ono, *J. Chem. Soc. Faraday Trans.* 90 (1994) 187–191.
- [114] T. Baba, *Catal. Surveys Jpn.* (2000) 17–29.
- [115] T. Baba, H. Yuasa, H. Handa, Y. Ono, *Catal. Lett.* 50 (1998) 83–85.
- [116] H. Handa, T. Baba, Y. Ono, *J. Chem. Soc. Faraday Trans.* 94 (1998) 451–454.
- [117] T. Yamaguchi, J.H. Zhu, Y. Wang, M. Komatsu, M. Ookawa, *Chem. Lett.* (1997) 989–990.
- [118] Y. Wang, J.H. Zhu, W.Y. Huang, *Phys. Chem. Chem. Phys.* 3 (2001) 2537–2543.
- [119] Y. Wang, W.Y. Huang, Y. Chun, J.R. Xia, J.H. Zhu, *Chem. Mater.* 13 (2001) 670–677.
- [120] K. Tanabe, T. Yamaguchi, *Catal. Today* 20 (1994) 185–198.
- [121] R.A. Sheldon, J. Dakka, *Catal. Today* 19 (1994) 215–246.
- [122] R.A. Sheldon, R.S. Downing, *Appl. Catal. A* 189 (1999) 163–183.
- [123] M.L. Kantam, B.M. Choudary, Ch.V. Reddy, K.K. Rao, F. Figueras, *Chem. Commun.* (1998) 1033–1034.
- [124] A. Corma, R.M. Martin-Aranda, *Appl. Catal. A* 105 (1993) 271–279.
- [125] M.J. Climent, A. Corma, R. Guil-Lopez, S. Iborra, *Catal. Lett.* 74 (2001) 161–167.
- [126] M.J. Climent, A. Corma, R. Guil-Lopez, S. Iborra, J. Primo, *Catal. Lett.* 59 (1999) 33–38.
- [127] G. Zhang, H. Hattori, K. Tanabe, *Appl. Catal.* 36 (1988) 189–197; G. Zhang, H. Hattori, *Appl. Catal.* 40 (1988) 183–190.
- [128] D. Tichit, M.N. Bennani, F. Figueras, R. Teissier, J. Kervennal, *Appl. Clay Sci.* 13 (1998) 401–415.
- [129] J.C.A.A. Roelofs, A.J. van Dillen, K.P. de Jong, *Catal. Today* 60 (2000) 297–303.
- [130] M.J. Climent, A. Corma, S. Iborra, A. Velty, *Catal. Lett.* 79 (2002) 157–163.
- [131] M.J. Climent, A. Corma, S. Iborra, J. Primo, *J. Catal.* 151 (1995) 60–66.
- [132] S. Sebt, A. Solhy, R. Tahir, S. Abdelatif, S. Boulaajaj, J.A. Mayoral, J.I. Garcia, J.M. Fraile, A. Kossir, H. Oumimoun, *J. Catal.* 213 (2003) 1–6.
- [133] K. Akutu, H. Kabashima, T. Seki, H. Hattori, *Appl. Catal. A* 247 (2003) 65–74.
- [134] R. Ballini, F. Bigi, R. Maggi, G. Sartori, *J. Catal.* 191 (2000) 348–353.
-

-
- [135] V.J. Bulbulbe, V.H. Deshpande, S. Velu, A. Sudalai, S. Shivasankar, V.T. Sathe, *Tetrahedron* 55 (1999) 9325–9332.
- [136] H. Kabashima, T. Katou, H. Hattori, *Appl. Catal. A* 241 (2001) 121–124.
- [137] H. Hattori, K. Kabashima, *Appl. Catal. A* 161 (1997) L33–L35.
- [138] K. Kabashima, H. Tsuji, H. Hattori, *React. Kinet. Catal. Lett.* 58 (1996) 255–259.
- [139] P.S. Kumbhar, J. Sanchez-Valente, F. Figueras, *Chem. Commun.* (1998) 1091–1092.
- [140] H. Kabashima, H. Tsuji, T. Shibuya, H. Hattori, *J. Mol. Catal. A* 155 (2000) 23–29.
- [141] B.M. Choudary, M.L. Kantam, Ch.V. Reddy, K.K. Rao, F. Figueras, *J. Mol. Catal. A* 146 (1999) 279–284.
- [142] I. Rodriguez, S. Iborra, F. Rey, A. Corma, *Appl. Catal. A* 194–195 (2000) 241–252.
- [143] A. Corma, S. Iborra, I. Rodriguez, M. Iglesias, F. Sanchez, *Catal. Lett.* 82 (2002) 237–242.
- [144] J.I. Tateiwa, A. Hosomi, *Eur. J. Org. Chem.* (2001) 1445–1448.
- [145] P. Mastrorilli, C.F. Nobile, G.P. Suranna, *J. Mol. Catal. A* 103 (1995) 23–29.
- [146] T. Kawabata, T. Mizugaki, K. Ebitani, K. Kaneda, *J. Am. Chem. Soc.* 125 (2003) 10486–10487.
- [147] M. Sasidharan, R. Kumar, *J. Catal.* 220 (2003) 326–332.
- [148] J. Barrios, R. Rojas, A.R. Alcanrara, J.V. Sinisterra, *J. Catal.* 112 (1988) 529–542.
- [149] J. Yamawaki, T. Kawate, T. Ando, T. Hanafusa, *Bull. Chem. Soc. Jpn.* 56 (1983) 1885–1886.
- [150] J.M. Campelo, M.S. Climent, J.M. Marinas, *React. Kinet. Catal. Lett.* 47 (1992) 7–11.
- [151] P. Laszlo, P. Pennetreau, *Tetrahedron Lett.* 26 (1985) 2645–2648.
- [152] K. Kabashima, H. Tsuji, H. Hattori, *Appl. Catal. A* 165 (1997) 319–325.
- [153] J.E.G. Mdoe, J.H. Clark, D.J. Macquarrie, *Synlett* (1998) 625–627.
- [154] U. Meyer, H. Gorzawski, W. F. Hölderich, *Catal. Lett.* 59 (1999) 201–206.
- [155] N.L. Wendler, H.L. Slates, M. Tishler, *J. Am. Chem. Soc.* 73 (1951) 3816–3818.
- [156] W.G. Dauben, R.A. Bunce, *J. Org. Chem.* 48 (1983) 4642–4648.
- [157] J.W. Muskopf, R.M. Coates, *J. Org. Chem.* 50 (1985) 69–76.
- [158] N. Harada, T. Sugioka, H. Uda, T. Kuriki, *Synthesis* (1990) 53–56.
- [159] T. Bui, C.F. Barbas III, *Tetrahedron Lett.* 36 (2000) 6951–6954.
- [160] J. Christoffers, U. Rössler, T. Werner, *Eur. J. Org. Chem.* (2000) 701–705.
- [161] D. Bensa, T. Constantieux, J. Rodriguez, *Synthesis* (2004) 923–927.
- [162] F. Seel, *Angew. Chem.* 76 (1964) 532–534.
- [163] H. Kabashima, H. Tsuji, H. Hattori, *Appl. Catal. A* 165 (1997) 319–325.
- [164] T. Seki, H. Kabashima, K. Akutsu, H. Tachikawa, H. Hattori, *J. Catal.* 204 (2001) 393–401.
- [165] M.A. Aramendia, V. Borau, C. Jiménez, J.M. Marinas, J.R. Ruiz, F.J. Urbano, *Appl. Catal. A* 244 (2003) 207–215.
- [166] Y. Wang, J.H. Zhu, J.M. Cao, Y. Chun, Q.H. Xu, *Micropor. Mesopor. Mater.*, 26 (1998) 175–184.
- [167] D.E. Jiang, G.C. Pan, B.Y. Zhao, G.P. Ran, Y.C. Xie, E.Z. Min, *Appl. Catal. A* 201 (2001) 169–176.
- [168] P. Kovacheva, K. Arishtirova, S. Vassilev, *Appl. Catal. A* 210 (2001) 391–395.
- [169] Y. Sakurai, T. Suzuki, K. Nakagawa, N. Ikenaga, H. Aota, T. Suzuki, *J. Catal.* 209 (2002) 16–24.
- [170] S. Freni, S. Cavallaro, N. Mondello, L. Spadaio, F. Frusteri, *Catal. Commun.* 4 (2003) 287–293.
- [171] K.D. Jung, O. S. Joo, S.H. Cho, S.H. Han, *Appl. Catal. A* 240 (2003) 235–241.
-

-
- [172] A.S. Ndou, N. Plint, N.J. Coville, *Appl. Catal. A* 251 (2003) 337–345.
- [173] A.S. Ndou, N.J. Coville, *Appl. Catal. A* 275 (2004) 103–110.
- [174] S. Coluccia, A.J. Tench, *Proceedings of the 7th International Congress on Catalysis Tokyo, Japan*, 1980, P1160.
- [175] G. Martra, T. Cacciatori, L. Marchese, J.S.J. Hargreaves, I.M. Mellor, R.W. Joyner, S. Cosuccia, *Catal. Today* 70 (2001) 121–130 and references therein.
- [176] V.R. Choudary, V.H. Rane, R.V. Gadre, *J. Catal.* 145 (1994) 300–311.
- [177] S. Utamapanya, K.J. Klabunde, J. Schlup, *Chem. Mater.* 3 (1991) 175–181.
- [178] B.M. Choudary, K. Mahendar, K.V.S. Ranganath, *J. Mol. Catal. A* 234 (2005) 25–27.
- [179] B.M. Choudary, R.S. Mulukutla, K.J. Klabunde, *J. Am. Chem. Soc.* 125 (2003) 2020–2021.
- [180] K.S.W. Sing, J. Rouquerol, in *Handbook of Heterogeneous Catalysis*, Vol. 2 (eds. G. Ertl, H. Knözinger, J. Weitkamp), Wiley, New York, 1997, p427.
- [181] W. G. Dauben, R.A. Bunce, *J. Org. Chem.* 48 (1983) 4642–4648.
- [182] P. Wieland, K. Miescher, *Helv. Chim. Acta* 33 (1950) 2215–2228.
- [183] S.J. Danishefsky, J.J. Masters, W.B. Young, J.T. Link, L.B. Snyder, T.V. Magee, D.K. Jung, R.C.A. Isaacs, W.G. Bornmann, C.A. Alaimo, C. A. Coburn, M.J. Di Grandi, *J. Am. Chem. Soc.* 118 (1996) 2843–2859.
- [184] L.A. Paquette, D. Backhaus, R. Braun, T.L. Underiner, K. Fuchs, *J. Am. Chem. Soc.* 119 (1997) 9662–9671.
- [185] T. Yamaguchi, *Catal. Today* 20 (1994) 199–218.
- [186] M. Hino, K. Arata, *J. Chem. Soc. Chem. Commun.* (1980) 851–852.
- [187] D.A. Ward, E.I. Ko, *J. Catal.* 157 (1995) 321–333.
- [188] V. Quaschnig, J. Deutsch, P. Druska, H.J. Niclas, E. Kemnitz, *J. Catal.* 177 (1998) 164–174.
- [189] X.M. Song, A. Sayari, *Catal. Rev. -Sci. Eng.* 38 (1996) 329–412.
- [190] W.M. Hua, F. Zhang, Z. Ma, Z. Gao, *Catal. Lett.* 65 (2000) 85–89.
- [191] J.C. Yori, C.L. Pieck, J.M. Parera, *Catal. Lett.* 64 (2000) 141–146.
- [192] B.Q. Xu, S.B. Cheng, X. Zhang, S.F. Ying, Q.M. Zhu, *Chem. Commun.* (2000) 1121–1122.
- [193] P.T. Patil, K.M. Malshe, P. Kumar, M.K. Dongare, E. Kemnitz, *Catal. Commun.* 3 (2002) 411–416.
- [194] A.Z. Khan, E. Ruckenstein, *J. Catal.* 139 (1993) 304–321.
- [195] S. Sugiyama, K. Shimodan, H. Hayashi, N. Shigemoto, K. Miyaura, K. Saitoh, J.B. Moffat, *J. Catal.* 141 (1993) 279–286.
- [196] P. Thomasson, O.S. Tyagi, H. Knözinger, *Appl. Catal. A* 181 (1999) 181–188.
- [197] J.H. Zhu, Y. Wang, Y. Chun, X.S. Wang, *J. Chem. Soc. Faraday Trans.* 94 (1998) 1163–1169.
- [198] R. Bal, B.B. Tope, T.K. Das, S.G. Hegde, S. Sivasanker, *J. Catal.* 204 (2001) 358–363.
- [199] J.H. Li, R.J. Davis, *Appl. Catal. A* 239 (2003) 59–70.
- [200] W.S. Wieland, R.J. Davis, J.M. Garces, *Catal. Today* 28 (1996) 443–450.
- [201] Y. Fu, T. Baba, Y. Ono, *Appl. Catal. A* 176 (1999) 201–204.
- [202] Z.-J. Li, H.A. Prescott, J. Deutsch, A. Trunschke, H. Lieske, E. Kemnitz, *Catal. Lett.* 92 (2004) 175–180.
- [203] Z. Liu, W.J. Jie, L. Dong, Y. Chen, *J. Solid State Chem.* 138 (1998) 41–46.
-

-
- [204] G. Leofani, M. Padovan, G. Tozzola, B. Venturelli, *Catal. Today* 41 (1998) 207–219.
- [205] K. Parida, V. Quaschnig, E. Lieske, E. Kemnitz, J. Mater. Chem. 11 (2001) 1903–1911.
- [206] F. Cavani, F. Trifiro, A. Vaccari, *Catal. Today* 11 (1991) 173–301.
- [207] A. Vaccari, *Catal. Today* 41 (1998) 53–71.
- [208] B.F. Sels, D.E. De Vos, P.A. Jacobs, *Catal. Rev. -Sci. Eng.* 43 (2001) 443–488.
- [209] D. Tichit, B. Coq, *Cattech* 7 (2003) 206–217.
- [210] V.R.L. Constantino, T.J. Pinnavaia, *Catal. Lett.* 23 (1994) 361–367.
- [211] E. Suzuki, M. Okamoto, Y. Ono, *J. Mol. Catal.* 61 (1990) 283–294.
- [212] K.K. Rao, M. Gravelle, J. Sanchez-Valente, F. Figueras, *J. Catal.* 173 (1998) 115–121.
- [213] A. Corma, V. Fornés, R.M. Martin-Aranda, F. Rey, *J. Catal.* 134 (1992) 58–65.
- [214] A.L. McKenzie, C.T. Fishel, R.J. Davis, *J. Catal.* 138 (1992) 547–561.
- [215] J.I. Di Cosimo, V.K. Díez, M. Xu, E. Iglesia, C.R. Apesteguía, *J. Catal.* 178 (1998) 499–510.
- [216] J. Shen, J.M. Kobe, Y. Chen, J.A. Dumesic, *Langmuir* 10 (1994) 3902–3908.
- [217] V.K. Díez, C.R. Apesteguía, J.I. Di Cosimo, *J. Catal.* 215 (2003) 220–233.
- [218] F. Prinetto, G. Ghiotti, R. Durand, D. Tichit, *J. Phys. Chem. B* 104 (2000) 11117–11126.
- [219] J. Shen, M. Tu, C. Hu, *J. Solid State Chem.* 137 (1998) 295–301.
- [220] S. Casenave, H. Martinez, C. Guimon, A. Auroux, V. Hulea, A. Cordoneanu, E. Dumitriu, *Thermochim. Acta* 379 (2001) 85–93.
- [221] S. Casenave, H. Martinez, C. Guimon, A. Auroux, V. Hulea, E. Dumitriu, *J. Therm. Anal. Cal.* 72 (2003) 191–198.
- [222] P.S. Kumbhar, J.S. Valente, J. Lopez, F. Figueras, *Chem. Commun.* (1998) 535–536.
- [223] K. Yamaguchi, K. Ebitani, T. Yoshida, H. Yoshida, K. Kaneda, *J. Am. Chem. Soc.* 121 (1999) 4526–4527.
- [224] D. Tichit, D. Lutic, B. Coq, R. Durand, R. Teissier, *J. Catal.* 219 (2003) 167–175.
- [225] D. Tichit, M.H. Lhouty, A. Guida, B.H. Chiche, F. Figueras, A. Auroux, D. Bartalini, E. Garrone, *J. Catal.* 151 (1995) 50–59.
- [226] M.J. Climent, A. Corma, S. Iborra, K. Epping, A. Velty, *J. Catal.* 225 (2004) 316–326.
- [227] H.A. Prescott, Z.-J. Li, E. Kemnitz, A. Trunschke, J. Deutsch, H. Lieske, A. Auroux, *J. Catal.* 234 (2005) 119–130.
- [228] www.sasol.com, product information.
- [229] A. Corma, V. Fornés, F. Rey, *J. Catal.* 148 (1994) 205–212.
- [230] G. Fornasari, M. Gazzano, D. Matteuzi, F. Trifiro, A. Vaccari, *Appl. Clay Sci.* 10 (1995) 69–82.
- [231] K.J.D. MacKenzie, R.H. Meinhold, B.L. Sherrieff, Z. Xu, *J. Mater. Chem.* 3 (1993) 1263–1269.
- [232] R.H. Meinhold, R.C.T. Slade, R.H. Newman, *Appl. Magn. Reson.* 4 (1993) 121–140.
- [233] W.T. Reichle, S.Y. Kang, D.S. Everhardt, *J. Catal.* 101 (1986) 352–359.
- [234] S. Miyata, *Clays Clay Miner.* 28 (1980) 50–56.
- [235] M.J. Climent, A. Corma, V. Fornés, A. Frau, R. Guil-López, S. Iborra, J. Primo, *J. Catal.* 163 (1996) 392–398.
- [236] H. Knözinger, *Adv. Catal.* 25 (1976) 184–271.
- [237] G. Busca, *Phys. Chem. Chem. Phys.* 1 (1999) 723–736.
-

-
- [238] N. Fripiat, R. Conanec, A. Auroux, Y. Laurent, P. Grange, *J. Catal.* 167 (1997) 543–549.
- [239] C. Morterra, A. Chiorino, G. Ghiotti, E. Garrone, *J. Chem. Soc. Faraday Trans. 1*, 75 (1979) 271–288.
- [240] C. Morterra, S. Coluccia, A. Chiorino, F. Boccuzzi, *J. Catal.* 54 (1978) 348–364.
- [241] F. Abbattista, S. Delmastro, G. Gozzelino, D. Mazza, M. Vallino, G. Busca, V. Lorenzelli, G. Ramis, *J. Catal.* 117 (1989) 42–51.
- [242] P. Nortier, P. Fourre, A.B. Mohammed Saad, O. Saur, J.C. Lavalley, *Appl. Catal.* 61 (1990) 141–160.
- [243] G. Busca, V. Lorenzelli, *Mater. Chem.* 7 (1982) 89–126.
- [244] J.C. Lavalley, *Cata. Today* 27 (1996) 377–401.
- [245] J.A. Lercher, C. Colombier, H. Noller, *J. Chem. Soc., Faraday Trans. 1*, 80 (1984) 949–959.
- [246] A.A. Davydov, M.L. Shepot'ko, A.A. Budneva, *Kinet. Catal.* 35 (1994) 299–306.
- [247] V. Solinas, I. Ferino, *Catal. Today* 41 (1998) 179–189.
- [248] E. Kemnitz, U. Groß, S. Rüdiger, C.S. Shekar, *Angew. Chem. Int. Ed.* 42 (2003) 4251–4254.
- [249] M.J. Climent, A. Corma, V. Fornés, R. Guil-Lopez, S. Iborra, *Adv. Synth. Catal.* 344 (2002) 1090–1096.
- [250] E.I. Ko, Sol-Gel Process, in *Handbook of Heterogeneous Catalysis* (eds. G. Ertl, H. Knözinger, J. Weitkamp), Wiley-VCH, Weinheim, 1997.
- [251] J.K. Murthy, U. Groß, S. Rüdiger, E. Ünveren, E. Kemnitz, *J. Fluorine Chem.* 125 (2004) 937–949.
- [252] S. Rüdiger, U. Groß, M. Feist, H.A. Prescott, C.S. Shekar, S. Troyanov, E. Kemnitz, *J. Mater. Chem.* 15 (2005) 588–597.
- [253] A. Hess, E. Kemnitz, *J. Catal.* 149 (1994) 449–457.
- [254] E. Kemnitz, A. Hess, G. Rother, S. Troyanov, *J. Catal.* 159 (1996) 332–339.
- [255] B. Adamczyk, O. Boesha, N. Weiherb, S.L.M. Schroederb, E. Kemnitz, *J. Fluorine Chem.* 101 (2000) 239–246.
- [256] T. Krahl, R. Stösser, E. Kemnitz, G. Scholz, M. Feist, G. Silly, J.-Y. Buzare, *Inorg. Chem.* 42 (2003) 6474–6483.
- [257] T. Krahl, E. Kemnitz, *Angew. Chem. Int. Ed.* 43 (2004) 6653–6656.
- [258] A. Demourgues, L. Francke, E. Durand, A. Tressaud, *J. Fluorine Chem.* 114 (2002) 229–236.
- [259] E. Kemnitz, D.-H. Menz, *Prog. Solid State Chem.* 26 (1998) 97–153.
- [260] D.J. Suh, T.-J. Park, *Chem. Mater.* 14 (2002) 1452–1454.
- [261] K. Niesz, P. Yang, G.A. Somorjai, *Chem. Commun.* (2005) 1986–1987.
- [262] T. Lopez, I. Garcia-Cruz, R. Gomez, *J. Catal.* 127 (1991) 75–85.
- [263] Y. Diao, W.P. Walawender, C.M. Sorensen, K.J. Klabunde, T. Ricker, *Chem. Mater.* 14 (2002) 362–368.
- [264] R. Portillo, T. Lopez, R. Gomez, B.A. Morales, O. Novaro, *Langmuir* 12 (1996) 40–44.
- [265] H.S. Jung, J.-K. Lee, J.-Y. Kim, K.S. Hong, *J. Collid Inter. Sci.* 259 (2003) 127–132.
- [266] M. Wojciechowska, M. Zielinski, M. Pietrowski, *J. Fluorine Chem.* 120 (2003) 1–11.
- [267] A.J. Lecloux, in *Catalysis: Science and Technology* (eds. J.R. Anderson, M. Boudart), Akademie-Verlag, Berlin, 1983, Vol.2, Chapt. 4 Texture of catalysts, 171–230.
- [268] D. Wallacher, N. Künzner, D. Kovalen, N. Knorr, K. Knorr, *Phys. Rev. Lett.* 92 (2004) 195704–195708.
-

-
- [269] H. Thoms, M. Epple, A. Reller, *Solid State Ionics* 101–103 (1997) 79–84.
- [270] <http://webbook.nist.gov/chemistry/>
- [271] H. Thoms, M. Epple, H. Viebrock, A. Reller, *J. Mater. Chem.* 5 (1995) 589–594.
- [272] Z.A. Starikova, A.I. Yanovsky, E.P. Turevskaya, N.Ya Turova, *Polyhedron* 16 (1997) 967–974.
- [273] J.M. Miller, *Prog. Nucl. Magn. Reson. Sp.* 28 (1996) 255–281.
- [274] P.J. Chupas, D.R. Corbin, V.N.M. Rao, J.C. Hanson, C.P. Grey, *J. Phys. Chem. B* 107 (2003) 8327–8336.
-

Lebenslauf

Name: Zhijian Li

Geburtsort: Zhangping, Fujian, P.R China

Geburtsdatum: 27.04.1977

Schulbildung

09.1983–06.1989 Shiyan Primary School, Zhangping, Fujian, P.R China

09.1989–06.1992 No.1 Middle School, Zhangping, Fujian, P.R China

09.1992–06.1995 No.1 High School, Zhangping, Fujian, P.R China

Hochschulbildung

09.1995–06.1999 Department of Chemistry, Nankai University, Tianjin, P.R.China
Bachelor of Science (Chemistry)

09.1999–07.2002 Department of Chemistry, Nankai University, Tianjin, P.R.China
Master of Science (Chemistry)

10.2002–08.2005 Promotion an der Humboldt-Universität zu Berlin
im Institut für Anorganische Chemie bei Prof. Dr. E. Kemnitz

Selbständigkeitserklärung

Hiermit erkläre ich, die vorliegende Arbeit selbständig ohne fremde Hilfe verfaßt und nur die angegebene Literatur und Hilfsmittel verwendet zu haben.

Zhijian Li

5 Juli 2005
